

**SPECTRAL PROPERTIES OF 1.3 μm InGaAsP SEMICONDUCTOR DIODE
LASERS**

By

JOSEPH EDWARD HAYWARD, B.ENG, M.ENG

A Thesis

Submitted to the School of Graduate Studies

in Partial Fulfilment of the Requirements

for the Degree

Doctor of Philosophy

McMaster University

© Copyright by Joseph Edward Hayward, April 1993

DOCTOR OF PHILOSOPHY (1993)
(Engineering Physics)

McMASTER UNIVERSITY
Hamilton, Ontario

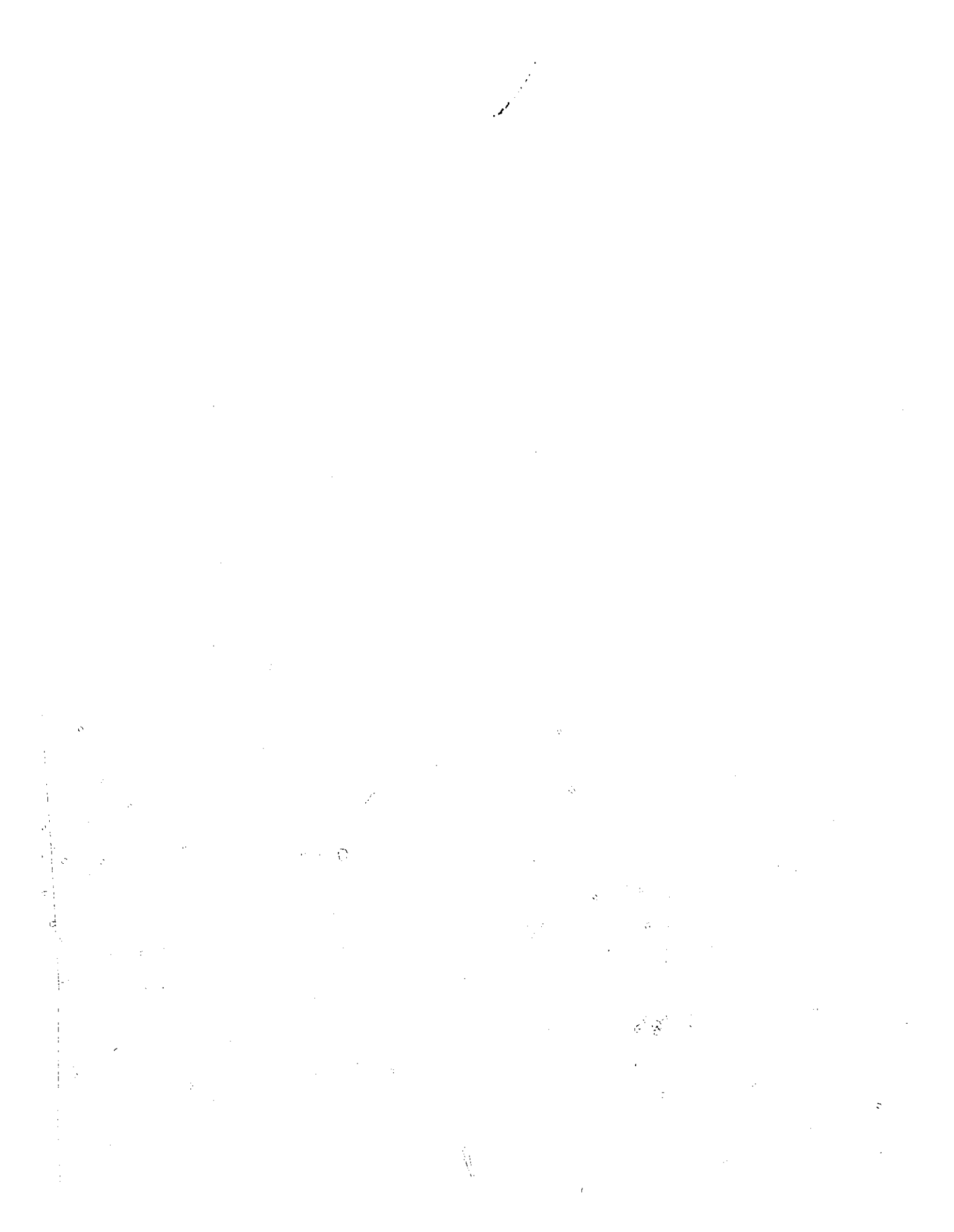
TITLE: Spectral Properties of 1.3 μm InGaAsP Semiconductor Diode Lasers

AUTHOR: Joseph Edward Hayward, B.Eng., M.Eng. (McMaster University)

SUPERVISOR: Professor D. T. Cassidy

NUMBER OF PAGES: xi,140

SPECTRAL PROPERTIES OF DIODE LASERS



Abstract

Physical mechanisms responsible for the above-threshold spectral output of 1.3 μm InGaAsP semiconductor diode lasers are presented and discussed. Measurements of the facet emission of a large number of devices indicate modulations in the below-threshold $R_m G_m$ product which can be used to predict and explain the shape of the above-threshold mode profile for output power levels of less than approximately 5 mW. Above-threshold measurements using devices incorporated into a short-external-cavity configuration show that a symmetric, nonlinear gain mechanism is required to explain the spectral properties for output power levels in a single mode which are greater than 5 mW. Thus it is concluded that both the effects of scattering centres and nonlinear gain are required to model accurately the spectral output of 1.3 μm InGaAsP semiconductor diode lasers.

Acknowledgments

I would like to thank my supervisor Dr. D. T. Cassidy for his guidance and support throughout the course of this work. F. H. Peters is also acknowledged for providing the electroluminescent data used in Chapter 4. I would also like to thank Glen Leinweber for many helpful recommendations. The financial support of the Natural Science and Engineering Research Council of Canada and McMaster University are gratefully acknowledged. Finally, I would like to thank Isabel, Nathaniel and Rebecca for their love and encouragement.

Table of Contents

	page
Chapter 1. Introduction	1
Chapter 2. Calculation of Residues	
2.1 Introduction	7
2.2 Experimental Technique	9
2.3 Correlation of Results	22
2.4 Modelling of Above Threshold Spectra	28
2.5 Summary	33
Chapter 3. Shape of $R_m G_m$ Profiles	
3.1 Introduction	35
3.2 The Fitting Coefficients	36
3.2 Variation of the Fitting Coefficients	38
3.4 Longitudinal Mode Spacing	47
3.5 Summary	50
Chapter 4. Comparison of Techniques to Measure Scattering Centres	
4.1 Introduction	53
4.2 Comparison of Techniques	54
4.3 Correlation of Results	58
4.4 Longitudinal Mode Sampling	62
4.5 Summary	71
Chapter 5. Nonlinear Gain in SXC Semiconductor Lasers	
5.1 Introduction	75
5.2 Survey of Documented Results	77
5.3 Predicted Results Excluding Nonlinear Gain	83
5.4 Experimental Technique	89
5.5 Model of Symmetric Nonlinear Gain	104
5.6 Summary	115
Chapter 6. Conclusion	
6.1 Introduction	119
6.2 Recommended Additional Research	119
6.3 Summary	122

Appendix A. Variation of $R_m G_m$ Fitting Coefficients	125
Appendix B. Numerical Technique for Determining Longitudinal Mode Powers	131
References	135

List of Figures

	page
Fig. 2.1	Schematic diagram of a Fabry-Perot laser structure incorporating a single, isolated scattering centre. 10
Fig. 2.2	Experimental apparatus used to resolve the below-threshold emission spectra of semiconductor diode lasers. 13
Fig. 2.3	Spectrally-resolved below-threshold emission of a typical index-guided semiconductor diode laser. 15
Fig. 2.4	Six $R_m G_m$ products for laser A at three different below-threshold current levels. 16
Fig. 2.5	Residues for laser A, calculated from the measured below-threshold $R_m G_m$ products. 18
Fig. 2.6	Residue analysis applied to laser A which operates single-mode or with a modulated above-threshold mode profile (ATMP). 19
Fig. 2.7	Residue analysis applied to laser k which operates with a smooth ATMP. 21
Fig. 2.8	Root-mean-square residue and a number (Δ) which is characteristic of the shape of the ATMP for 32 different lasers. 23
Fig. 2.9	Reproducibility of rms residue measurements for four different index-guided lasers. 25
Fig. 2.10	Effect of correcting the rms residue for the amount of spontaneous emission in the laser. 28
Fig. 2.11	Measured and predicted above-threshold emission spectra for laser A. 31
Fig. 2.12	Measured and predicted above-threshold emission spectra for laser H. 32

	page
Fig. 3.1	Effect of fitting parameters on the shape of the below-threshold $R_m G_m$ profile. 37
Fig. 3.2	Below-threshold $R_m G_m$ profiles for generic gain-guided and index-guided devices. 44
Fig. 4.1	Degree of polarization (DOP) of the electroluminescence distributed along the active region length of a planar-buried-heterostructure laser (laser Z). 56
Fig. 4.2	Residue analysis applied to the laser which is characterized by the DOP plot indicated in Fig. 4.1. 57
Fig. 4.3	Correlation plot and best-fit line for the discrete scattering parameter (σ) and the rms residue (Γ) of sixteen different lasers. 60
Fig. 4.4	The effect of the phase shift ϕ on the calculation of a normalized rms residue (Γ/Γ_0). 65
Fig. 4.5	Bounds of the minimum and maximum normalized rms residue (Γ/Γ_0) due to variations in the phase shift (ϕ) for an isolated scatterer placed in the active region. 66
Fig. 4.6	DOP of the electroluminescence of a gain-guided laser (laser i) which indicates the presence of a scattering centre near the midpoint of the active region. 68
Fig. 4.7	Residue analysis applied to the laser which is characterized by the DOP plot indicated in Fig. 4.6. 69
Fig. 4.8	DOP of the electroluminescence of an index-guided device (laser V) which indicates the presence of a scattering centre near the midpoint of the active region. 70
Fig. 4.9	Residue analysis applied to the laser which is characterized by the DOP plot indicated in Fig. 4.8. 71

	page
Fig. 5.1	Predicted evolution of the optical power in the longitudinal modes for a solitary Fabry-Perot laser and for the same device incorporated into a short-external-cavity configuration. 85
Fig. 5.2	Predicted evolution of the optical power in the side modes of a short-external-cavity laser for a variety of effects. 87
Fig. 5.3	Schematic diagram of the experimental apparatus used to monitor the effects of nonlinear gain on the spectral output of SXC diode lasers. 90
Fig. 5.4	The evolution of the mode powers with increasing injection current for laser X. 93
Fig. 5.5	The evolution of the mode powers with increasing injection current for laser D. 95
Fig. 5.6	The mode evolution curves obtained by cycling through a number of free spectral ranges of the external cavity to excite the same resonant mode of laser D. 98
Fig. 5.7	The mode evolution curves obtained for three different resonant modes within the intrinsic $R_m G_m$ profile of laser H. 101
Fig. 5.8	The predicted effect of a symmetric nonlinear gain mechanism on the evolution of the mode powers for a short external cavity laser. 107
Fig. 5.9	The predicted effect of a spectral hole burning mechanism on the evolution of the mode powers for various values of the hole depth α_2 . 109
Fig. 5.10	The predicted effect of a spectral hole burning mechanism on the evolution of the mode powers for various values of the hole width α_3 . 110
Fig. 5.11	The predicted influence of the amount of optical feedback from the external mirror on the appearance of spectral hole burning effects. 112
Fig. 5.12	The predicted influence of a single, isolated scatterer in the centre of the active region on the appearance of spectral hole burning effects. 114

Handwritten text, possibly bleed-through from the reverse side of the page. The text is extremely faint and illegible. A vertical dotted line is visible near the center of the page.

List of Tables

	page
Table 3.1 Fitting Coefficients For Laser F	39
Table 3.2 Variation of Fitting Coefficients For Laser F	40
Table 3.3 Variation of Index-Guided Coefficients	42
Table 3.4 Variation of Gain-Guided Coefficients	42
Table 3.5 Longitudinal Mode Spacing Parameters	49
Table A.1 Index-Guided Devices	126
Table A.2 Gain-Guided Devices	129



Chapter 1. Introduction

An understanding of the physical mechanisms which affect the above-threshold spectral output of 1.3 μm InGaAsP semiconductor diode lasers is important since these devices are used in commercial applications, particularly in the areas of telecommunications and near-infrared spectroscopy. An increased knowledge of these physical mechanisms allows for accurate modelling of device behaviour and for the possibility of providing manufacturers with a diagnostic tool for assessment of production processes to increase device yield or for application-oriented device selection.

In optical-fibre based telecommunications systems the number and strength of the longitudinal lasing modes affects many system operation parameters. Chromatic dispersion in the optical fibre reduces the maximum transmission rate for systems using multi-longitudinal mode sources as compared to systems using single mode lasers. In addition, mode partition noise is a mechanism whereby the presence of multiple-longitudinal modes in the source laser results in a decrease in the signal-to-noise ratio at the optical receiver.[1, p.883] In spectroscopic applications, the ability to alter the wavelength of semiconductor lasers by changing a combination of the injection current and the active region temperature has been exploited to probe absorption transitions in diverse molecular systems.[2] It is clear that sources lasing in a single longitudinal mode are preferred since the presence of other modes leads to difficulty in discriminating

between transitions.

The obstacles encountered with multiple-longitudinal mode lasers have provided the impetus to manufacture devices which lase in a single longitudinal mode. Distributed-feedback lasers,[1, p.631] composite-cavity lasers,[3] and short-external-cavity lasers[4] have been manufactured to provide for single mode selection.

The most economical 1.3 μm semiconductor diode lasers which explicitly lack any intentional mode selection mechanisms differ primarily in the methods of light confinement in the active region. Gain-guided devices rely on a lateral variation of the gain in order to confine the laser mode whereas a lateral refractive index step confines the light in an index-guided device. Apart from obvious structural differences, gain- and index-guided devices differ in several important respects. The injection current required to achieve lasing threshold in gain-guided devices tends to be approximately 5-10 times greater than that for index-guided lasers. From the viewpoint of this work, the most important differences between the two devices are the characteristics of the above-threshold spectra. Gain-guided devices tend to lase in multiple-longitudinal modes with a smooth mode envelope whereas index-guided devices tend to lase predominantly in a single mode or in multiple modes with a highly modulated mode envelope.

A number of theories have been postulated to account for the observed differences in the above-threshold spectral output of gain- and index-guided lasers. One of the most reported and yet controversial postulates concerns the amount of spontaneous emission coupled into the longitudinal modes (the spontaneous emission factor) for each

of the device types. Accounting for the number of carriers in the inversion and the number of photons in the laser cavity, a rate equation analysis indicates that single-mode behaviour is obtained if it is assumed that a small number of spontaneous photons are coupled into the longitudinal modes, akin to a gas laser. A multi-moded spectrum can similarly be predicted if the coupling of spontaneous photons is assumed to be significantly larger. It has thus been postulated that the spontaneous emission factor for gain-guided devices is typically one to two orders of magnitude greater than that for index-guided devices. It has been reported that curved phase fronts in the modes of gain-guided devices can account for the increase in the spontaneous emission factor.[5] This postulate has been debated using both classical and quantum mechanical arguments.[6,7,8] Although an increase in the spontaneous emission factor can account for the observation that gain-guided devices tend to lase in multiple longitudinal modes and index-guided devices tend to lase more single-moded, the theory cannot account for the fact that some index-guided devices exhibit an above-threshold spectral output with a highly modulated mode envelope.

Inhomogeneous gain saturation resulting from nonlinear gain mechanisms has been proposed in an attempt to explain the modulation characteristics and the spectral output of semiconductor diode lasers. Several mechanisms have been advanced to account for nonlinear gain effects. Spectral hole burning[9] and population beating[10] have been postulated to account for the observation that index-guided devices lase more single-moded than predicted from the results of accepted values of the spontaneous

emission factor. Nonlinear gain due to induced gain and index gratings[11] and carrier heating[12] attempt to account for the modulation bandwidth of semiconductor diode lasers. The mathematical description of each of the nonlinear gain mechanisms is complicated, often involving the use of density matrices. Another drawback to the nonlinear gain theories is that phenomenological parameters are often used in the models to describe measurements performed on a small number of devices.

Polarization-resolved and spatially-resolved electroluminescence measurements have indicated that the material in the active region is non-uniform.[13] It was found that scattering centres exist along the active region of many 1.3 μm semiconductor diode lasers. A correlation was demonstrated between the number and strength of the scattering centres and the characteristics of the above-threshold spectral output. Those devices which showed small amounts of scattering along the active region were characterized by a multi-mode spectrum with a smooth mode envelope. Index-guided devices typically displayed large amounts of intracavity scattering and were characterized by single-mode operation or multi-mode operation with a strongly modulated mode envelope. A Fabry-Perot model incorporating a single, isolated Rayleigh scatterer predicted that the presence of the intracavity scattering centre should be manifested as modulations in the product $R_m G_m$ where R_m and G_m are the reflectance and the single pass gain of the m^{th} mode.[14] Characteristics of the modulations in the $R_m G_m$ product and the correlation of these modulations with the above-threshold spectral output of 1.3 μm semiconductor diode lasers form the major subject of the dissertation.

The dissertation is divided into 6 chapters. A residue which is characteristic of internal scattering is extracted from the below-threshold spectra by fitting a smooth function to the $R_m G_m$ profile. The correlation between the residue and the shape of the above-threshold mode envelope for 32 devices is discussed in Chapter 2. The residue is also used to predict the above-threshold spectral tuning characteristics of selected devices. For all of the devices studied in the experiment described in Chapter 2, the coefficients of the parameters of the function which was fit to the $R_m G_m$ profile are collected and analyzed in Chapter 3. In Chapter 4, data obtained from the polarization-resolved and spatially-resolved electroluminescence technique and the measurement of the characteristic residue are compared. An experiment using a short-external-cavity laser to monitor the effects of nonlinear gain on the evolution of the optical power in the longitudinal modes with increasing injection current is described in Chapter 5. Conclusions and recommendations for future research are discussed in Chapter 6.

The work presented in this dissertation has been summarized in four manuscripts which have been published in scientific journals,[15,16] accepted for publication,[17] or submitted for publication.[18]

Chapter 2. Calculation of Residues

2.1 Introduction

Semiconductor diode lasers (SDL's) display, depending on such parameters as the light confinement mechanism, laser operating temperature and the bias current, a wide range of longitudinal mode spectral signatures. For example, it has been observed that gain-guided lasers tend to operate on multiple longitudinal modes, that index-guided lasers tend to operate more single moded than do gain-guided devices, and that the spectral output of some devices evolves, when the operating temperature and bias current are varied, from single-mode operation to multi-mode operation with a strongly modulated mode envelope. A number of theories have been presented to explain the observed above- threshold spectra of SDL's; among these theories are enhanced spontaneous emission[5] and nonlinear gain.[9,10] These theories can explain the observation that index-guided lasers tend to more single-mode operation than do gain-guided devices; however, the theories cannot account for spectral features such as strongly modulated mode envelopes.

Scattering of light in the active region of a semiconductor diode laser affects the above-threshold spectral output through resonant enhancement of selected modes. This is the mechanism responsible for the single-mode characteristics of distributed-

feedback,[1 p.631] and composite-cavity lasers.[4] Peters and Cassidy[13] have shown a correlation between the scattering properties along the length of the active region of SDL's, as determined from the measurement and analysis of spatially-resolved and polarization-resolved electroluminescence, and the above-threshold spectra. They found that lasers which operated in a single mode or displayed a modulated mode envelope tended to scatter more light than lasers which operated with a smooth mode envelope. A Fabry-Perot model incorporating the strength and position of these scattering centres predicted that a modulation should occur in the product $R_m G_m$, where R_m and G_m are the reflectance and single-pass gain of the m^{th} mode.[14] By using pulses from a xenon laser, DeChiaro created damage-induced centres in the active region of SDL's which alter the above-threshold spectral output and which create a noticeable modulation in the mode profile.[19]

This chapter consists of a report on measurement of the modulation of the below-threshold $R_m G_m$ product of more than 30 commercially-available 1.3 μm InGaAsP semiconductor diode lasers and on the correlation of this modulation with the above-threshold mode profile (ATMP). It is found that lasers which tend to operate in a single mode or with a modulated mode envelope exhibit modulation features in the $R_m G_m$ product and that lasers which tend to have a smooth above-threshold mode profile do not exhibit such modulation features. It is also found that gain-guided lasers tend to have a smooth ATMP, whereas index-guided lasers tend to operate on a single mode or with a modulated ATMP. It is shown, by including the measured modulation features in an

appropriate model of SDL devices,[20] that the above-threshold spectral characteristics of the lasers can be predicted. The results obtained provide further evidence that scattering in the active region dominates other mechanisms which may influence the above-threshold spectral output of SDL's such as enhanced spontaneous emission[5] and nonlinear gain.[9,10]

This chapter is organized as follows: Section 2.2 provides a description of the technique to extract the modulations in the below-threshold $R_m G_m$ products; Section 2.3 reports on the correlation of these modulations with the above-threshold mode profile; Section 2.4 shows the results of using the modulation features to predict the above-threshold spectral tuning characteristics; and, Section 2.5 provides a summary.

2.2 Experimental Technique

Figure 2.1 is a schematic diagram of the active region of an SDL cavity with a single, isolated scattering centre located a distance L_1 from facet 1 and L_2 from facet 2. The effect on the spectral output of the scattering centre has been calculated.[14] If the scattering centre scatters a fraction σ^2 of the light back into the mode and transmits

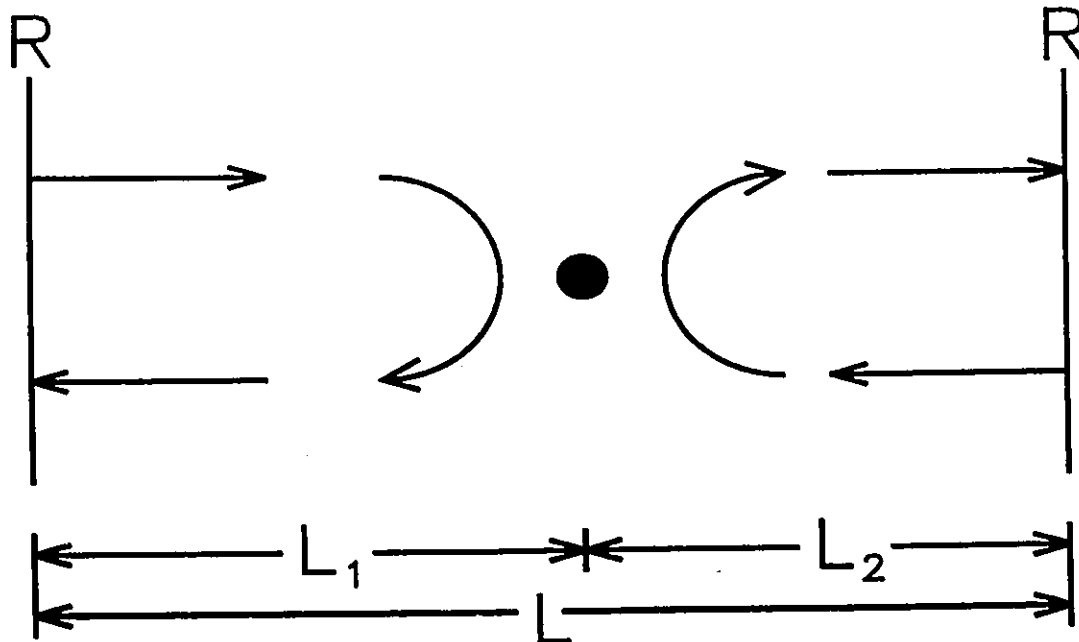


Figure 2.1

Schematic diagram of a Fabry-Perot laser structure (length L) incorporating a single, isolated scattering centre a distance L_1 from the left facet. The scattering centre is denoted by the solid dot. The arrows in the active region indicate the direction of propagation of the electric field.

a fraction τ^2 , then the intensity I_{1m} of the m^{th} mode just before it strikes facet 1 is:

$$I_{1m} = \frac{(|\delta_m|^2)(1+R_{2m}G_m)/[1-2\sqrt{RG_{1m}}\sigma \cos(2k_m L_1)+RG_{1m}^2\sigma^2]}{1-R_{1m}R_{2m}G_m^2} \quad (2-1)$$

where R is the reflectance of the facets, $(|\delta_m|^2)$ is the amount of spontaneous emission which couples into mode m , k_m is the propagation constant of mode m , $G_m=G_{1m}G_{2m}$ is the single pass-gain of the m^{th} mode over the full cavity of length L , G_{1m} is the single-pass

gain for the m^{th} mode over the distance L_i between facet i and the scattering centre, and,

$$R_{im} = \frac{R\tau^2}{1 - 2\sqrt{RG_{im}}\sigma\cos(2k_m L_i) + RG_{im}^2\sigma^2}, \quad i=1,2 \quad (2-2)$$

is the effective reflectance of facet i for the m^{th} mode. For small σ (σ measured [14] to be $\leq 10^{-2}$),

$$R_{im} \approx R\tau^2[1 + 2\sqrt{RG_{im}}\sigma\cos(2k_m L_i)] \quad (2-3)$$

and the reflectances of the facets appear to vary sinusoidally about the mean or unperturbed value R . For a mode of the full cavity, the resonance condition is $\cos[2k_m L] = 1$, and since $L = L_1 + L_2$, $\cos[2k_m L_1] = \cos[2k_m(L - L_2)] = \cos[2k_m L_2]$. Thus R_{1m} and R_{2m} vary with the same period when sampled at the resonant frequencies of the full cavity.

The $R_m G_m$ product, or $\sqrt{R_{1m} R_{2m}} G_m$ product for an asymmetric laser, can be measured experimentally. The mode sum/minimum technique [21] was used to measure the product. Since scattering should cause the $R_m G_m$ product to vary with mode number, a smooth function of the form,

$$[RG]_m^{\text{fit}} = R \exp\left(\frac{a_1}{a_5 s_m^4 + a_4 s_m^3 + a_3 s_m^2 + a_2 s_m + 1}\right) \quad (2-4)$$

was fit to the data, where s_m is the mode spacing normalized to the mode spacing near mode zero and mode zero is defined as the strongest mode near threshold. The form for

the fitting function was chosen to be consistent with a previous analytic model,[20] and the order of the polynomial in s_m was chosen to yield a good fit. A representative set of values for the fitting parameters is $a_1=1.04$, $a_2=1.33 \times 10^{-3}$, $a_3=1.55 \times 10^{-3}$, $a_4=3.36 \times 10^{-4}$, and $a_5=3.47 \times 10^{-6}$. Subsequently, a normalized residue can be formed:

$$RESIDUE = \frac{\sqrt{R_{1m}R_{2m}}G_m - [RG]_m^{fit}}{[RG]_m^{fit}} \quad (2-5)$$

Substituting for R_{1m} and R_{2m} from Eq. (2-2) and assuming a device with a weak, single scattering centre, one obtains

$$RESIDUE = \sigma \sqrt{R} \cos(2k_m L_1)(G_{1m} + G_{2m}) \quad (2-6)$$

since $\tau^2 R G_m = [RG]_m^{fit}$. RESIDUE is a measure of the amount of scattering in the device. If there is little or no scattering, then RESIDUE should be small or equal zero. If there is strong scattering, then RESIDUE should be large.

The $R_m G_m$ product was measured by using below-threshold emission spectra for pumping levels which gave peak $R_m G_m$ values in the range 0.7 to 0.95, since it was found that the $R_m G_m$ product could be measured reproducibly under these conditions. The below-threshold emission spectra of the devices were acquired with the experimental configuration depicted in Fig. 2.2. The light from the front facet of the laser diode (LD) was collected and collimated using a multielement, antireflection-coated optic (L1). A neutral-density filter (ND, optical density = 0.9) which was placed in front of the collimating optic, provided partial immunity from optical feedback. A polarizing beam

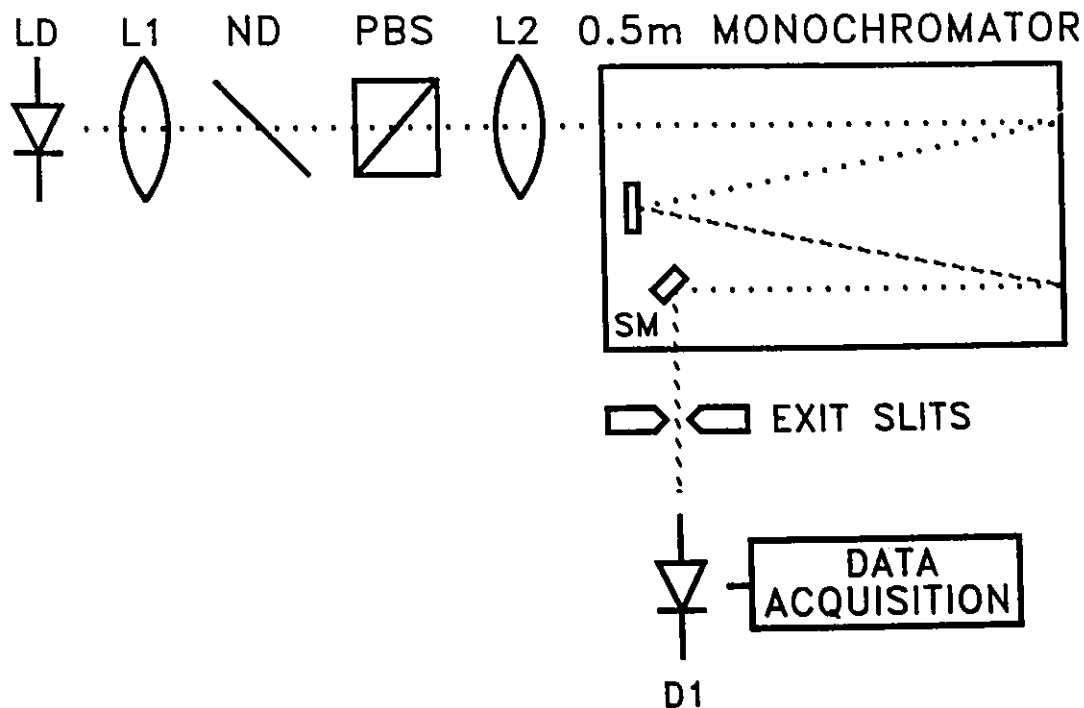


Figure 2.2

Block diagram depicting the experimental apparatus used to resolve the below-threshold emission spectra of semiconductor diode lasers. The dotted line indicates the path of the laser beam.

splitter (PBS) was placed in the beam path to isolate the predominant TE portion of the light from the laser. The light was then focused into a Jarrell-Ash 0.5-m monochromator using an $f/6$ lens (L2). The emission spectra were resolved by using a ruled grating blazed for a wavelength of $1.0\ \mu\text{m}$ in conjunction with a $50\text{-}\mu\text{m}$ -wide exit slit. A small-area ($\sim 1.0\ \text{mm}$ diameter), low-noise InGaAs detector (D1) and conventional lock-in amplifier techniques (time constant $\sim 100\ \text{ms}$) enhanced the detection sensitivity. The monochromator was equipped with a General Scanning mirror assembly (SM) with

position feedback placed near the exit slit of the instrument. The angular position of the scanning mirror was computer-controlled, which facilitated the acquisition of a large number of data points (4096) for each below-threshold spectrum. The gain control of the scanning mirror electronics was adjusted so that approximately 100 data points were collected for each longitudinal mode. The laser temperature was stabilized by electronic feedback techniques.

To calculate the $R_m G_m$ product from the laser emission spectra, both the mode sum and the mode minima must be determined,[21] and this requires parsing the acquired emission spectrum into individual modes. Parsing the spectrum was facilitated by calculating the first derivative of the acquired data using a central difference approximation with a spacing of ten points. A zero crossing of the derivative record corresponded to the position of a peak in the longitudinal mode spectrum. An example of a typical longitudinal mode spectrum and the corresponding derivative record are shown in Fig. 2.3. The positions of the mode minima were determined as one half of the distance between the peak of the mode of interest and the adjacent mode peaks. The points constituting the mode were then subjected to a sliding 5-point average. The value of the mode minimum was defined as the mean of the short-wavelength minimum and the long-wavelength minimum (referenced to the mode peak) of the averaged mode record. Note that the effect of the averaging operation and the monochromator response function on the experimentally determined $R_m G_m$ product was reduced by deconvolution.[21] The response function of the monochromator was estimated from the

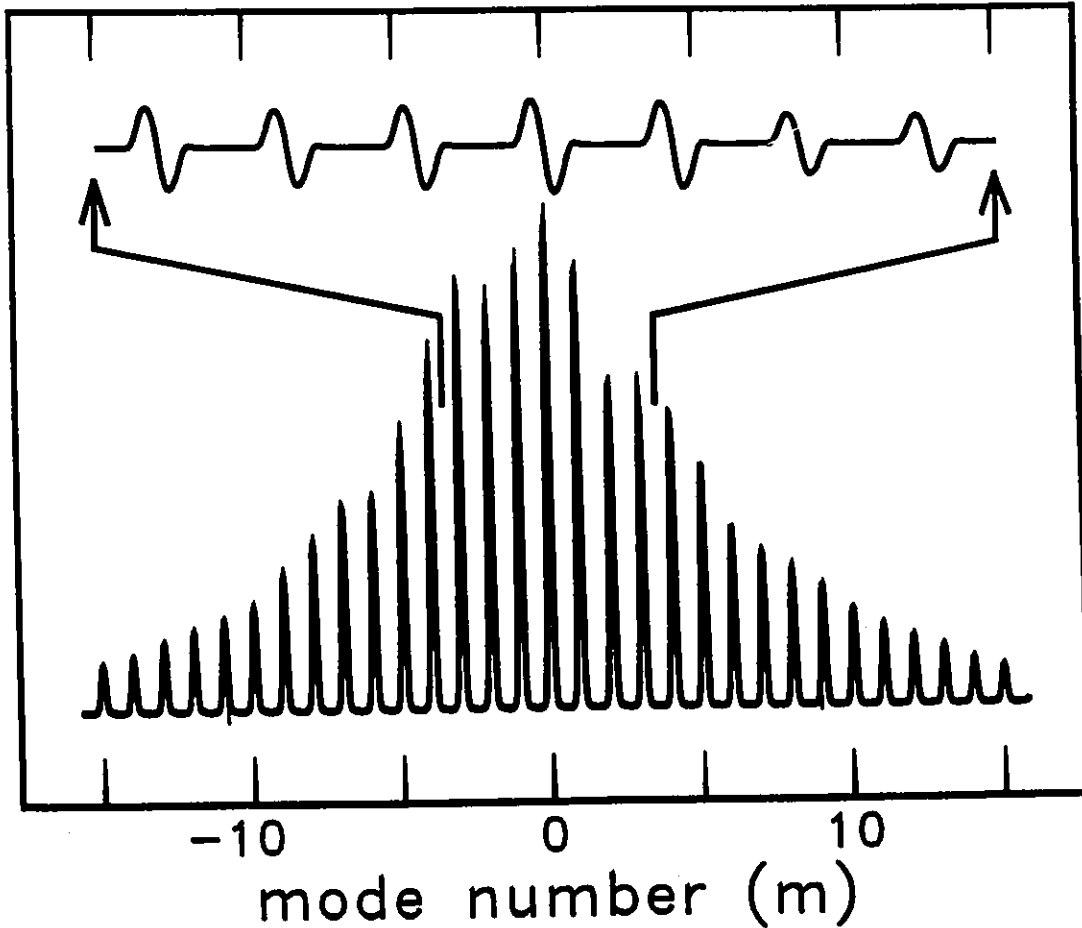


Figure 2.3

Spectrally-resolved below threshold emission of a typical index-guided semiconductor diode laser. The top trace represents an expanded first derivative record calculated across 7 modes. The record was used to facilitate parsing the spectrum into individual modes.

above-threshold spectra.

The results of the analysis of experimental data for an SDL operating with a modulated ATMP are shown in Fig. 2.4. The figure shows six $R_m G_m$ products calculated

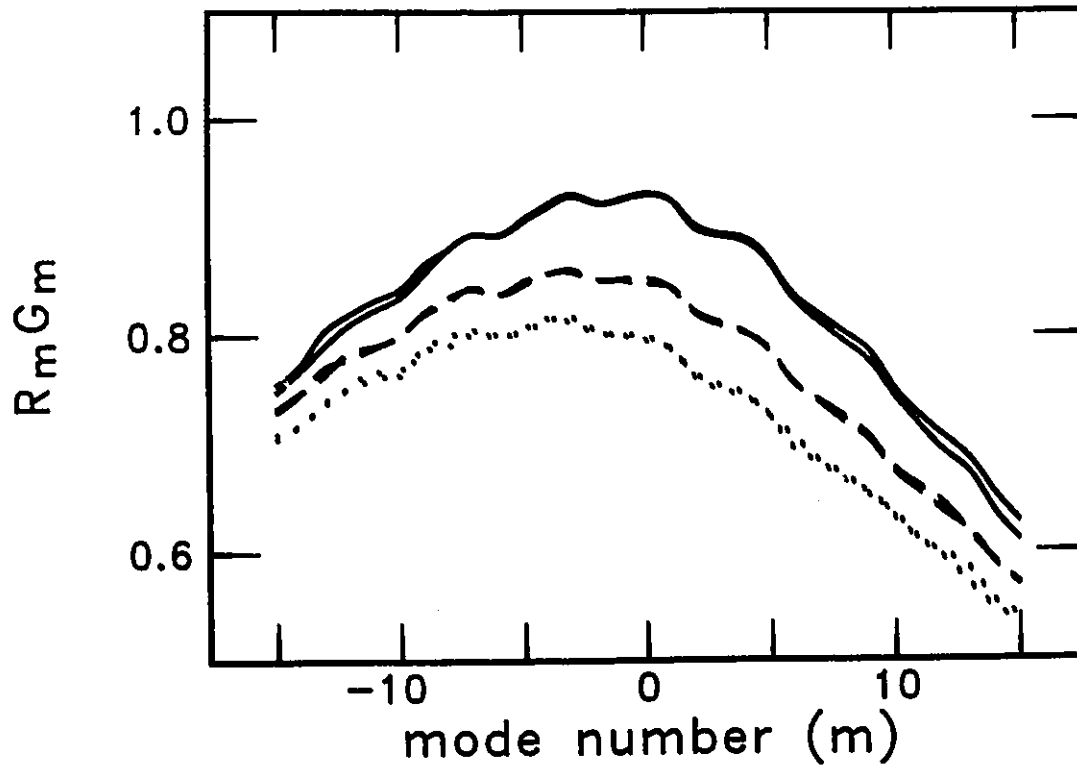


Figure 2.4

Six $R_m G_m$ products for laser A at three different below-threshold current levels; I_{th} -0.5 mA (solid curves), I_{th} -1.0 mA (dashed curves) and I_{th} -1.5 mA (dotted curves). The $R_m G_m$ values were determined from the emission spectra for 15 modes on either side of the $R_m G_m$ peak. Small modulations are evident in all the profiles.

by using the mode-sum/minimum method.[21] The emission spectra corresponding to these profiles were acquired at three different laser bias currents (I_{th} -0.5 mA, I_{th} -1.0 mA and I_{th} -1.5 mA), which corresponded to peak $R_m G_m$ values of 0.92, 0.85 and 0.81, respectively. (For gain-guided lasers, the three bias currents were I_{th} -3.0 mA, I_{th} -6.0 mA and I_{th} -9.0 mA. These bias currents resulted in peak $R_m G_m$ values similar to those

obtained for the lower-threshold index-guided devices.) Repetition of the acquisition procedure at the same current levels results in a set of six $R_m G_m$ products. A modulated gain profile is evident in all cases. Notice that the position of the modulation features (in mode space) remains fixed as the current level is varied. This observation is consistent with a wavelength-dependent effective reflectance resulting from scattering centres in the active region of the device.

The residues for the $R_m G_m$ products shown in Fig. 2.4 are shown in Fig. 2.5. They indicate a near-sinusoidal wavelength dependence of the facet effective reflectance. The position and the magnitude of the modulation features are consistent for each of the six residues, especially those nearest mode zero. The consistency of the residues at different current levels is important, since it removes the restriction of comparing devices at exactly the same $R_m G_m$ values.

The $R_m G_m$ product and residue corresponding to the highest current level for the device discussed above are reproduced in Fig. 2.6. The rms value of the residue, Γ , is a measure of the magnitude of the deviation of the amplitude of the modulation feature about the best-fit $R_m G_m$ value and is thus a measure of the size of the modulation features in the residue record. If there is little or no scattering, then the modulation features are small and Γ is expected to have a small value, whereas a large amount of scattering produces a large value of Γ . The value of Γ was calculated over the 11 modes centred about mode zero and is indicated in the bottom of the figure. The significance of the above-threshold spectra at the right of Fig. 2.6 is discussed below.

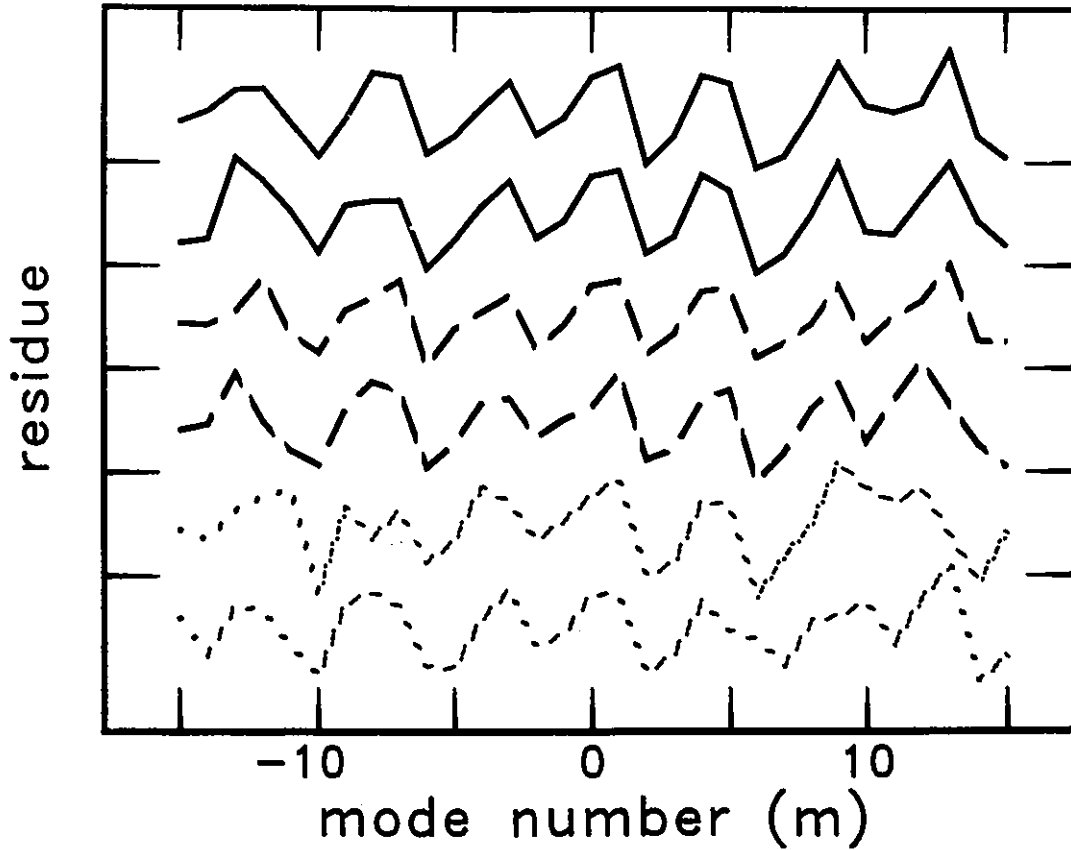


Figure 2.5

Residues for laser A, calculated from the $R_m G_m$ products depicted in Fig. 1 at the three current levels: I_{th} -0.5 mA (solid curves), I_{th} -1.0 mA (dashed curves) and I_{th} -1.5 mA (dotted curves). The spacing between ordinate tic marks is 0.02. The bottom residue represents a non-offset plot, and each subsequent residue has been subjected to a sequential offset of 0.02 for clarity of presentation. Sinusoidal modulation features with a period of approximately four modes are evident.

Depending on the active region temperature and the bias current, the longitudinal-mode spectrum of a SDL can range from a single mode, to regions which exhibit large modulations of the spectral envelope. A number characterizing the structure

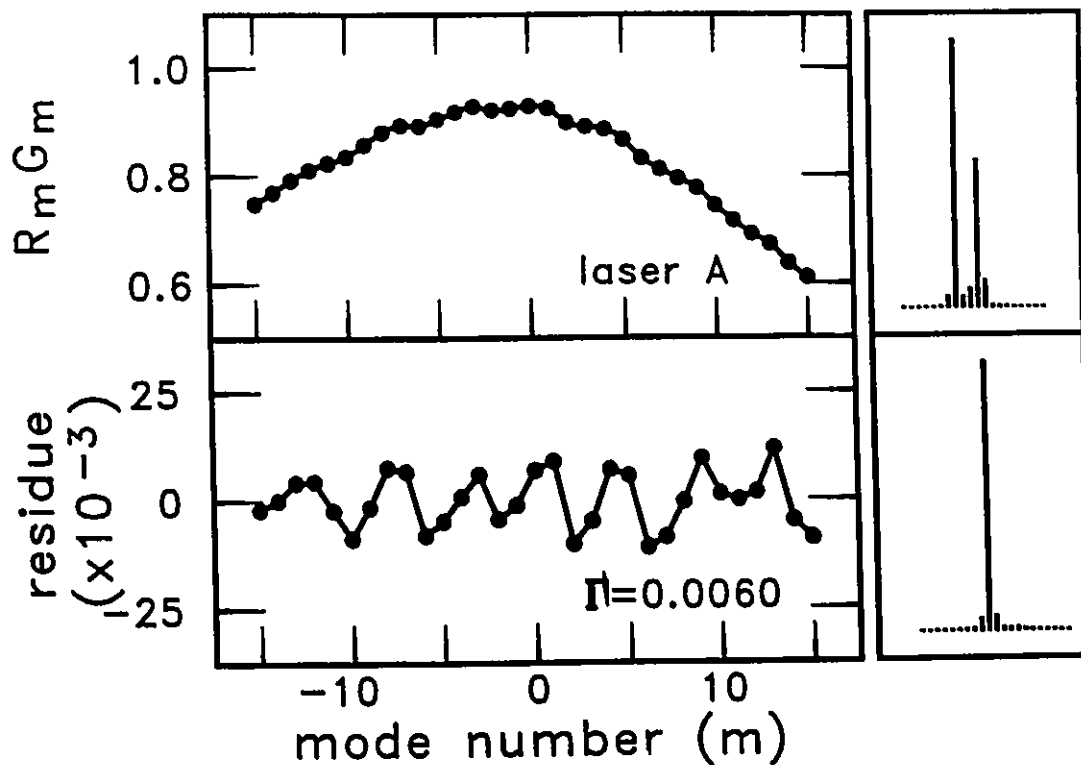


Figure 2.6

Residue analysis applied to laser A which operates single-mode or with a modulated ATMP. The $R_m G_m$ product indicates the presence of significant modulation features. The normalized residue is shown in the bottom of the figure. The spectra resulting in the minimum $[\log(\zeta_{\min}) = -3.615]$ and maximum $[\log(\zeta_{\max}) = -1.738]$ second moments indicate that the laser can operate with a single-mode region or with a strongly modulated envelope region, depending on the laser temperature and bias current.

of different mode envelopes can be calculated on the basis of the second moment of the above threshold spectra about mode zero (the strongest mode). This characteristic

number, ζ , is defined by

$$\zeta = \frac{\sum s_m^2 I_m}{\sum I_m} . \quad (2-8)$$

Note that the second moment is normalized to the power in all the modes. A laser which tends to run in a single mode would have a small second moment, whereas a laser with a modulated mode envelope would have a large second moment. Multiple-longitudinal-mode operation (typical of gain-guided devices) would be characterized by a second moment lying somewhere between these two values.

The spectral output of each laser was recorded for bias currents ranging from threshold to twice threshold current and temperatures ranging from 25 to 35 °C. The electronic gain control on the scanning mirror was adjusted such that approximately 30 modes were recorded. The spectra resulting in the minimum and maximum second moment obtained over the search range for laser A, an index-guided laser, are displayed on the right of Fig. 2.6.

In comparison, Fig. 2.7 represents the results of a similar analysis applied to a laser with a smooth gain profile. The $R_m G_m$ product in the top of the figure indicates no significant modulation features, and the corresponding rms residue is approximately one third that of laser A (c.f. Fig. 2.6). The spectra resulting in the minimum and maximum second moments for this laser (laser k, a gain-guided laser) are presented at the right of the figure. Within the bias current and temperature bounds of the search region,

the laser exhibits only multiple-longitudinal-mode emission with a smooth mode envelope.

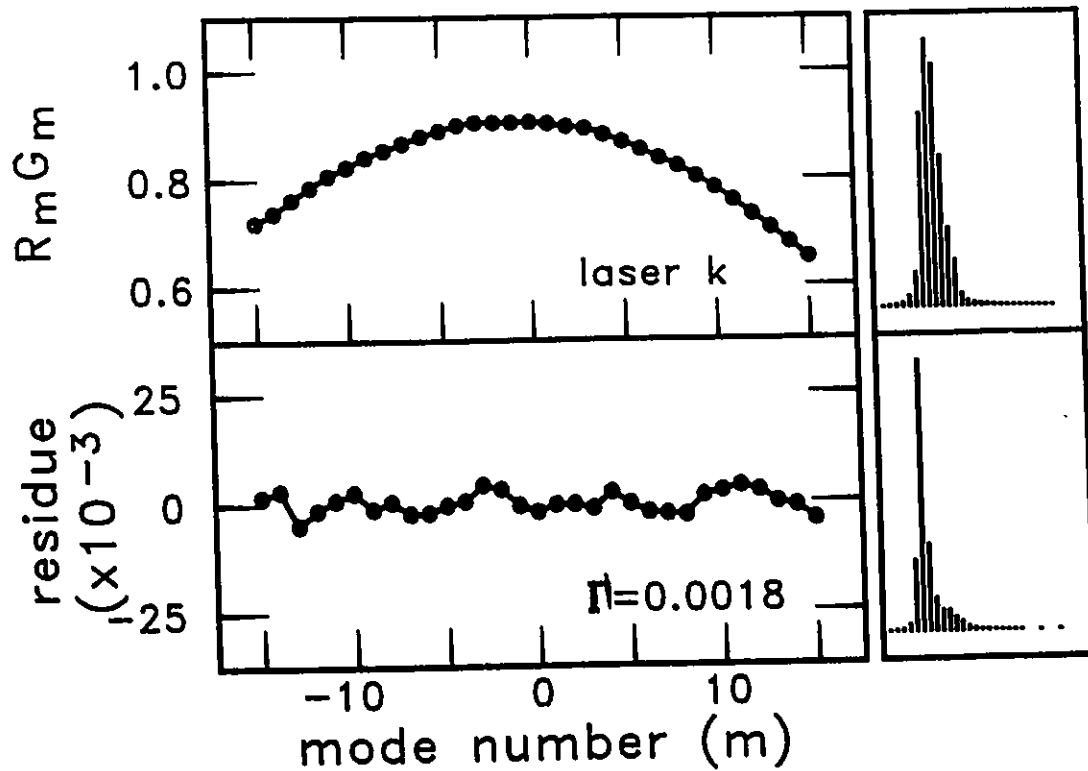


Figure 2.7

Residue analysis applied to laser k which operates with a smooth ATMP. The $R_m G_m$ product as a function of mode number is shown in the top of the figure. The normalized residue is notably smaller than that for laser A. The spectra resulting in the minimum [$\log(\zeta_{\min}) = -2.218$] and maximum [$\log(\zeta_{\max}) = -2.696$] second moments displayed to the right indicate that the laser operates with a smooth mode envelope.

2.3 Correlation of Results

The measurement and analysis technique has been applied to 32 different 1.3 μm lasers (21 index-guided[22,23] and 11 gain-guided[24,25 p.178] from five manufacturers. Note that all the lasers which were tested are reported - no screening of data was implemented. (The **only** laser which was subjected to different numerical processing was laser S, an index-guided device. An eight term least-squares fit was required to calculate the residue, in order to accommodate a slow variation in the $R_m G_m$ product.) Figure 2.8 shows a compilation of the results obtained for the lasers which were tested. The rms residue, Γ , is plotted along the ordinate. Plotted along the abscissa is Δ which is defined as:

$$\Delta = \log \zeta_{\max} - \log \zeta_{\min} \quad (2-9)$$

where ζ_{\max} is the maximum second moment of the ATMP and ζ_{\min} is the minimum second moment of the ATMP as obtained from the search of the above threshold spectra. Δ is a measure of the shape of the ATMP. The use of the difference as a characteristic parameter ensures that a laser with both strongly modulated mode envelope and single-mode operating regions is assigned a larger value than a laser which exhibits only one of these attributes.

The position of the laser identification letter in Fig. 2.8 represents the mean value of the rms residues for the six below-threshold current levels. The amplitude of the

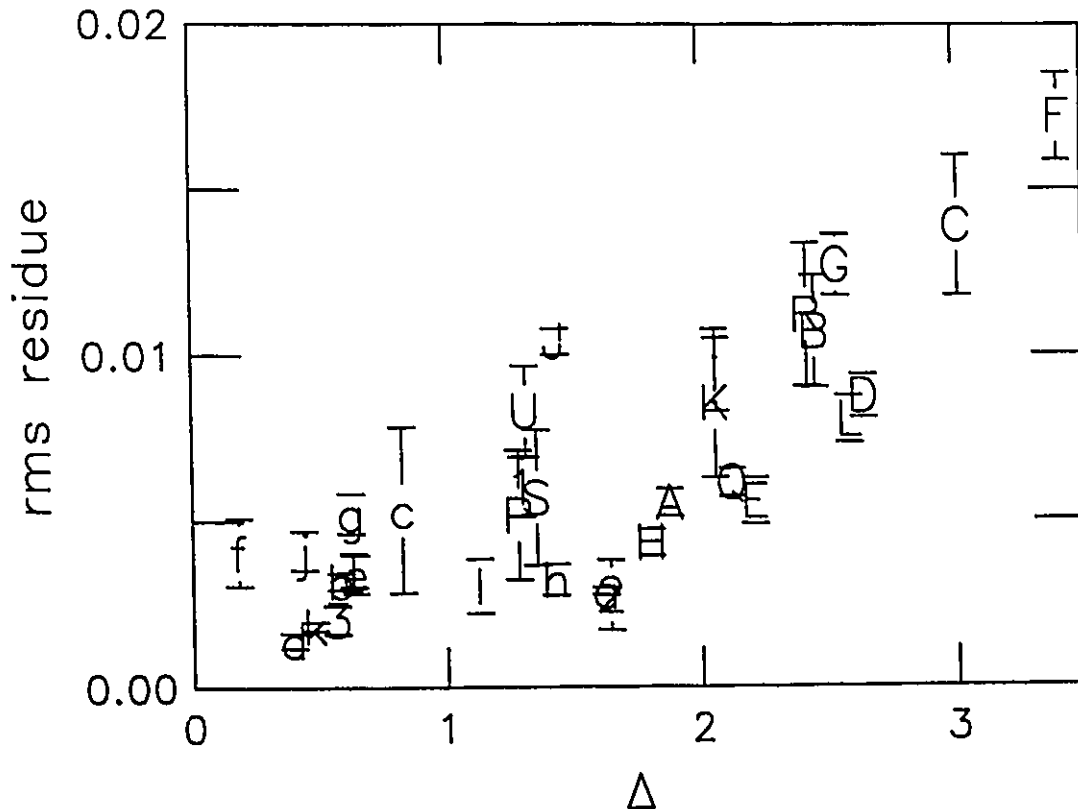


Figure 2.8

Root-mean-square residue and a number (Δ) which is characteristic of the shape of the ATMP for 32 different lasers. The ordinate of the laser identification label represents the mean of six rms residue calculations. The amplitude of the error bars represents one standard deviation from the mean. Gain-guided lasers are represented by lowercase letters. Index-guided lasers are represented by uppercase letters except for arrowhead-buried-crescent devices, which are represented by numbers.

error bars represents one standard deviation of the six calculated rms residues and is indicative of: (i) any variation of the amplitude of the modulation features as a function of current level and (ii) reproducibility of the measurements. The magnitude of the error

bars is determined to a large extent by the dependence of the residue on current. For a single scattering centre, the residue depends on G_{1m} and G_{2m} [c.f. Eq.(2-5)], which depend on the pumping level. Neither G_{1m} nor G_{2m} are known. To take this pumping level dependence into account, the residues for different lasers were obtained over a similar range of $R_m G_m$ values. Points which lie outside the error bars are considered distinct and meaningful.

Reproducibility of the calculated rms residue values was confirmed by repeating measurements of four index-guided devices. The below-threshold emission spectra for the repeated series of measurements were acquired approximately 1 month after the original measurements. During this time other devices were characterized, and many optical alignment adjustments were required. The results of the reproducibility measurements are summarized in Fig. 2.9. In all cases the mean rms residues of the repeated results are well within one standard deviation of the original results. The large extent of overlap of the error bars is an excellent indicator that the modulations in the $R_m G_m$ product are from an intrinsic device property and not manifestations of optical feedback or wavelength-dependent transmission of the optical system. (Other monochromators were also used in the experimental technique, yielding similar results).

The results depicted in Fig. 2.8 indicate that there is a correlation between the structure of the above-threshold spectra and the rms residue calculated by using the below threshold spectra. Gain-guided SDL's are identified on the graph with lowercase letters. These lasers tend to lase in multiple longitudinal modes with a smooth mode envelope

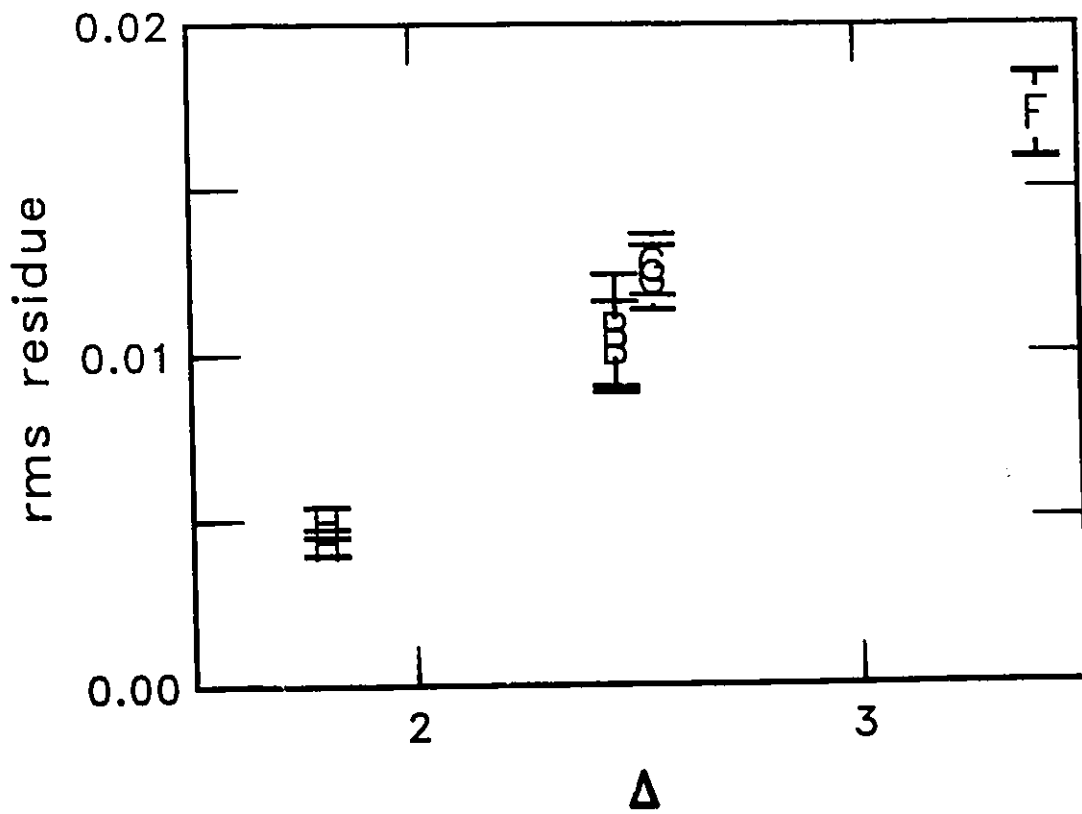


Figure 2.9

Plot similar to Fig. 2.8 with an expanded abscissa showing reproducibility analysis for four different index-guided lasers. Measurements of the residues were repeated after a span of approximately one month. The extent of overlap of the error bars confirms a high degree of reproducibility.

and are found predominantly in the lower left-hand portion of the graph. Conversely, large rms residue values are obtained for devices which lase in a single mode or which exhibit a modulated mode envelope. Index-guided devices are indicated in the figure by uppercase letters, except for arrowhead-buried-crescent devices which are indicated by numbers. Note that data for laser A are shown in Fig. 2.6 and those for laser k are shown

in Fig. 2.7.

The linear-correlation coefficient, r , is a statistic which is often used to determine the extent to which two variables can be considered correlated. Calculation of the statistic for the variables Γ and Δ which are plotted in Fig. 2.8 yields a value of $|r|=0.81$. The probability that a random set of data points would have an experimental linear-correlation coefficient equal to $|r|$ has a known probability density function.[26,p.310] Estimating the integral of this probability density function, the calculated value of the probability for $|r|=0.81$ for 32 ordered pairs is approximately 2×10^{-8} . Physically, this low value of the probability means that for one billion experiments involving uncorrelated variables ($|r|=0$), one would expect 32 points to have a linear-correlation coefficient as large as $|r|=0.81$ only 20 times. Based on the value of the linear-correlation coefficient, it can be confidently stated that the rms residue Γ and the shape of the ATMP (characterized by Δ) are highly correlated.

The amount of spontaneous emission is an important factor in determining the extent to which scattering centres affect the above-threshold spectral output of SDL's.[27] It was found that lasers with large amounts of spontaneous emission are less affected by internal scattering than are devices with small amounts of spontaneous emission. Spontaneous emission masks the effect of scattering centres on the spectral output of diode lasers.[27] Experiments also indicate that the amount of spontaneous emission produced is correlated with the laser threshold current, and thus measurements which are to be correlated with the effects of scattering centres may be normalized with respect to

the threshold current.[27]

The residue calculated in this work is essentially a measure of the effective facet reflectance from internal scattering. Any perturbations in the effective reflectance are a direct result of the effect of scattering centres in the laser. Thus, to determine the influence of the scattering centre on the ATMP, one must take into account the effects of spontaneous emission. Figure 2.10 shows the result of applying the threshold current normalization to the lasers tested in the experiment. Since gain-guided lasers tend to have a larger threshold current than do index-guided devices, the effect of correcting for the amount of spontaneous emission is that gain-guided devices tend to reside nearer the Δ axis.

The linear-correlation coefficient obtained after correcting for the amount of spontaneous emission was calculated to be $|r|=0.72$. The corresponding probability that this value of $|r|$ would be obtained from an uncorrelated parent population was calculated to be approximately 3×10^{-6} . Although the linear-correlation coefficient was higher when the rms residue was not corrected for the amount of spontaneous emission ($|r|=0.81$), it can be shown that there is no significant difference between the two correlation coefficients.[28 p.204] (The 99% confidence interval for $|r|=0.81$ was calculated to be from $|r|=0.56$ to $|r|=0.92$.)

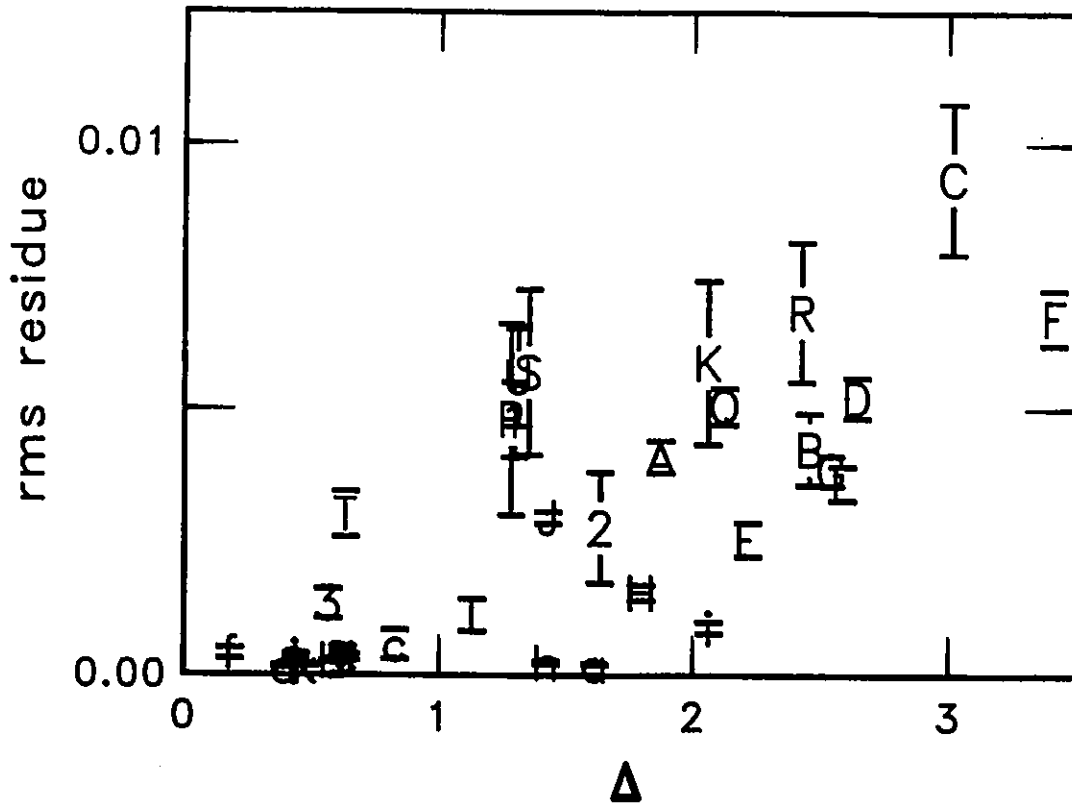


Figure 2.10

Effect of correcting the rms residues of Fig. 2.8 for the amount of spontaneous emission in the laser. As a result of applying the correction, gain-guided lasers (represented by lowercase letters), which have a higher threshold current than index-guided devices (represented by uppercase letters and numbers) tend to reside nearer the Δ axis.

2.4 Modelling of Above Threshold Spectra

The position, in mode space, of the $R_m G_m$ modulation features was found to be independent of laser bias current (c.f. Fig. 2.5). This observation is consistent with

wavelength-dependent variations in the facet reflectance resulting from scattering centres in the active region of the laser. If scattering is the dominant mechanism determining the above-threshold spectral output of SDL's, then the modulation features (residue) measured by using the below-threshold emission spectra of a device should provide sufficient information to predict the above-threshold mode profile. The purpose of this section is to compare the predicted above-threshold spectrum of a SDL with the measured spectrum.

The model used to predict the above-threshold spectra was based on a model of an homogeneously broadened SDL.[14,20] The facet reflectance was determined by adding the calculated residue (such as that shown in Fig. 2.5) to a wavelength-independent facet reflectance of 0.32. The constant component of the reflectance was calculated by using the refractive index difference at the laser facet. The fraction of spontaneous emission coupled into each mode (spontaneous emission factor, β) were set equal to one another for all devices.[27] The width of the gain spectrum was obtained from the least-squares fit to the $R_m G_m$ product [cf. Eq. (2-4)]. The gain peak was allowed to tune linearly with the pump (equivalent to laser bias current) term.

The pump term was increased from a value of 0 until the peak $R_m G_m$ values obtained from the model and from the experimental data were equivalent. The sum of the modelled mode intensities was calculated and compared with the total optical power in the modes of the emission spectra, and this provided an optical power calibration for the model. The gain peak tuning rate was fixed by matching a measured ATMP and the below-threshold mode profile with the model output at equivalent output power levels.

After the tuning rate was fixed, additional modelled spectra were generated on the basis of the equivalent optical powers of measured spectra.

Figure 2.11 shows the measured and predicted above threshold mode profiles of an index-guided SDL (laser A in Fig. 2.8) for a range of bias currents. The modeled spectra at the right in Fig. 2.11 were generated by fixing the pumping rate at a value based on the optical power of the corresponding measured spectra at the left in the figure. The variable γ adjacent to each measured spectrum in Fig. 2.11 indicates the ratio of the optical powers in the measured above-threshold spectra to the below-threshold emission spectra used to calculate the residue. The model predicts the profile of the above-threshold spectra and the evolution of the modes as a function of bias current.

The measured and predicted above-threshold mode profiles for an additional index-guided device (laser H in Fig. 2.8) are shown in Fig. 2.12. The threshold current of this laser was approximately twice as large as that of the device whose spectra are depicted in Fig. 2.11, and the amount of spontaneous emission in the model was accordingly larger. The results depicted in Fig. 2.12 indicate a similar measured and predicted spectra, with the exception of the spectrum at the highest bias current. It should be noted that this modelling procedure was applied to four other lasers, and similar results were obtained.

The results depicted in Fig. 2.11 indicate that the model accurately predicts the measured above-threshold spectra even for power ratios, γ , in excess of 50. The fact that the residue retains its physical significance at such large power ratios is an excellent

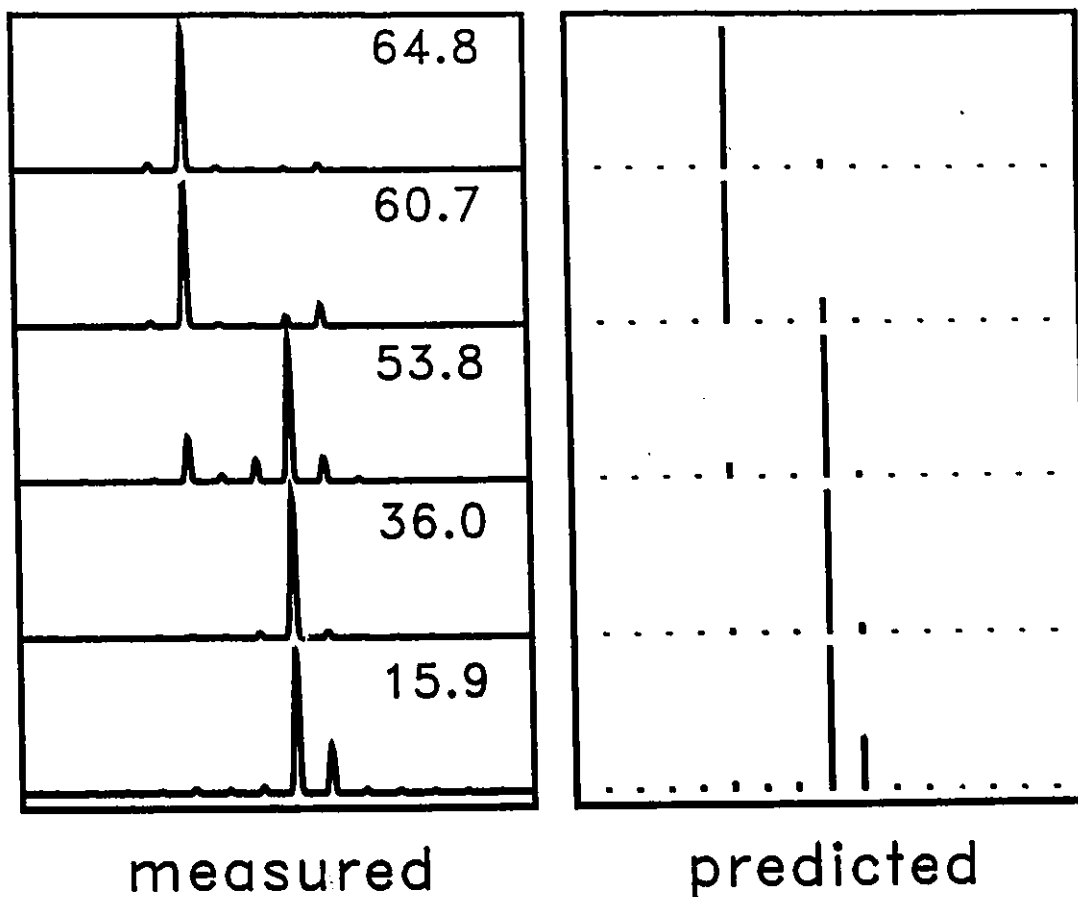


Figure 2.11

Measured and predicted above-threshold emission spectra for laser A. Adjacent measured and predicted spectra correspond to equivalent optical power levels. The power ratio, γ , which is the ratio of the optical powers in the measured above-threshold spectra and the below-threshold emission spectra used to calculate the residue, is indicated at the right of the measured spectra.

indicator that scattering is a dominant mechanism in determining the above-threshold mode profile. If this were not the case, one could expect that non-linear effects such as spectral hole burning[9] would begin to affect the above-threshold mode profile.

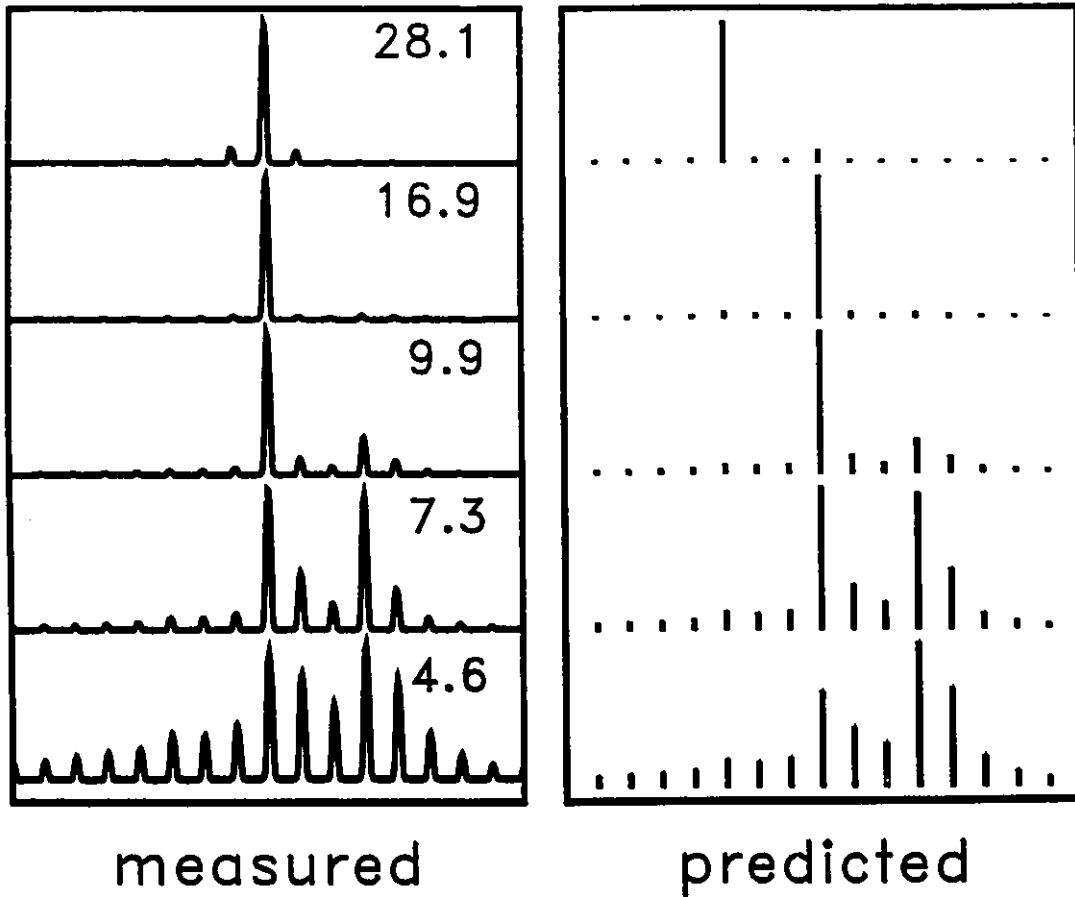


Figure 2.12

Measured and predicted above-threshold emission spectra for laser H. Adjacent measured and predicted spectra correspond to equivalent optical power levels. The power ratio, γ , is indicated to the right of the measured spectra.

2.5 Summary

Predicted modulations in the $R_m G_m$ product of semiconductor diode lasers were confirmed through the measurement of the $R_m G_m$ product for more than 30 commercially available devices. The $R_m G_m$ product was measured by using the below-threshold emission spectra, and a characteristic residue, which represents the facet effective reflectance, was extracted for each laser. Excellent reproducibility of the residues was confirmed by repeating measurements for a number of devices.

Assigning an rms residue to each laser involved in the study indicated a strong correlation between the amplitude of the modulation features and the deviation of the above-threshold mode profile from a smooth mode envelope. In general, lasers which operated single-mode or on multiple modes with a strongly modulated mode envelope had larger characteristic rms residues than did lasers which operated with a smooth mode profile. This supports the hypothesis that the longitudinal mode spectrum is governed to a large extent by the strength and position of scattering centres in the active region of the laser.

Nonlinear phenomena, such as spectral hole burning,[9] have been postulated to account for the above-threshold spectral output of SDL's. If nonlinear mechanisms determine the above-threshold spectra, then the influence of nonlinear effects below threshold should be weak, since nonlinear effects vary with the square of the optical power. The results indicate that scattering is the dominant mechanism, since the above-

threshold spectra can be predicted by using measurements accumulated below threshold. Using the modulation features in the $R_m G_m$ product as an effective facet reflectance, it was found that the features of the measured above-threshold spectra could be modelled for a large range of output power levels if the gain peak was allowed to tune across the residue record.

The results of the experiment indicate that the effect of internal scattering on the above-threshold spectral output may dominate over any effects caused by nonlinear gain,[9,10] or enhanced spontaneous emission.[5] Therefore the effect of scattering in the active region must be accounted for in any realistic modelling of the spectral output of 1.3 μm semiconductor diode lasers.

Chapter 3. Shape of $R_m G_m$ Profiles

3.1 Introduction

In Chapter 2, a method of extracting a residue from the below-threshold $R_m G_m$ profiles of semiconductor lasers was discussed. It was found that the magnitude of modulations in the profile, as characterized by the rms residue, was correlated with the shape of the above-threshold mode envelope. A smooth function was fit to the profile in order to extract the characteristic residue. If the residue is a physically significant quantity, then it would be expected that the smooth function used to extract the residue would also be physically significant.

The purpose of this chapter is to record information pertaining to each of the five coefficients used to construct the functional form of the smooth $R_m G_m$ profile. The rate of change of each of the coefficients with the measured peak of the $R_m G_m$ profile, $(RG)_{\max}$, was calculated for all of the devices studied for the residue experiment discussed in Chapter 2. It is anticipated that the information provided in this chapter will serve as a useful reference for future modelling of the spectral behaviour of devices. The importance of each of the five coefficients to the overall shape of the $R_m G_m$ profile is discussed in Section 3.2. The variation of the coefficients with the measured values of $(RG)_{\max}$ is presented in Section 3.3. The physical significance of the calculated variations

is also discussed in this section. The wavelength dependence of the longitudinal mode spacing is discussed in Section 3.4 and Section 3.5 contains a summary of the results.

3.2 The Fitting Coefficients

The smooth function, which was fit to the measured below-threshold $R_m G_m$ profile using a least-squares algorithm is:

$$[RG]_m^{fit} = R \exp \left(\frac{a_1}{a_5 s_m^4 + a_4 s_m^3 + a_3 s_m^2 + a_2 s_m + 1} \right) \quad (3-1)$$

where R is the facet reflectance, s_m is the mode spacing normalized to the mode spacing near mode zero and mode zero is defined as the strongest mode near threshold. The fitting function was written in a form: (i) which is consistent with a previous analytic model; [20] (ii) so that physical significance can be ascribed to the coefficients; and, (iii) to yield a good fit. The residue was subsequently obtained by subtracting the smooth function from the measured profile and normalizing the result.

It has been suggested that the polynomial in s_m should take the form of a Lorentzian, $a_1(1+a_3 s_m^2)^{-1}$, with $a_3=1/2000$ and $a_2=a_4=a_5=0$. [29,30] In this context, it is apparent that the coefficient a_3 determines the width of the $R_m G_m$ profile. Although it is expected that a_3 should be the dominant coefficient, introduction of additional coefficients into the model allows for any deviation from a true Lorentzian profile.

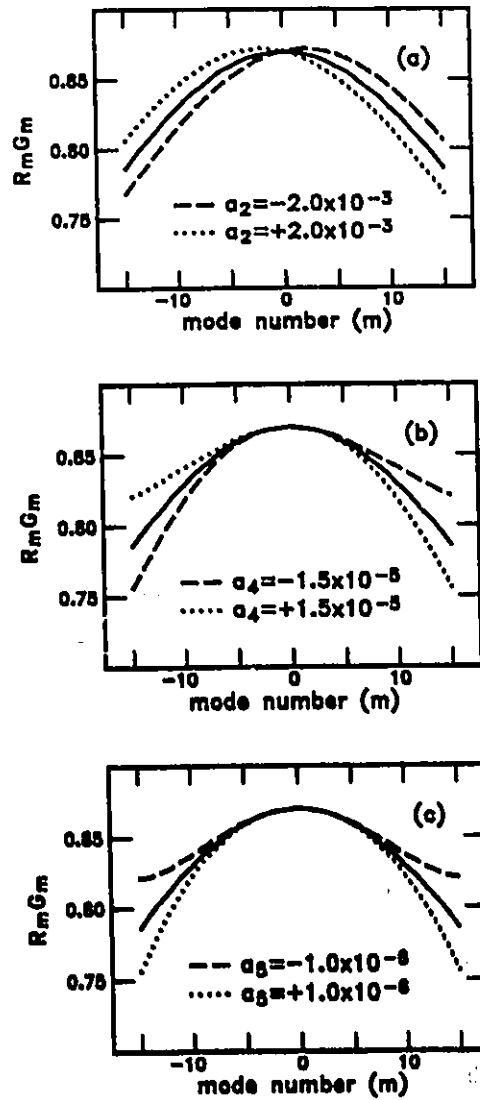


Figure 3.1

Effect of fitting coefficients on the shape of the below-threshold $R_m G_m$ profile. The results for selected values of the coefficients a_2 , a_4 , and a_5 are shown in (a), (b), and (c) respectively. The solid curve in each figure shows the profile for $a_1=1.0$, $a_3=1/2000$ and all other a_i 's set equal to zero.

The effects of each of the coefficients a_i on the shape of the below-threshold $R_m G_m$ profile can be discerned from Eq. (3-1) by factorization of the polynomial in s_m , although a pictorial representation is more tangible. Figure 3.1 shows the effect of positive and negative values of each of the coefficients a_2 , a_4 , and a_5 . The values of a_1 and a_3 were set equal to 1.0 and 1/2000 respectively. The results depicted in Fig. 3.1 indicate that: (i) a_2 shifts the peak of the profile toward positive or negative mode numbers; (ii) a_4 skews the $R_m G_m$ profile; and, (iii) a_5 increases or decreases the gain for modes far from the peak of the profile.

3.2 Variation of the Fitting Coefficients

As discussed in Chapter 2, a least-squares fit to the measured $R_m G_m$ profile was performed on 32 devices in order to extract the characteristic residue for each device. The values of each of the coefficients of the fitting function for the six measured below-threshold $R_m G_m$ profiles (at three different injection current levels) of laser F, an index-guided device, are shown in Table 3.1. The values $(RG)_{\max}$ shown in Table 3.1 represent the peak values obtained from the measured $R_m G_m$ profiles for laser F.

The value of $(RG)_{\max}$ shown in Table 3.1 is a measure of the injection current level relative to the threshold current of the device. Since the shape of the $R_m G_m$ profile of a laser changes as threshold is approached,[31 p.182] the correlation of each of the coefficients a_i with the value of $(RG)_{\max}$ was examined. Table 3.2 shows the results of

Table 3.1 Fitting Coefficients For Laser F

F	I_m -0.5mA		I_m -1.0mA		I_m -1.5mA	
	Trial #1	Trial #2	Trial #1	Trial #2	Trial #1	Trial #2
a_1	1.039	1.050	1.018	1.021	0.971	0.972
a_2	-2.04e-03	-1.91e-03	-1.57e-03	-1.43e-03	-9.47e-04	-1.01e-03
a_3	1.31e-03	1.21e-03	1.16e-03	1.21e-03	1.17e-03	1.17e-03
a_4	3.25e-05	2.92e-05	3.05e-05	2.89e-05	3.17e-05	3.29e-05
a_5	-2.20e-06	-2.07e-06	-1.69e-06	-1.97e-06	-1.66e-06	-1.55e-06
$(RG)_{max}$	0.926	0.937	0.903	0.904	0.858	0.860

fitting a linear equation of the form;

$$a_i = b_i + n_i(RG)_{max}, \quad i = 1 \text{ to } 5 \quad (3-2)$$

to the dependent variables a_i using the six available points shown in Table 3.1 for laser F. The a_i intercept is indicated by the variable b (associated error σ_b) and the slope is indicated by the variable n (associated error σ_n). The errors σ_b and σ_n were calculated by estimating the parent standard deviation, which is the quantity minimized in the fitting procedure.[26 p.114]

The linear correlation coefficient, r , is also displayed in the table. A positive (negative) value of this statistic indicates that the dependent variable a_i increases if the independent variable increases (decreases). Examining the functional form for the

Table 3.2 Variation of Fitting Coefficients For Laser F

F	b	σ_b	n	σ_n	r
a ₁	0.10	0.02	1.01	0.02	1.00
a ₂	1.0e-02	1.7e-03	-1.3e-02	1.5e-03	-0.97
a ₃	2.5e-04	6.8e-04	1.1e-03	6.1e-04	0.62
a ₄	5.5e-05	2.2e-05	-2.7e-05	1.9e-05	-0.53
a ₅	4.3e-06	1.9e-06	-6.8e-06	1.7e-06	-0.87

probability distribution of the linear correlation coefficient, it can be determined that for 6 observations, there is a 10 percent probability of obtaining $|r| \geq 0.73$ for an uncorrelated parent population.[26 p.310] For the purposes of the ensuing analysis, it will be assumed that the correlation is statistically significant only if $|r| \geq 0.73$.

The analysis used to generate the values shown in Table 3.2 for laser F has been applied to all of the 32 devices involved in the residue study discussed in Chapter 2. The results are tabulated and shown in Appendix A. The information contained in this table should provide assistance to future researchers in attempts to model the spectral output of the measured devices. Using the linear form shown in Eq. (3-2), the values provided in Appendix A, and a value of $(RG)_{\max}$ for a given device, the shape of the $R_m G_m$ profile can be determined.

In an attempt to discern any trends in the variation of the fitting coefficients with the injection current, the mean values of the slopes and intercepts were calculated and categorized by the guiding mechanism of the laser. Table 3.3 and Table 3.4 show the results for the index-guided and gain-guided devices respectively. The final column in each table indicates the percentage of devices included in the analysis, i.e., those devices with fitting coefficients satisfying the significance criterion, $|r| \geq 0.73$. There were 32 devices available for study, consisting of 21 index-guided devices and 11 gain-guided devices.

The results tabulated in Table 3.3 and Table 3.4 indicate that the slope and intercept values for the a_1 and a_3 coefficients for both the index-guided and gain-guided devices are equal within the limits of the errors. Physically, it is expected that the rate of change of the coefficient a_1 with $(RG)_{\max}$ would be the same for lasers with different guiding mechanisms since both these parameters are indicators of the injection current level relative to the threshold condition. Although the slope and intercept values for the coefficient a_3 are equal within the error bounds for both device types, the magnitude of the error and the small number of significant devices (final column in Table 3.3 and Table 3.4) render specific conclusions about the coefficient difficult. The negative value of the slope for the coefficient a_3 indicates that the width of the measured below-threshold $R_m G_m$ profile increases slightly as the injection current is increased. It is generally accepted that the width of the $R_m G_m$ profile decreases as the injection current is increased.[32 p.20]

Table 3.3 Variation of Index-Guided Coefficients

	b	σ_b	n	σ_n	Significant Devices (%)
a ₁	-0.09	0.03	1.25	0.03	100.0
a ₂	4.19e-02	3.43e-03	-4.61e-02	2.83e-03	85.7
a ₃	2.90e-03	1.04e-03	-1.71e-03	8.13e-04	61.9
a ₄	4.75e-04	9.40e-05	-5.00e-04	7.39e-05	21.0
a ₅	3.19e-05	6.57e-06	-3.39e-05	5.20e-06	66.7

Table 3.4 Variation of Gain-Guided Coefficients

	b	σ_b	n	σ_n	Significant Devices (%)
a ₁	-0.06	0.02	1.21	0.02	100.0
a ₂	1.29e-02	1.93e-03	-1.52e-02	1.60e-03	81.8
a ₃	3.14e-03	3.14e-04	-1.77e-03	2.58e-04	45.5
a ₄	2.03e-04	2.41e-05	-2.09e-04	2.05e-05	90.9
a ₅	1.94e-05	2.58e-06	-1.81e-05	2.12e-06	81.8

Figure 3.2 indicates a comparison between the effects of the calculated values of the slopes and intercepts of the coefficients a_2 , a_4 and a_5 for index-guided and gain-guided devices. Since the values of the slopes and intercepts for a_1 and a_3 were found to be equal within the bounds of the errors for both device types, the values of these parameters was set equal to the mean of the values found in Table 3.3 and Table 3.4. The below-threshold $R_m G_m$ profiles have been calculated over 61 modes for $(RG)_{max}$ values ranging from 0.5 to 0.9.

As threshold is approached from below, the value of $(RG)_{max}$ increases and the curves in Fig. 3.2 indicate that the profiles shift toward larger mode numbers. As in previous figures, larger mode numbers represent modes with shorter wavelengths (higher energies of photons in the mode). This wavelength-tuning effect is a result of the rate of change of the coefficient a_2 (c.f. Fig. 3.1). The tabulated results indicate that the calculated slope for the coefficient a_2 for index-guided devices is approximately three times greater than that for the gain-guided devices. The increased slope for the index-guided devices is manifested as an increased wavelength-tuning of the $R_m G_m$ profile for a given increase in gain, as depicted in Fig. 3.2. The shift of the peak in the $R_m G_m$ profile toward higher energies with increasing injection current is documented,[32 p.20] although the physical reason for the increased tuning for index-guided devices remains unclear.

Calculations of the gain spectra at different injection levels for undoped InGaAsP[25 p.88] suggest that the gain distribution is skewed toward longer wavelengths.

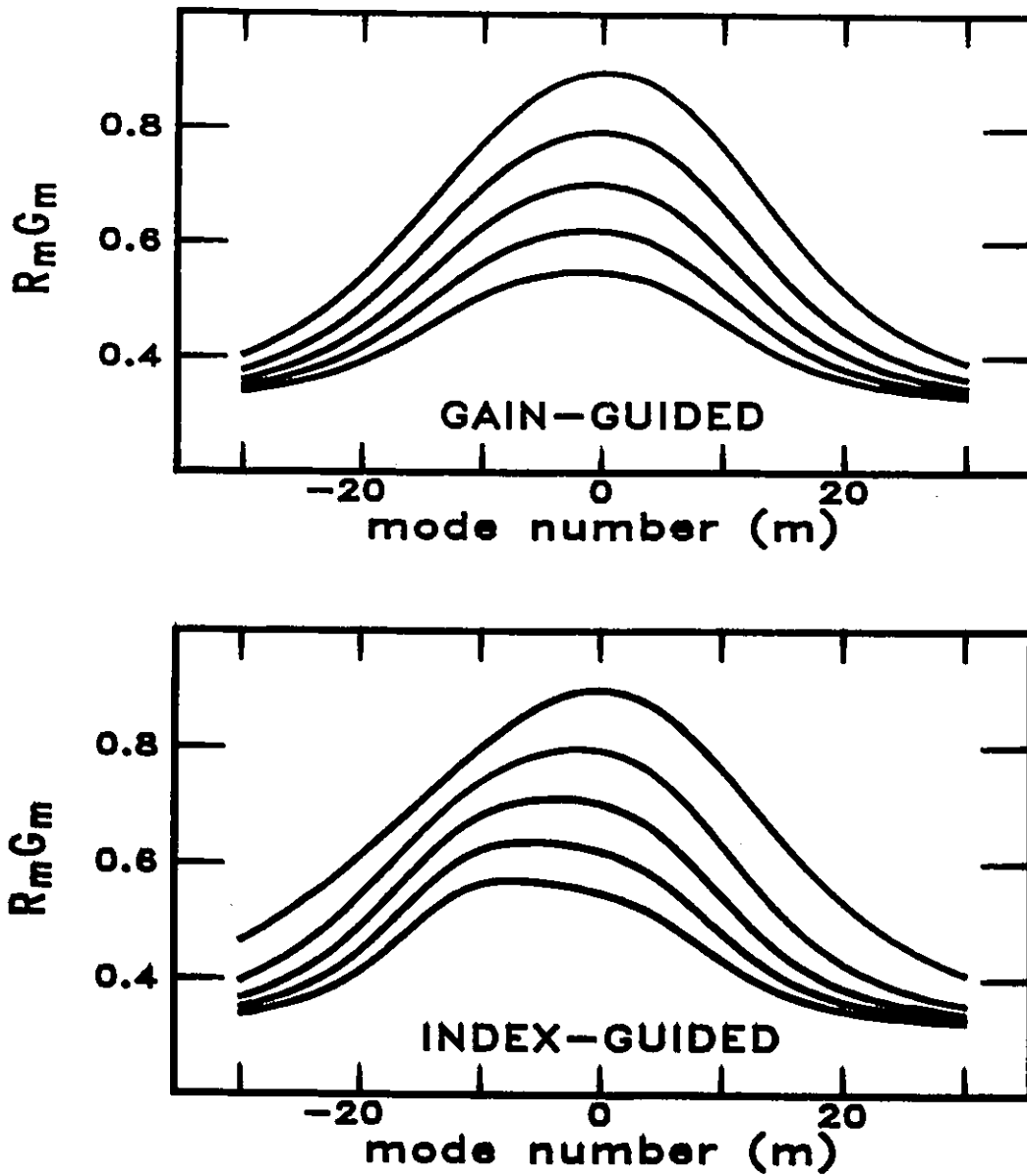


Figure 3.2

Below-threshold $R_m G_m$ profiles for generic gain-guided (a) and index-guided (b) devices based on the values in Table 3.3 and Table 3.4 respectively. The curves are generated for $(RG)_{\max}$ values of 0.5 to 0.9 in increments of 0.1.

A visual inspection of the published curves also suggests that the extent of the skew decreases as the injection level increases. In Eq. (3-1), the coefficient a_4 is responsible for the skew. The tabulated values of the intercept and slope for the coefficients a_4 indicate that, for both index-guided and gain-guided devices, the below-threshold $R_m G_m$ profile is skewed toward long wavelengths and the skew decreases with increasing injection level (negative slope). These observations are in agreement with the gain spectra calculations.[25 p.88] The curves shown in Fig. 3.2 also indicate that the magnitude of the skew for index-guided devices is larger than that for gain-guided structures. The cause of the influence of the guiding mechanism on the magnitude of the skew is unknown.

The contribution of the a_5 coefficient to the shape of the below-threshold $R_m G_m$ profile is smaller in comparison to the contribution of the a_3 coefficient by at least one order of magnitude for those modes spaced less than ten mode spacings from the peak of the profile. Thus, any effects caused by the a_5 coefficient will be overshadowed by the a_3 coefficient, for a narrow region about the peak of the $R_m G_m$ profile. Although it is not obvious from Fig. 3.2, the a_5 coefficient decreases the value of the $R_m G_m$ product for those modes far from the peak of the profile, particularly for the larger values of $(RG)_{max}$. This suggests that as the laser approaches the threshold current condition, a Lorentzian approximation for the gain distribution is no longer valid for those modes spaced far from the peak of the gain profile.

The values of the slopes and intercepts for an assumed linear dependence of

each fitting coefficient in Eq. (3-1) on the maximum value of the below-threshold $R_m G_m$ profile are the major result of this chapter. If the below-threshold spectra of a specific device requires investigation, the values provided in Appendix A should allow predictions of the shape of the below-threshold $R_m G_m$ profile at any current injection level (c.f. Fig. 3.2). Predictions of the above-threshold mode envelope, particularly for index-guided devices, would require information concerning the modulations in the $R_m G_m$ profile due to the presence of scattering centres. The results presented in Table 3.3 and Table 3.4 could be used to model the $R_m G_m$ profile [for a given value of $(RG)_{max}$] of a generic index-guided or gain-guided device respectively, since these values represent the average values of a large number of commercial devices.

The greatest concern regarding the analysis presented in this section is the large variability in the values for the a_3 coefficient (c.f. the error values in Table 3.3 and Table 3.4). It is this coefficient which is the dominant factor in assessing the width of the below-threshold $R_m G_m$ profile. An inspection of the values in Appendix A indicates that the full-width at half-maximum (FWHM) of the profile can vary between 10 and 50 modes, representing a large range of values. One may expect that the shape of the above-threshold mode envelope would be strongly correlated with the width of the below-threshold $R_m G_m$ profile and that a narrow profile width would translate into a smaller number of lasing modes. However, above threshold, there are usually less than ten modes which lase. Thus, it is the shape of the $R_m G_m$ profile in a narrow region about the profile peak, coupled with the imposed modulations due to the presence of scattering centres,

which determine the above-threshold mode envelope. In a narrow, ten mode region about the peak in the below-threshold $R_m G_m$ profile, there is little difference between profiles with a FWHM of 30 and 70 modes. Above threshold, the magnitude of the non-lasing modes, which are distant from the peak of the $R_m G_m$ profile, will be most affected by the width of the profile, as determined by the a_3 coefficient. These non-lasing modes were not measured and hence, no conclusion on the correlation of the magnitude of the non-lasing modes with the width of the profile can be put forth.

3.4 Longitudinal Mode Spacing

To calculate the below-threshold $R_m G_m$ profile, the longitudinal mode spectrum was parsed into individual modes. Thus, the position of the peak of each longitudinal mode was available after performing the parsing procedure. Refractive index variations in the active region material result in dispersive effects in the cavity, causing a variation in the longitudinal mode spacing.[31 p.242] Using the measured position of the longitudinal mode peaks, an examination of the longitudinal mode spacing was conducted for each device.

The mean of the mode spacings closest to mode 0 was first calculated to extract a normalization constant. The mode spacings for the 15 modes on either side of mode 0 were then calculated and normalized, resulting in 30 values of the mode spacing across the $R_m G_m$ profile. For the purposes of performing a polynomial fit to the data, the

numbering convention for the mode spacings was as follows; mode spacing -15 corresponded to the spacing between mode -15 and mode -14, mode spacing -14 corresponded to the spacing between mode -14 and mode -13, *et cetera*. The longitudinal mode spacing data was calculated from all six available below-threshold $R_m G_m$ profiles for each device. A linear least-squares fit was then performed on the mode spacing data. Subsequently, the slope and intercept data for the six cases was averaged, yielding a mean value for the slope and intercept for each device. It should be noted that a quadratic function was also fit to the data as a test of curvature in the mode spacing profile. It was found that the contribution of the quadratic term was at least an order of magnitude smaller than that of the linear term even for mode spacing -15.

The effective group index of a laser waveguide depends upon both the composition of the active region material and the energy separation from the band gap.[33] Table 3.5 shows the mean values of the slope and intercepts for both index-guided and gain-guided devices. The tabulated values indicate that the variation of the longitudinal mode spacing across the below-threshold $R_m G_m$ profile is independent of the guiding mechanism, within the error bounds of the relevant slopes and intercepts. Each of the devices involved in the study emitted in the 1.3 μm wavelength region and it is expected that the active regions of all of the devices were fabricated from a similar material (InGaAsP) and that lasing occurred at a similar energy level relative to the bandgap energy.

Combining the values for the index-guided and gain-guided devices in

Table 3.5, the slope and intercept for the variation of the mode spacing, averaged over all devices, is indicated in the final row of the table. Note that the slope of the mode spacing variation is negative, indicating that the spacing increases with wavelength. Published results indicate that the effective group index for InGaAsP/InP waveguide structures decrease with increasing wavelength.[33] Since the mode spacing varies inversely with the effective group index, the results agree with the documented trend. (It should be noted that the wavelength-dependent dispersion of the monochromator was calculated, and it was determined that the instrument had a negligible effect on the mode spacing.)

Table 3.5 Longitudinal Mode Spacing Parameters

	b	σ_b	n	σ_n
GAIN-GUIDED	0.99944	0.00002	-0.00217	0.00021
INDEX-GUIDED	0.99919	0.00004	-0.00200	0.00031
TOTAL	0.99927	0.00003	-0.00206	0.00028

The results presented in this section could provide valuable information to researchers modelling refractive index effects in 1.3 μm semiconductor diode lasers. A

measurement of the length of the device as well as an accurate wavelength calibration of the monochromator would be required to determine the effective group index of the waveguide structure. The effective group index is an important parameter required for modelling a variety of effects, particularly the waveguiding properties in the active region.[34]

3.5 Summary

In this chapter, the smooth profile which was fit to the measured below-threshold $R_m G_m$ profile was examined. This profile was used to extract the residues discussed in Chapter 2. The fitting coefficients for each of the 32 commercial devices used for the residue study were calculated and a linear relationship between the coefficients and the maximum value of the $R_m G_m$ profile was examined. For each device tested, the values of the slope and intercept for the fitting coefficients were calculated and are tabulated in Appendix A. Upon averaging values according to device type (either index- or gain-guided), discernible differences between the wavelength-tuning coefficient (a_2) and the profile skew coefficient (a_4) were established. Variation of the a_2 and a_4 coefficients with the injection current agreed with accepted results. Specific conclusions involving trends in the a_3 coefficient, (which characterized the profile width) could not be put forth because this coefficient varied considerably for different devices. The spacing of the longitudinal modes across the $R_m G_m$ profile was also examined and a

linear relationship was established between the intermode spacing and the mode number.

The results reported in this chapter provide valuable data to researchers requiring information regarding the shape of the $R_m G_m$ profile or the longitudinal mode spacing of 1.3 μm semiconductor diode lasers. For example, the data characterizing the shape of the $R_m G_m$ profile (shown in Appendix A) was used to model linewidth effects in specific 1.3 μm semiconductor diode lasers.[35]

Chapter 4. Comparison of Techniques to Measure Scattering Centres

4.1 Introduction

The results reported in Chapter 2 suggest that the presence of scattering centres in the active region of 1.3 μm InGaAsP/InP semiconductor diode lasers is an important mechanism in determining the above-threshold longitudinal mode profile of these devices. Using different experimental techniques or devices, other researchers have reached similar conclusions.[4,13,19] The effect of the strength and position of scattering centres in the active region of semiconductor diode lasers can account for the observation that index-guided lasers tend to lase in a single longitudinal mode, whereas gain-guided devices tend to exhibit a more multi-longitudinal mode spectral output.

Two related studies have reported the observation that intrinsic scattering centres in the active region of commercially-available semiconductor lasers significantly affect the shape of the above-threshold mode profile. Polarization-resolved and spatially-resolved electroluminescence measurements of light through the substrate[13] and below-threshold measurements of the facet emission to obtain the $R_m G_m$ product (where R_m is the reflectance and G_m the single pass gain of the m^{th} longitudinal mode) indicate that the above-threshold spectral output can be explained by considering the effects of scattering centres along the length of the device. (The below-threshold measurements of the $R_m G_m$

product were discussed in Chapter 2.) The purpose of this chapter is to report on the correlation between the results obtained in these studies. This chapter is organized as follows: Section 4.2 compares the results obtained from the experimental techniques, Section 4.3 discusses the correlation between the two studies, and Section 4.4 discusses some pertinent aspects of mode sampling of the effective facet reflectance. Section 4.5 provides a summary.

4.2 Comparison of Techniques

Spatially-resolved and polarization-resolved electroluminescence measurements have revealed a correlation between the amount of light scattered from the active region through the substrate of a semiconductor diode laser and the above-threshold mode profiles of the devices.[13] In general it was found that lasers having large values of discrete or total scattering tended to run single-mode or with a highly modulated above-threshold mode envelope. Devices which had small values of the scattering parameters tended to lase on multiple-longitudinal modes with a smooth mode envelope. Total scattering is a measure of the total amount of light from the active region which is scattered through the substrate and discrete scattering is a statistical measure of the degree of localization of the scattering. A Fabry-Perot model incorporating the strength and position of a single scattering centre enables accurate prediction of the above-threshold mode profile for selected devices.[14]

As explained in Chapter 2, examination of the facet emission has indicated that a correlation exists between the modulations in the below-threshold $R_m G_m$ profile and the above-threshold spectral signature. It was found that lasers showing large modulation features in the below-threshold $R_m G_m$ profile tended to run single-mode or with highly modulated above-threshold mode profiles. A residue which is characteristic of the modulation features was extracted from the below-threshold spectra by fitting a smooth function to the measured $R_m G_m$ profile. Accurate predictions of the above-threshold mode profile of the devices were obtained by incorporating the residue in a model of an homogeneously-broadened laser[20] as effective reflectance variations.

If scattering in the active region of diode lasers is a dominant mechanism which determines the above-threshold properties of the devices, and if the spatially- and polarization-resolved electroluminescence technique accurately reflects the extent to which scattering affects the spectral output, a strong correlation should exist between the amount of scattering in the active region as measured through the substrate and the magnitude of the modulation features in the below-threshold $R_m G_m$ profile.

The data depicted in Figure 4.1 and Figure 4.2 for a planar-buried-heterostructure (PBH) laser shows a correlation between the results obtained from the two experimental techniques. Figure 4.1 shows the degree of polarization along the length of the active region of a PBH semiconductor laser (laser Z) as obtained from spatially and polarization-resolved electroluminescence measurements. The differences between the degree of polarization below-threshold (broken line) and above-threshold (solid line)

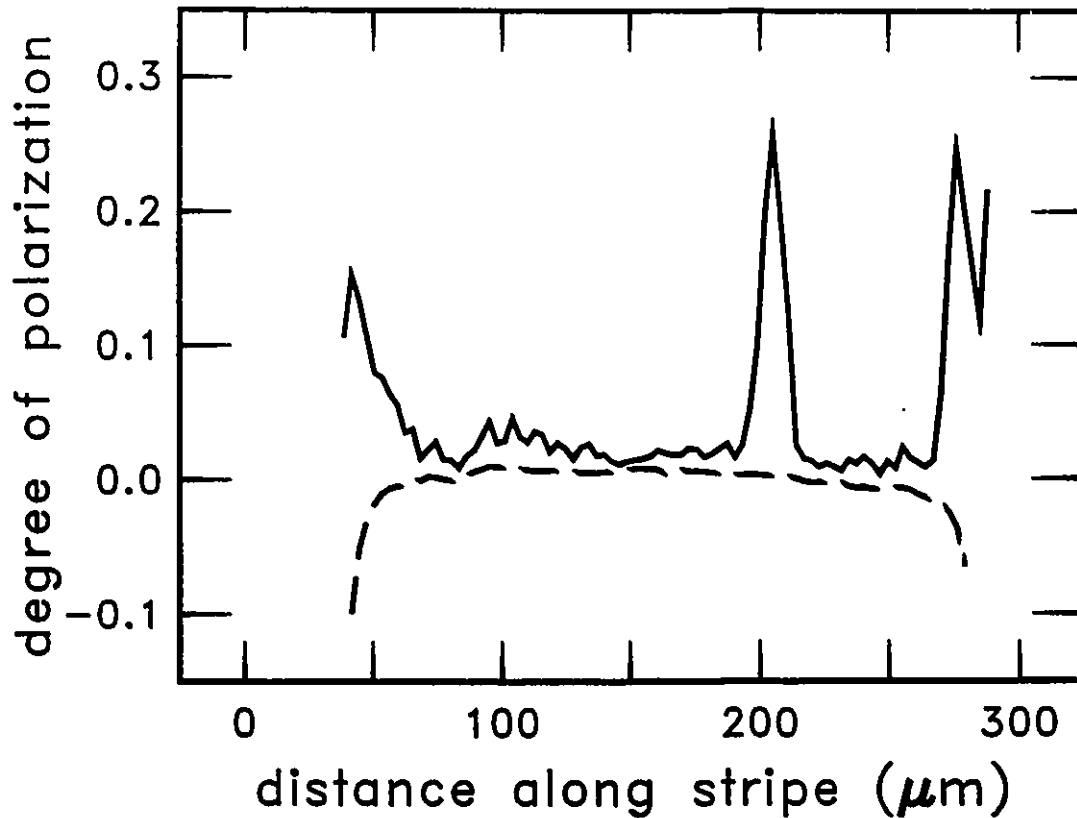


Figure 4.1

Degree of polarization (DOP) of the electroluminescence distributed along the active region length of a planar buried heterostructure laser. The dashed and solid lines indicate the results of the DOP measurement below and above threshold respectively. The active region stripe spans the distance between the 0 and 300 μm tic marks on the abscissa. The spike at a distance of approximately one-third the active region length from the right laser facet indicates the presence of a strong scattering centre at this location.

indicate the presence of a strong scattering centre located at a distance of approximately one-third the active region length from the right facet of the laser. Incorporation of the position of the scattering centre in a Fabry-Perot model[14] predicts a sinusoidal effective

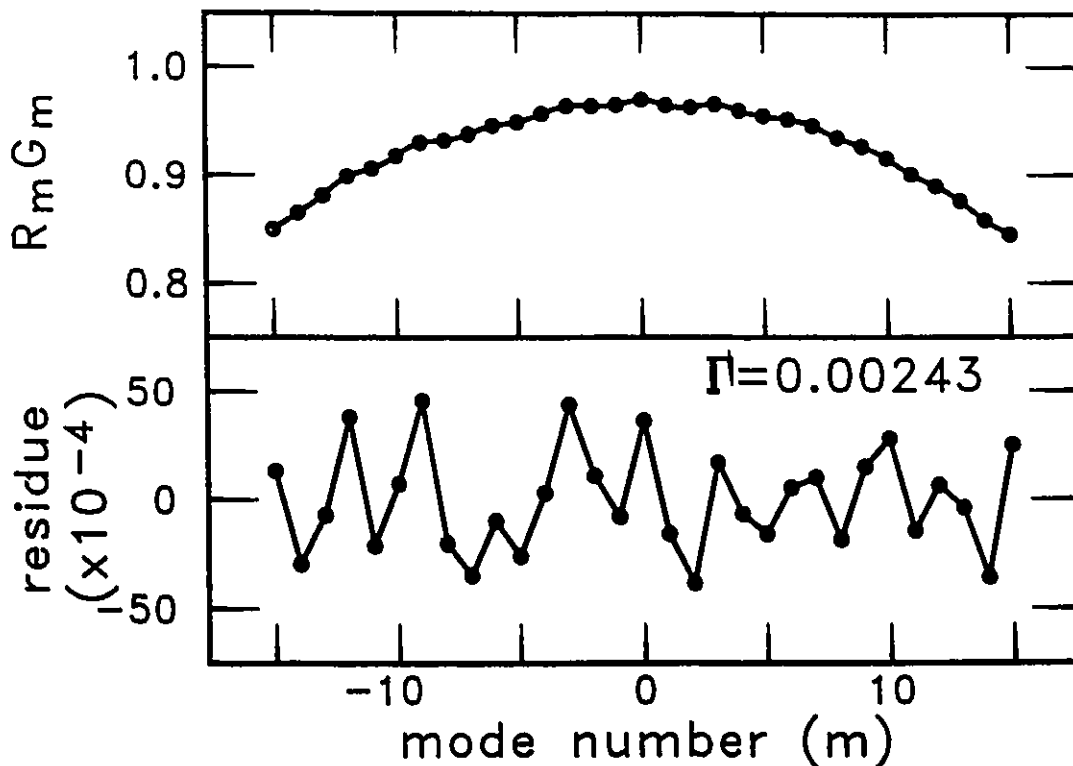


Figure 4.2

Residue analysis applied to the laser which is characterized by the degree of polarization plot indicated in Fig. 4.1. The $R_m G_m$ product indicates the presence of modulation features. The normalized residue is shown in the bottom of the figure and indicates a quasi-sinusoidal functional dependence on the mode number with a period of approximately three mode spacings. The rms residue, Γ is also indicated in the figure.

reflectance variation with a period of approximately three mode spacings.

The below-threshold $R_m G_m$ profile for this device, obtained using the mode-sum/minimum method,[21] is indicated at the top of Fig. 4.2. Significant modulation features are evident. Following the method discussed in Chapter 2, a smooth function

was fit to the $R_m G_m$ profile.[20] The normalized residue depicted at the bottom of Fig. 4.2 was constructed by subtracting the best-fit profile from the data and dividing by the best-fit gain. The root-mean-square (rms) residue Γ , which characterizes the magnitude of the modulation features is calculated as the standard deviation of the normalized residue record. Γ is calculated over the 21 points centred about mode 0, where mode 0 is defined as being the strongest mode. (It will be recalled that in Chapter 2, Γ was calculated over 11 points centred about mode 0. The rationale for choosing a larger interval will be explained in Section 4.4.) Note that the normalized residue has a sinusoidal functional dependence on mode number with a period of approximately three mode spacings. This is the period predicted from the position of the localized scattering centre shown in Fig. 1 as obtained from a Fabry-Perot laser model. It is evident that a correlation exists between the modulation features in the below-threshold $R_m G_m$ profile and the position of scattering centres in the active region obtained by the spatially and polarization resolved electroluminescence technique. Using a similar method, DeChiaro reported a correlation between the below-threshold mode profile and the positions of damage-induced scattering sites.[19]

4.3 Correlation of Results

The spatially and polarization resolved electroluminescence data and the below-threshold $R_m G_m$ profiles were examined for 16 lasers [5 gain-guided, 3 arrowhead

buried crescent (ABC), and 8 planar buried heterostructure (PBH)]. The correlation plot for these devices is shown in Figure 4.3. Gain-guided lasers are represented by lower-case letters, planar buried heterostructure devices are represented by upper-case letters and the numbers represent arrowhead buried crescent devices. (Those devices which were studied in this experiment as well as the experiment outlined in Chapter 2 are designated with the same identification label.) Each ordered pair represents measurements obtained on the same device from each technique. Plotted along the abscissa is the discrete scattering parameter σ/β for each device. This scattering parameter is measured through the device substrate and is a measure of the strength and localization of the scatterer (as observed through the substrate), normalized to the amount of spontaneous emission (β) in the device. The rms residue, Γ , as measured from an examination of the facet emission, is also normalized to the amount of spontaneous emission (β). Γ/β is plotted on the ordinate. The value of the ordinate represents the mean value of six rms residues, as calculated from six different measurements of the below-threshold spectra at identical bias current levels.

A linear least-squares fit to the ordered pairs was calculated and the best-fit line is indicated in Fig. 4.3. The intercept of the best-fit line is approximately equal to zero. This result is expected, because a device without scattering centres should exhibit no discrete scattering ($\sigma=0$) and a smooth $R_m G_m$ profile ($\Gamma=0$). Note that the gain-guided devices which were tested lie on the best-fit line close to the origin. Gain-guided devices tend to operate with smooth above-threshold mode profiles and exhibit negligible

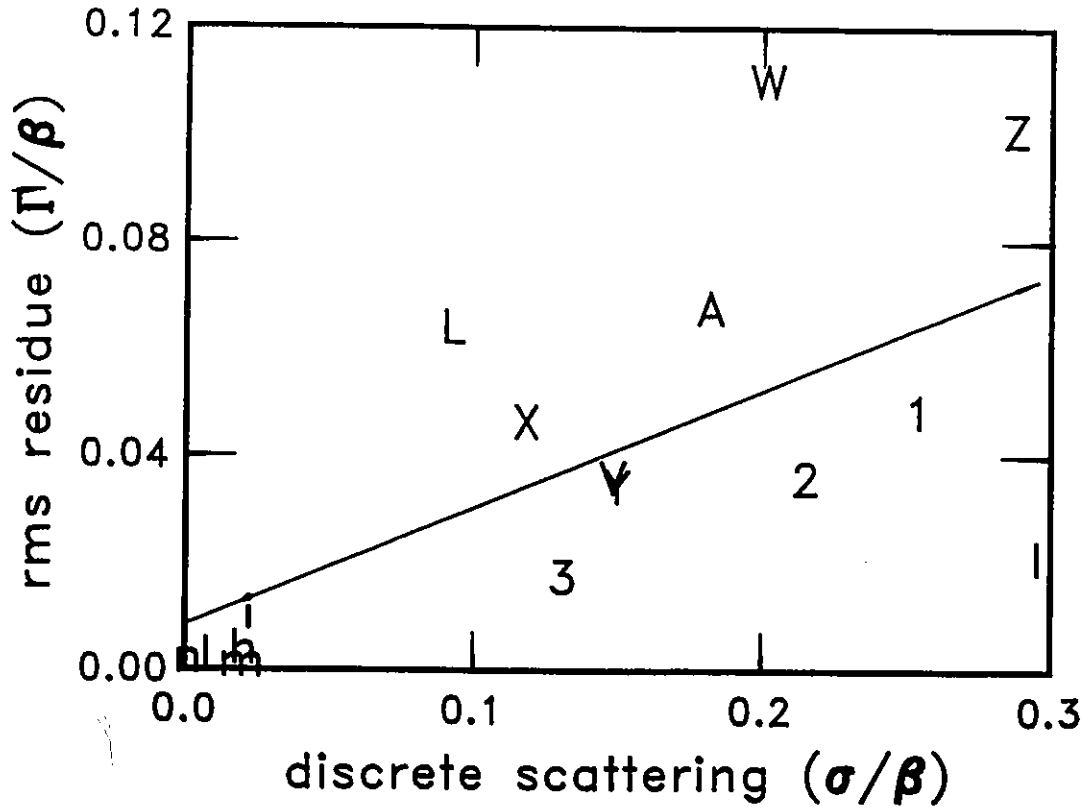


Figure 4.3

Correlation plot and best-fit line for the discrete scattering parameter (σ) and the rms residue (Γ) of sixteen different lasers. The value of the discrete scattering parameter normalized to the amount of spontaneous emission in the device (σ/β) is plotted on the abscissa. The ordinate of the laser identification label represents the mean of six rms residue calculations (Γ) normalized to the amount of spontaneous emission in the device (β). Gain-guided lasers are represented by lower case letters and planar-buried-heterostructure devices are represented by upper case letters. Arrowhead-buried-heterostructure lasers are represented by numbers.

scattering and thus are characterized by small rms residues. In addition, the large amount of spontaneous emission associated with gain-guided devices tends to mask the influence of any scattering centres.[27]

From the results depicted in Fig. 4.3, it appears that a weak correlation exists between σ/β and Γ/β . A stronger correlation was anticipated and it was expected that most points would lie closer to a best-fit line. There are several reasons for the dispersal of the ordered pairs about the best-fit line. First, for the modelling of the above-threshold mode profile from measurements through the device substrate, it has been assumed that the scattering centres along the length of the active region are Rayleigh scatterers.[14] Since the polarization- and spatially-resolved electroluminescence measurements are collected through the substrate, this technique would over- or under-estimate the amount of light scattered in the direction of the facet if there were any directional anisotropies for the scattering of light by these centres. It is the amount of light scattered in the direction of the facet which determines the magnitude of the modulation features in the below-threshold $R_m G_m$ profile and hence the value of Γ/β . Secondly, the longitudinal modes sample the effective facet reflectance such that phase relationships could be manifested as reductions in the magnitude of the modulation features (rms residue Γ). The topic of mode sampling will be discussed in the next section. Finally, although the correlation between σ/β and Γ/β appears weak, it is important to explore pertinent statistical quantities before the correlation can be adequately assessed.

The linear correlation coefficient (r) is a statistical quantity which allows the capability to assess the correlation of two variables.[26 p.119] The value of this statistic was calculated to be $|r|=0.65$. A Monte Carlo simulation using 100,000 independent trials was conducted to assess the probability of achieving the value of $|r|$ from a

random parent population (for which $|r|$ is approximately equal to zero). A random number was chosen for each measured value of σ/β in order to generate 16 uncorrelated ordered pairs. From the simulation, it was found that the probability that a set of sixteen uncorrelated ordered pairs has a correlation coefficient greater than 0.65 is approximately 0.004. Thus, only 40 times in 10,000 trials would one expect a set of 16 uncorrelated ordered pairs to be linearly correlated as well as the data presented in Fig. 4.3. Interpolated from a probability distribution table for the linear correlation coefficient,[26 p.311] the probability of exceeding the value $|r|=0.65$ in a random sample of 16 observations taken from an uncorrelated parent population is approximately 0.007. From the analysis of the statistics, it can be concluded that the correlation is stronger than a preliminary visual inspection may indicate.

4.4 Longitudinal Mode Sampling

As indicated in the previous section, the manifestation of the sampling of the effective facet reflectance by the longitudinal modes can explain some deviations of the ordered pairs in Fig. 4.3 from the best-fit line.

It will be recalled from Eq. (2-3), that for a single scattering centre which scatters a small fraction σ^2 back into the mode and transmits a fraction τ^2 , the effective

facet reflectance of facet #i for the m^{th} mode is given by:

$$R_{im} \approx R\tau^2[1+2\sqrt{R}G_{im}\sigma \cos(2k_m L_i)] \quad (4-1)$$

where R is the reflectance of the facets, k_m is the propagation constant of mode m , and G_{im} is the single pass gain for the m^{th} mode over the distance L_i between facet #i and the scattering centre. Accounting for the spacing of the Fabry-Perot resonances of the full cavity, the dependence of the facet reflectance on the mode index m becomes:

$$R_i(m) \approx R\tau^2[1+2\sqrt{R}G_i(m)\sigma \cos(2\pi m \frac{L_i}{L} + \phi)] \quad (4-2)$$

where $\phi=2k_0L_i$ represents a phase shift and includes the propagation constant of mode $m=0$ and the distance L_i between facet #i and the scattering centre. The value of ϕ changes by 2π radians for a change in L_i of typically $0.2 \mu\text{m}$. The spatial resolution of the electroluminescence technique is approximately $1.0 \mu\text{m}$ and thus the phase shift ϕ can not be measured. It should also be recalled that for a mode of the full cavity, the resonance condition is $\cos[2k_m L] = 1$, and since $L = L_1+L_2$, $\cos[2k_m L_1] = \cos[2k_m(L-L_2)] = \cos[2k_m L_2]$ - that is, the sinusoidal modulation of the facet reflectance caused by the larger pseudo-cavity are aliased into those of the smaller pseudo-cavity. (The pseudo-cavity is defined as being composed of one laser facet and the scattering centre.) Thus R_{1m} and R_{2m} vary with the same period when sampled at the resonant frequencies of the full cavity.

Inspection of Eq. (4-2) indicates that the rate at which the longitudinal modes

sample the effective facet reflectance depends only on the ratio L_1/L . Thus, parameters which alter the refractive index of the active region or the optical frequency of the longitudinal modes, such as bias current or active region temperature, will have a negligible effect on the position (in mode space) where the longitudinal mode samples the effective facet reflectance, provided that the parameter change is uniform over the length of the cavity.[36]

Figure 4.4 shows the effect of the phase shift ϕ on the calculation of the rms residue Γ for L_1/L values of 0.50 and 0.25 for the case of a single, isolated scatterer. The rms residue plotted in Fig. 4.4 was normalized to the maximum value of the rms residue occurring at $\phi = 0$, which is defined as Γ_0 . For the condition $L_1/L = 0.50$, the longitudinal modes of the laser sample the effective reflectance exactly twice per cycle - the Nyquist sampling rate. At this limiting sampling rate, it is expected that the amplitude of the sampled signal strongly depends on the phase relationship between the original signal (effective reflectance) and the sampling signal (longitudinal mode spectrum). The results displayed by the solid line in Fig. 4.4 indicate that the normalized rms residue Γ/Γ_0 varies between 1.0 and 0.0 depending on the value of the phase term ϕ if the effective reflectance is sampled at the Nyquist rate. The variation of Γ/Γ_0 with phase for the condition $L_1/L = 0.25$ is shown by the dashed line in Fig. 4.4. In this case the sampling rate is twice the Nyquist rate, and variations in ϕ have a much smaller effect on the magnitude of the rms residue. A normalized rms residue at $\phi = 0$ of $\Gamma/\Gamma_0 = 0.707$ is the value expected for a sinusoidal oscillation with a peak-to-peak amplitude of 2.0.

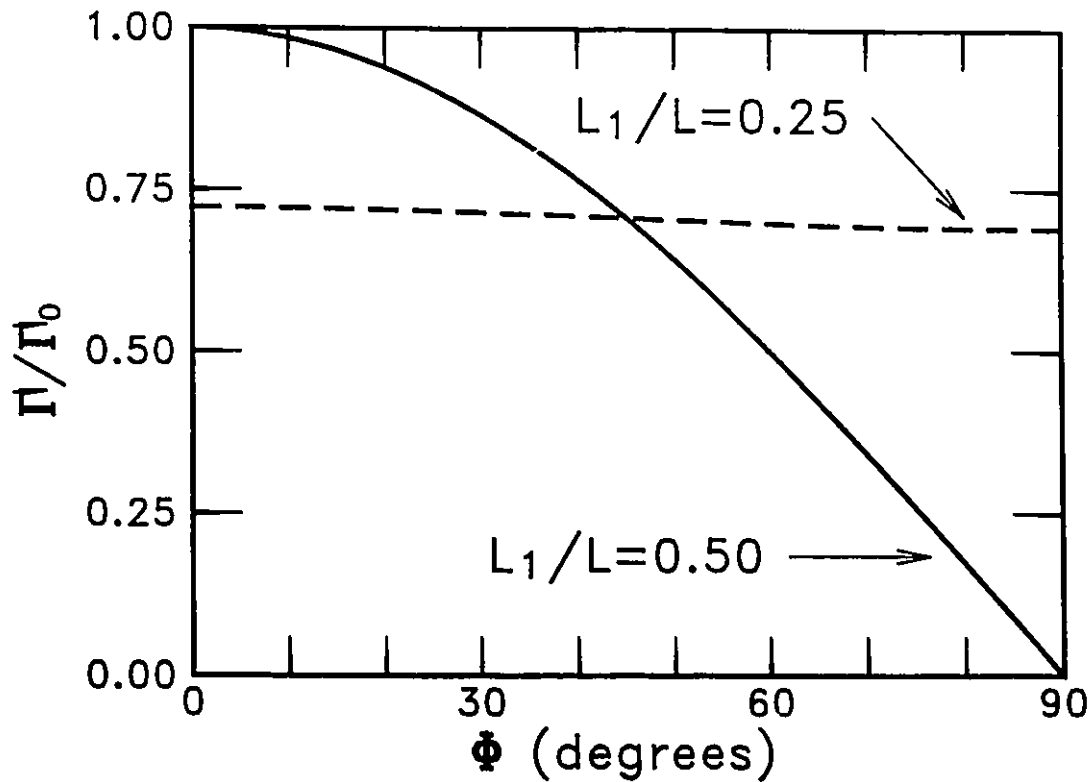


Figure 4.4

The effect of the phase shift ϕ on the calculation of a normalized rms residue (Γ/Γ_0). The solid line indicates the results expected for an isolated scatterer positioned at the centre of the active region ($L_1/L = 0.50$). The dashed line indicates a similar analysis applied to an isolated scatterer positioned such that $L_1/L = 0.25$.

Figure 4.5 shows the bounds of the minimum and maximum normalized rms residues as a result of phase shift variations for the full range of normalized scattering lengths $L_1/L = 0.0$ to $L_1/L = 0.5$. Values of Γ_{\max}/Γ_0 and Γ_{\min}/Γ_0 for $0.5 < L_1/L \leq 1.0$ are easily obtained by noting that the curves are symmetric about the line $L_1/L = 0.5$. The physical concept illustrated in Fig. 4.5 is that a scatterer near the centre of the active

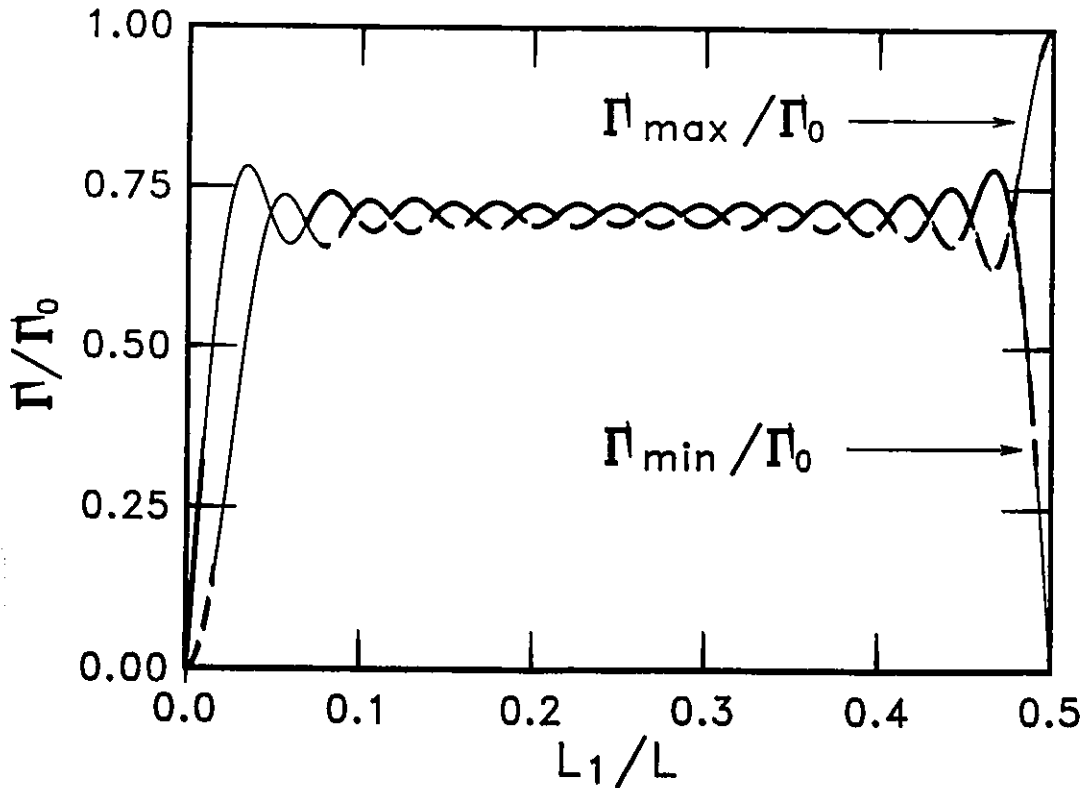


Figure 4.5

Bounds of the minimum and maximum normalized rms residue (Γ/Γ_0) due to variations in the phase shift (ϕ) for an isolated scatterer placed in the active region. The position of the scatterer is plotted along the abscissa as a fraction of the total active region length (L_1/L). The maximum (minimum) achievable rms residue for a given scatterer position is indicated by the solid(dashed) line.

region may or may not result in modulations in the longitudinal mode profile depending on the value of the phase term ϕ . Examination of light scattered through the substrate of a selected device using the spatially- and polarization- resolved electroluminescence may indicate a strong scatterer in the centre of the active region. Modulations in the $R_m G_m$ profile as obtained from the below-threshold facet emission of this same device may not

be evident (due to the value of the phase term ϕ) and the above-threshold spectra of the laser would show no manifestations of this scattering centre. These results have been observed in several lasers. The decrease in the values of Γ_{\max}/Γ_0 and Γ_{\min}/Γ_0 for small values of L_1/L results because the rms residue is calculated over a finite number (21) of longitudinal modes. Scattering centres near the laser facets (small values of L_1/L) result in modulations whose period is large compared to the width of the gain profile, resulting in small values of the rms residue. [In Chapter 2, rms residues were calculated over 11 longitudinal modes. A larger mode interval (21) was used for the analysis in this chapter in an attempt to collect residue data for scattering centres close to the laser facets.]

Figures 4.6 through 4.9 show the degree of polarization and residue plots for two lasers which have isolated scatterers near the centre of the active region; $L_1 = L_2 = 0.5L$. In the case of the first laser, a gain-guided device, (laser i in Fig. 4.3) the degree of polarization plot of Fig. 4.6 indicates the presence of a scatterer near the centre of the active region. The residue for this device is indicated in Fig. 4.7 and a modulation component with a period of two mode spacings is evident. Figure 4.8 depicts the degree of polarization plot for a second device, an index-guided laser (laser V in Fig. 4.3). The scatterer near the active region centre is approximately three times stronger than the previous device although the residue for laser V, as indicated in Fig. 4.9, does not exhibit a modulation component with a period of two mode spacings. The magnitudes of the modulation features in the residues of devices i and V in relation to the strength of the isolated scattering centres depicted in the degree of polarization plots are

consistent with the postulate that a scatterer near the centre of the active region may or may not result in modulations in the longitudinal mode profile depending on the value of the phase term ϕ .

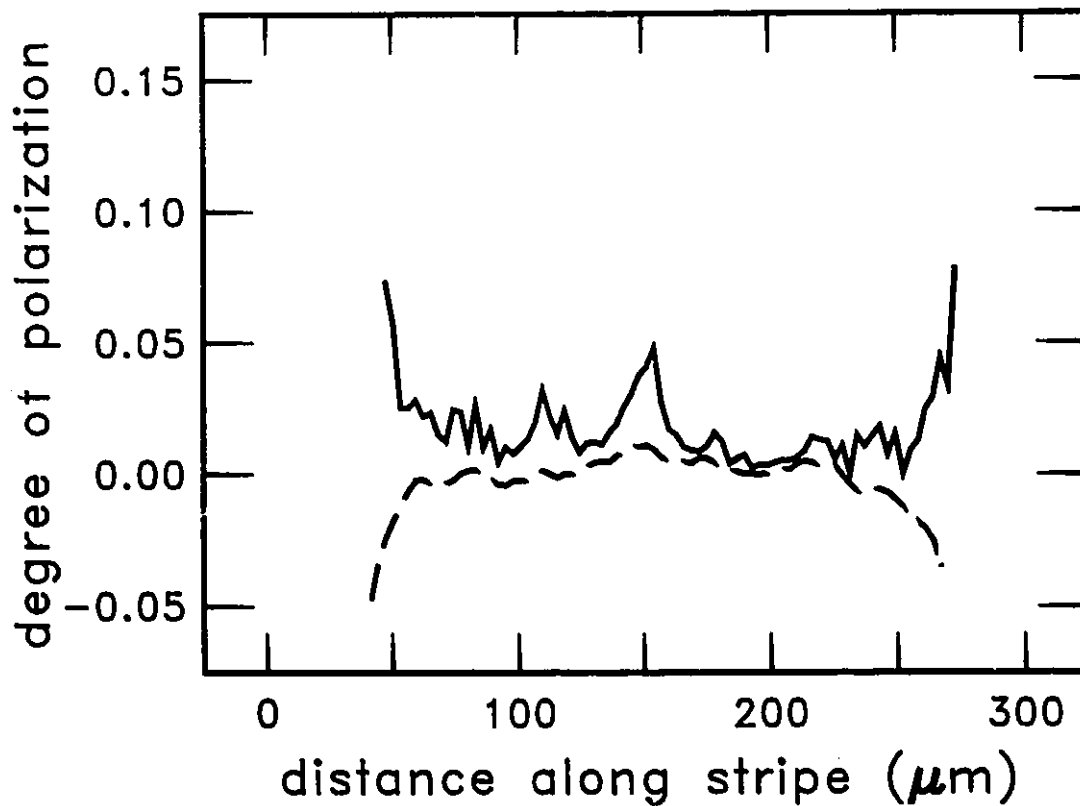


Figure 4.6

Degree of polarization (DOP) of the electroluminescence of a gain-guided laser which indicates the presence of a scattering centre near the midpoint of the active region length. The dashed and solid lines indicate the results of the DOP measurement below and above threshold respectively.

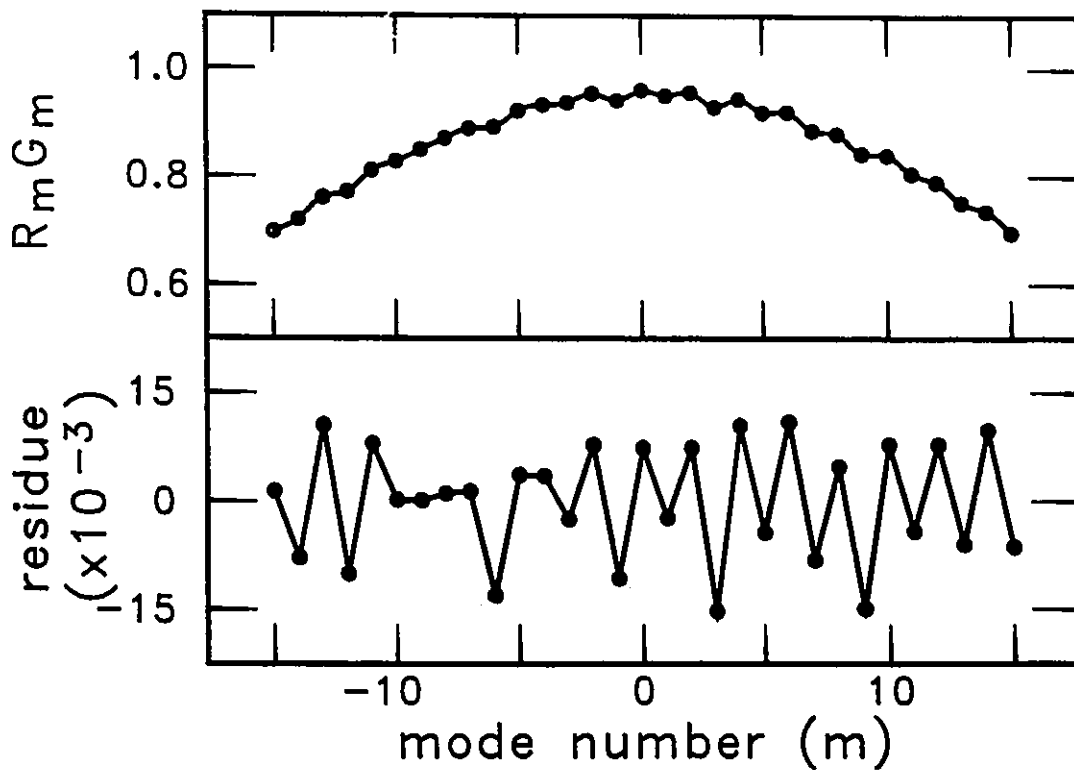


Figure 4.7

Residue analysis applied to the laser which is characterized by the degree of polarization plot indicated in Fig. 4.6. The normalized residue is shown in the bottom of the figure and indicates the presence of a modulation feature with a period of two mode spacings.

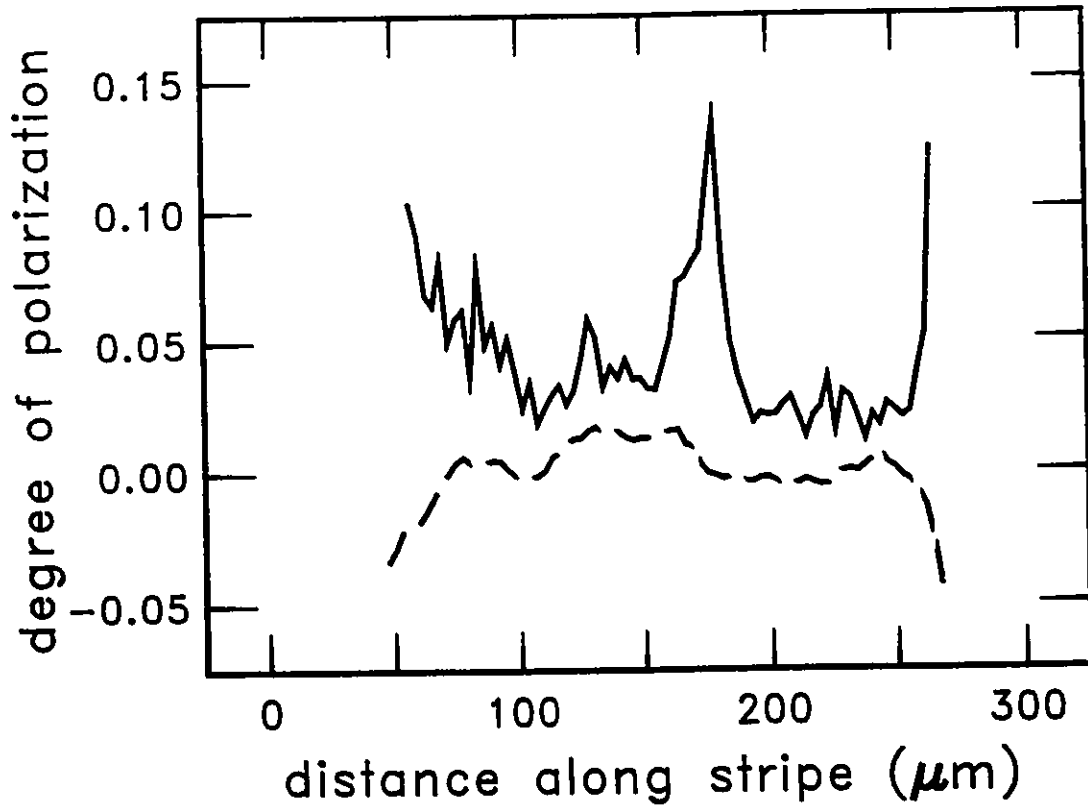


Figure 4.8

Degree of polarization (DOP) of the electroluminescence of a planar buried heterostructure laser which indicates the presence of a scattering centre near the midpoint of the active region length. The dashed and solid lines indicate the results of the DOP measurement below and above threshold respectively. Note that the DOP of the dominant spike is approximately a factor of three larger than the midpoint DOP spike of the gain-guided laser depicted in Fig. 4.6.

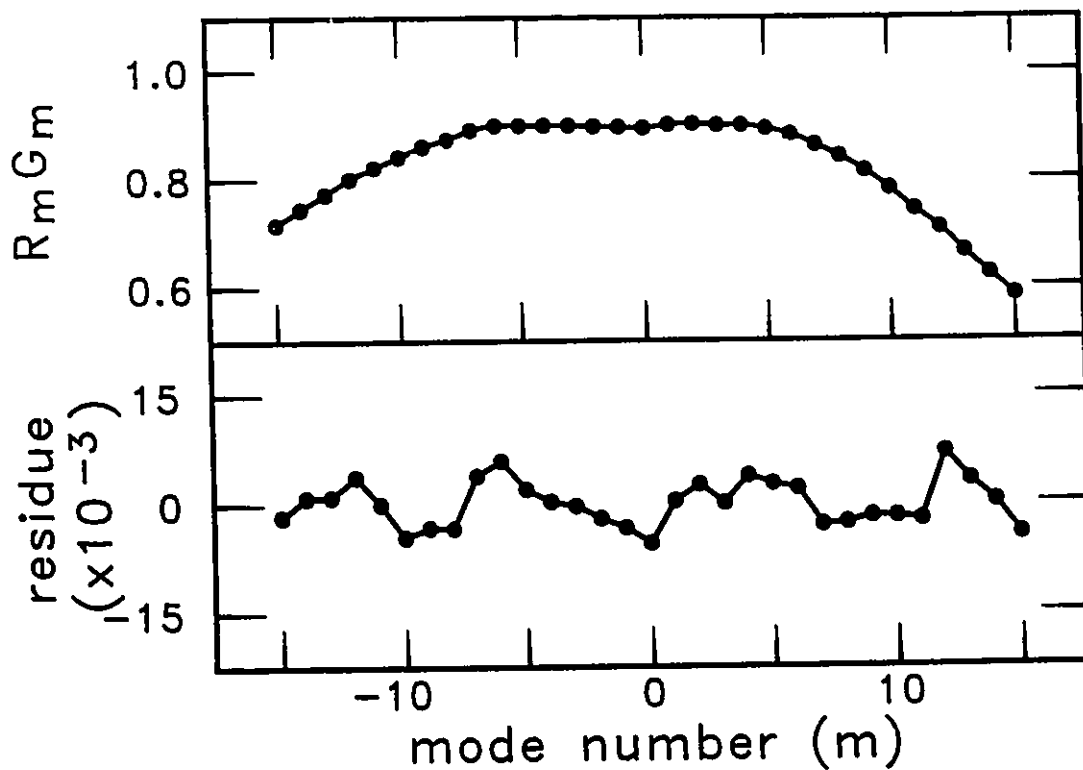


Figure 4.9

Residue analysis applied to the laser which is characterized by the degree of polarization plot indicated in Fig. 4.8. The absence of a modulation feature with a period of two mode spacings in the normalized residue shown in the bottom of the figure is taken to indicate the effect of longitudinal mode sampling near the Nyquist rate.

4.5 Summary

Sixteen $1.3 \mu\text{m}$ semiconductor diode lasers were studied and the correlation between the discrete scattering parameter (σ/β) as measured through the substrate by the

spatially and polarization resolved electroluminescence technique and the magnitude of modulation features in the $R_m G_m$ product (Γ/β) as measured from the facet emission has been reported. A strong correlation between σ/β and Γ/β was expected since both of the techniques measure the effects of light scattering along the length of the active region of the diode lasers. Visual inspection of a correlation plot of the two variables indicated a large dispersal of the ordered pairs about the best-fit line suggesting a seemingly weak correlation. Upon closer inspection of the statistics of the correlation coefficient using a Monte Carlo analysis, it was found that there was only a small probability (less than 0.5 percent) that ordered pairs obtained from an uncorrelated parent population would have a correlation coefficient as large as that of the data.

Several postulates were suggested to account for the large dispersal of the data points about the best-fit line. The strength and position of an isolated scattering centre in the active region determines the amplitude and the period of the effective facet reflectance. For certain lasers, it was observed that the period of the modulations in the below-threshold $R_m G_m$ product coincided with results predicted using the position of a localized scattering centre in a Fabry-Perot model as obtained from measurements of light scattered through the substrate (c.f. Fig. 4.1 and Fig. 4.2). The amplitude of the modulations in the measured below-threshold $R_m G_m$ profile are determined to a large extent by the position (in mode space) where the longitudinal modes sample the effective facet reflectance. For those scattering centres residing near the centre of the active region, the phase relationship between the sampling signal (the longitudinal modes) and

the original waveform (the effective facet reflectance) is particularly important. For certain phase conditions the scattering centre can have the effect of making little or no contribution to the measured modulations in the below-threshold $R_m G_m$ profile. Due to the importance of this phase relationship, measurements obtained through the substrate using the spatially- and polarization- resolved electroluminescence technique can over- or under-estimate the influence of scattering centres in determining the above-threshold spectral output.

It is important to note that the spatially- and polarization-resolved electroluminescence technique measures light scattered through the substrate. To predict the above-threshold longitudinal mode profile of a device using the strength and position of the scattering centre, it was assumed that the centre behaved as a Rayleigh scatterer.[14] If the Rayleigh scattering model is inappropriate, then the scattering centre in the active region of the device may exhibit anisotropic light scattering, resulting in an over- or under-estimation of the strength of the scattering in the direction of the mode by the spatially- and polarization-resolved electroluminescence technique. In contrast, the modulation features in the below-threshold $R_m G_m$ profile were measured by examining the facet emission of the laser and thus indicate the amount of light scattered along the axis of the active region.

Scattering centres distributed along the length of the active region of $1.3 \mu\text{m}$ semiconductor diode lasers provide a mechanism for the longitudinal mode selectivity in these devices, but the effects of sampling of the facet reflectivity by the longitudinal

modes and the amount of light scattered along the axis of the active region must be taken into account to predict the above-threshold mode profile. The effect of an anisotropic scatterer in the active region of a device would be to scatter unequal amounts of light in the direction of the facet and in the direction of the substrate. Measurements of scattering parameters using the spatially- and polarization-resolved electroluminescence technique do not include the effects of longitudinal mode sampling nor the amount of scattering in the direction of the facet, and thus this technique is better suited to determine the quality of the material in the active region. However, measurement of the modulation in the $R_m G_m$ profile as obtained from the below-threshold facet emission measures the amount of light scattered along the axis of the active region and includes the effects of longitudinal mode sampling. Thus, measurement of the below-threshold facet emission is the preferred technique to provide an accurate estimate of the effect of scattering centres on the spectral output.

Chapter 5. Nonlinear Gain in SXC Semiconductor Lasers

5.1 Introduction

In Chapter 2, it was shown that the above-threshold spectral output of 1.3 μm semiconductor diode lasers could be predicted based upon the modulations imposed on the $R_m G_m$ profile owing to the presence of scattering centres in the active region of the devices. Modulations in the $R_m G_m$ profile were measured by examining the below-threshold longitudinal mode spectral output of a large number of commercial devices. For sufficiently large optical power levels inside the active region, it has been predicted that the shape of the above-threshold mode envelope will be determined by nonlinear gain mechanisms, the magnitude of which increase with the photon density in the active region.[9,37,38,39]

Numerous documents have been published concerning nonlinear gain mechanisms in semiconductor devices. Theories regarding the origin of the nonlinear gain have been forwarded in an attempt to explain certain aspects of static or dynamic device behaviour. Existing models of device behaviour are often extended with phenomenological nonlinear terms to account for experimental observations. However, the calculation of parameters for the required device behaviour are often inconsistent with measured results. A survey of the documented results concerning nonlinear gain

phenomena is presented in Section 5.2.

The effect of scattering centres has not been coupled with nonlinear gain phenomena to model the above-threshold spectra of semiconductor devices. In Chapter 2, it was reported that the effect of scattering centres must be incorporated in any realistic model of the spectral output of semiconductor diode lasers. Thus, the importance of nonlinear gain phenomena in determining the shape of the above-threshold mode envelope becomes circumspect.

An experiment was designed to explore the possibility that nonlinear gain mechanisms are important in determining the shape of the mode envelope at large optical power levels. Using optical feedback supplied by a short-external-cavity (SXC), the evolution of the longitudinal modes with injection current was studied for several 1.3 μm semiconductor diode lasers. To facilitate isolation of the different mechanisms responsible for the shape of the mode evolution curves, the SXC was incorporated into a model of an homogeneously-broadened device.[20] The predicted mode evolution curves based upon an SXC source without the inclusion of nonlinear gain phenomena are discussed in Section 5.3. The apparatus used for collecting the data and the experimental results are described in Section 5.4.

Section 5.5 shows the results of including a symmetric nonlinear gain term in an homogeneously-broadened model for Fabry-Perot semiconductor lasers in an attempt to model the results of the experiment. A summary is provided in Section 5.6.

5.2 Survey of Documented Results

In the early 1970's, two theories of nonlinear gain phenomena in GaAs semiconductor diode lasers were reported in attempts to explain the static[37] and dynamic[38] spectral properties of semiconductor diode lasers. The theory of spectral hole burning[37] predicts a symmetric gain suppression about a lasing mode whereas the theory of anomalous interaction of spectral laser modes[38] predicts a nonlinear effect which is highly asymmetric. These theories provided the stimulus for many postulates regarding nonlinear gain effects and serve as a starting point for a survey of documented results.

Nishimura *et al* used a semiclassical density matrix formalism for electron-photon interactions to predict a gain decrease in a narrow spectral region centred about the optical frequency of the lasing mode.[37] The predicted width of the spectral hole was approximately one to two mode spacings and was dependent upon an assumed intraband relaxation rate. Relaxation rates of approximately 10^{-12} seconds were required to guarantee suppression of the non-lasing side modes at current levels of approximately 1.1 times the threshold current. Experimental verification of these results was not provided.

The density matrix formalism has been revised and extended in attempts to explain the spectral output of semiconductor lasers. For instance, it was found that for certain AlGaAs laser devices, the spectral output became increasingly single-moded as the

injection current was increased.[39] The extent to which the devices were single-mode was assessed by measuring only the intensity of the first short wavelength mode (i.e. the first mode on the short wavelength side of the strong single mode). This gain suppression effect could not be explained from a standard rate equation analysis of the device. A spectral hole burning theory was subsequently invoked to explain the observed spectral purity of these devices.[9,40] Intraband relaxation times of approximately 300 femtoseconds were required to model the longitudinal mode spectra. It should be noted that reduction of the first short wavelength mode is consistent with the shift of the gain peak toward longer wavelengths with increasing current injection. The first long wavelength mode should also have been measured in order to assess the extent to which the gain peak shift affected the mode intensities. Asada and Suematsu[41] also predicted gain suppression caused by spectral hole burning in InGaAsP devices. The prediction of increased single mode behaviour was also confirmed by measuring only the first short wavelength mode.

Several above-threshold spectra reported by Nakamura *et al*[39] exhibit a highly modulated mode profile. Modulated mode profiles were described in Chapter 2. Here it was shown that the shape of the mode profile could be explained by considering the effect of scattering centres and that the effects of nonlinear gain were not required to model accurately the above-threshold mode profiles.

A number of researchers have measured the gain recovery dynamics of semiconductor diode lasers in an attempt to relate material parameters to

phenomenological time constants associated with nonlinear gain mechanisms. Data obtained from pump-probe experiments of GaAlAs laser diodes using 100 fs optical pulses revealed that spectral hole burning effects must take place on a time scale much shorter than 100 fs.[42] These results do not support the phenomenological intraband relaxation time of 300 fs required by Yamada and Suematsu[9,40] to model the spectral output of GaAlAs devices. A carrier heating model was postulated to account for the observed gain dynamics.[42] Data obtained from a similar experiment using InGaAsP optical amplifiers and 180 fs optical pulses indicated that carrier heating, not spectral hole burning was the dominant nonlinear effect in this material.[43] The carrier heating effect is believed to contribute an asymmetric component to the nonlinear gain of a device.[11] Using 150 fs pulses, Mark and Mørk concluded that the effect of carrier heating and spectral hole burning make comparable contributions to gain nonlinearities in InGaAsP semiconductor diode lasers.[44] This result has been supported by Frankenberger and Schimpe from modulation spectroscopy measurements of InGaAsP diode lasers.[45] Surprisingly, Eom and Su measured the frequency response of InGaAsP semiconductor lasers and concluded that spectral hole burning was the dominant nonlinear gain mechanism.[46] The abundance of contradictory conclusions which have been reported indicates that measurements of the gain dynamics cannot isolate the principal mechanism for gain nonlinearities in semiconductor diode lasers.

A nonlinear gain mechanism in which a lasing mode causes changes in gain which differ in magnitude on the short and long wavelength sides of the mode, is referred

to as an asymmetric nonlinear gain mechanism. Bogatov *et al* used anti-reflection coated GaAs-AlGaAs lasers in an external cavity with two reflective diffraction gratings as optical feedback elements, and obtained lasing in two spectral modes.[38] A nonlinear interaction was observed which was dependent on the optical frequency spacing of the two modes as well as the position (in optical frequency space) of one mode relative to the other mode. It was found that the nonlinear interaction was strongest on the long wavelength side of a mode. It was postulated that the observed effects could be explained by dynamic variations in the electron density which result in variations of the complex dielectric constant. This theory was extended using a density matrix formalism to include three-mode interactions in semiconductor lasers by Kazarinov *et al* who postulated that a tendency to single mode operation in AlGaAs Fabry-Perot lasers was the result of both spectral hole burning and population beating.[10] Kazarinov *et al* noted that spectral hole burning leads to multi-mode oscillation[10] and not more single-mode oscillation as claimed by Yamada and Suematsu[9,40]. The population beating mechanism was required to obtain single-mode oscillation.[10] The density matrix formalism has been extended to a generalized multi-mode laser by Agrawal[47] who concluded that the intraband relaxation rate of 300 fs ensures that spectral hole burning is the dominant nonlinear gain mechanism. Interestingly, Sargent *et al*[48] also used a density matrix formalism for a multi-mode laser and concluded that population pulsations were as important as spectral hole burning. The differing conclusions for the generalized theory can be attributed to discrepancies in the assumed magnitudes of the relaxation rates.

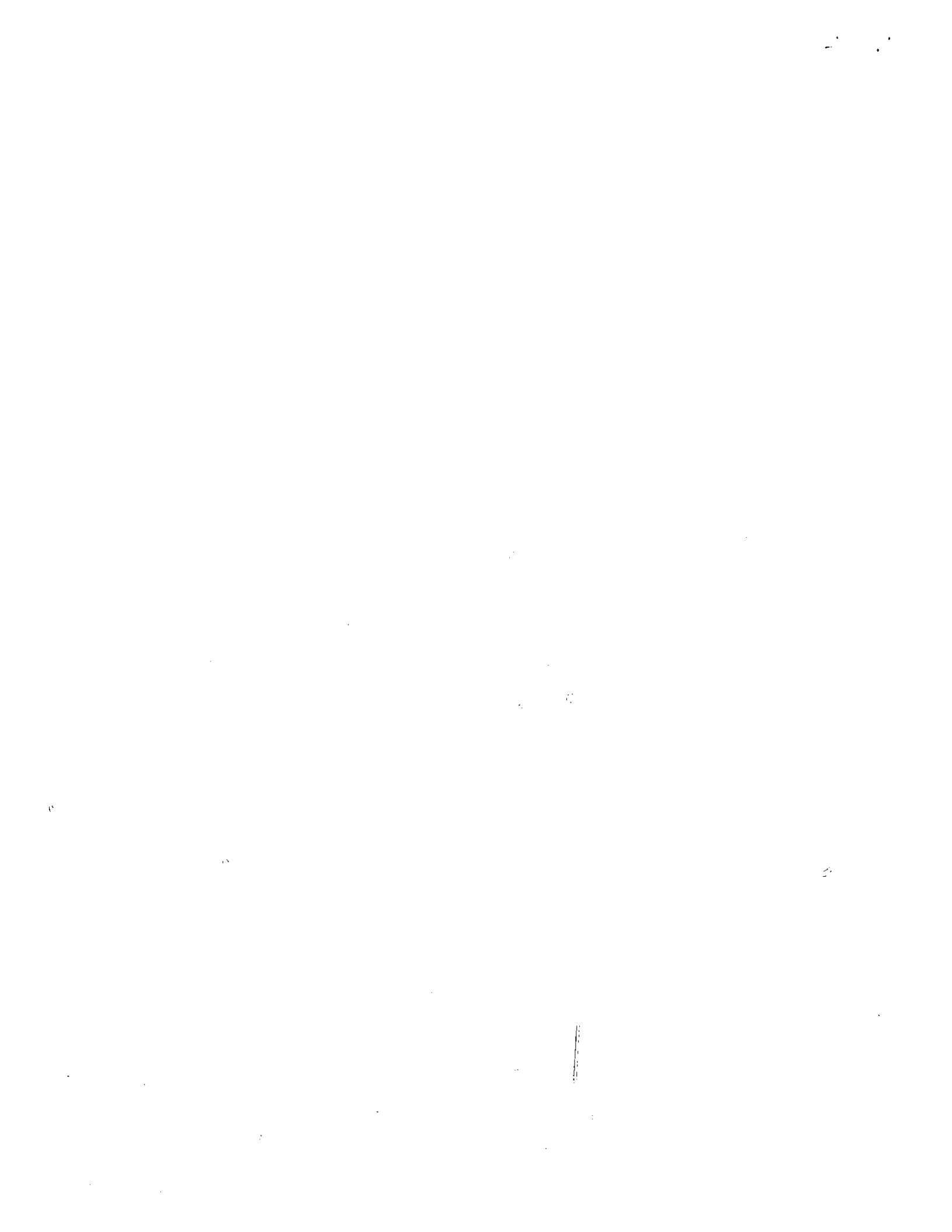
The presence of a dielectric grating owing to the cavity standing wave has also been proposed to explain asymmetric nonlinear gain in semiconductor lasers. Based upon measurements of the electrical frequency response of InGaAsP lasers, it has been postulated that the standing wave induces a refractive index grating along the axis of the device.[12,49] This effect is similar to the spatial hole burning mechanism in gas lasers and it differs from the population beating mechanism in that it is a spatial rather than a temporal effect. The dielectric grating effect has been disputed on two fronts. Since refractive index gratings are responsible for the mode properties of distributed feedback (DFB) devices, Lassen *et al* analyzed the Fabry-Perot laser as a DFB laser and found that the contribution of the dielectric grating to the nonlinear gain do not agree with experimental measurements of gain asymmetries.[50] It has also been suggested that carrier diffusion tends to remove the spatial holes caused by the cavity standing wave.[51]

Regardless of the governing physical mechanism, nonlinear gain is thought to play an important role in the dynamic properties of semiconductor diode lasers. One of the most important effects caused by nonlinear gain is a reduction in the modulation bandwidth of semiconductor diode lasers.[32,p.88] Channin was one of the first to postulate that gain saturation could explain the anomalously large damping of relaxation oscillations in certain semiconductor injection lasers.[52] Channin also noted that increased spontaneous emission into the laser mode (spontaneous emission factor) could account for increased damping of the relaxation oscillations.[52] Since the frequency and the damping rate of the relaxation oscillations determines the small signal modulation

bandwidth of semiconductor lasers,[32 p.86] considerable interest has been generated in the effect of nonlinear gain phenomena on the modulation response of devices. Studies of the frequency response of 1.3 μm InGaAsP devices indicate that nonlinear gain limits the modulation bandwidth to approximately 20 GHz.[53,54] Other dynamic characteristics which are thought to be affected by nonlinear gain include harmonic and intermodulation distortions[55] and optical frequency chirp.[32 p.119]

The references cited in this section do not comprise an exhaustive list of the mechanisms or effects of nonlinear gain in semiconductor diode lasers. Rather, the references reflect the author's estimation of seminal papers on the topics discussed. For the interested reader, reviews detailing nonlinear phenomena in semiconductor lasers are provided by Shore and McCall[56] and Petermann.[32]

None of the works cited in this section consider the effect of scattering centres in the active region of semiconductor diode lasers. It has been concluded from the results outlined in previous chapters that the shape of the below- and above-threshold mode envelope can be explained if the effect of scattering centres are included in an homogeneously-broadened model of semiconductor lasers. In attempts to explain the spectral output of diode lasers, nonlinear gain phenomena are often invoked in cases where the scattering centre postulate could account for the observed spectral output. Ignorance of the effect of scattering centres as a mode selection mechanism as well as the continuing controversy concerning the important gain saturation processes, leads one to ponder the existence of nonlinear gain phenomena. For this reason, a study of the



spectral characteristics of semiconductor diode lasers under high optical power operation was undertaken.

5.3 Predicted Results Excluding Nonlinear Gain

A semiconductor laser in a short-external-cavity (SXC) configuration has been used to provide a source operating in a single longitudinal mode with side-mode suppression ratios (SMSR) approaching those attainable with distributed feedback devices.[57,58] InGaAsP SXC lasers have been used as tunable sources in spectroscopic applications for the purposes of trace gas detection.[59] It was postulated that the single-mode characteristics of SXC lasers could be exploited in an experiment designed to probe possible effects resulting from nonlinear gain phenomena.

If the effects of nonlinear gain are important in determining the above-threshold spectral output of semiconductor diode lasers, it would be difficult to separate the effects caused by the individual modes in a multi-moded source. Proper alignment of a planar mirror in a short-external-cavity configuration results in resonant enhancement of a single longitudinal mode. The intense single-mode source should enable isolation of nonlinear gain phenomena for the solitary mode. The effects of nonlinear gain should be manifested as changes in the optical power of the side modes adjacent to the resonant mode. Careful measurement of the evolution of the power of the side modes with increasing injection current should provide the ability to: (i) confirm the existence of

nonlinear gain phenomena; and, (ii) assess the symmetry of the dominant nonlinear gain process. The wavelength dependence of nonlinear gain can also be studied by measuring the evolution of the side modes for a number of strong single modes within the intrinsic $R_m G_m$ profile of the semiconductor laser. An individual longitudinal mode can be selected and enhanced by altering the length of the short-external-cavity.

Before discussing the observations obtained using the experimental technique, it is worthwhile to consider the predicted evolution of the modes with increasing injection current for an SXC source without including the effects of nonlinear gain. Effects which can alter the shape of the modal evolution curve include: (i) drifts in the length of the external cavity resulting from variations in the position of the external mirror; (ii) wavelength tuning of the intrinsic $R_m G_m$ profile with temperature; and, (iii) variations in the amount of optical feedback provided by the external mirror. An understanding of the manifestation of these effects on the shape of the modal evolution curve facilitates the interpretation of the mode evolution curves derived from experimental measurements.

Figure 5.1 compares the predicted evolution of the modes with increasing injection current for a solitary device and a device incorporated into a short- external-cavity configuration. The optical powers in each of the longitudinal modes were calculated using a model for an homogeneously-broadened Fabry-Perot laser.[20] Figure 5.1(a) shows the predicted results for a solitary device assuming a spontaneous emission factor, β , of 10^{-3} . Incorporating a short-external-cavity configuration into the model as a sinusoidal variation of the facet reflectance with a period of 10 mode spacings,

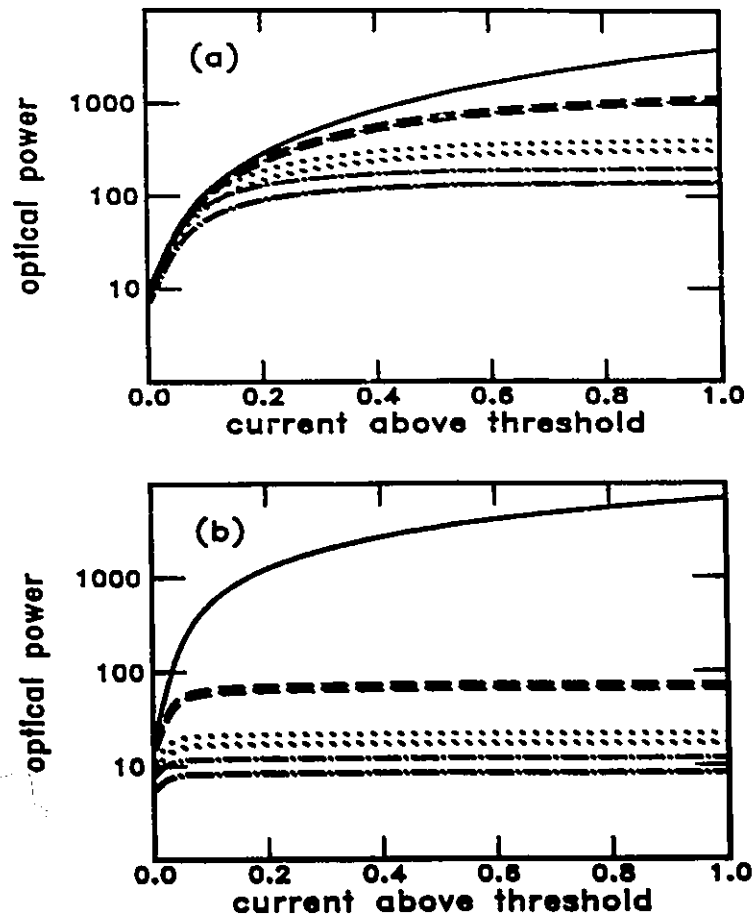


Figure 5.1

Predicted evolution of the optical power in the longitudinal modes for a solitary Fabry-Perot laser (a) and for the same device incorporated into a short- external-cavity configuration (b). The resonant mode is indicated by the solid line and the side modes are designated by the line styles: ± 1 (---), ± 2 (···) and ± 3 (-·-). In all cases, the side mode with the higher photon energy ($+n$) has a lower optical power than the corresponding mode with the lower photon energy ($-n$). The results shown in (b) for the short-external-cavity indicate a strong single mode source for which the optical power of the resonant mode is at least two orders of magnitude larger than that of the neighbouring side modes.

Fig. 5.1(b) indicates the predicted values of the mode powers. The peak-to-peak value of the reflectance modulation was chosen to be 0.02, based upon measurements of the near-field distribution of InGaAsP structures.[57] For the magnitude of reflectance modulation chosen, the most intense side modes (modes ± 1) are smaller than the resonant mode (mode 0) by approximately two orders of magnitude. Since the optical power in the resonant mode is much larger than that of the other side modes, nonlinear gain effects will be dominated by the optical power contained within the strong single mode.

The series of graphs shown in Figure 5.2 indicate predictions of the shape of the mode evolution curves for a variety of effects other than nonlinear gain for an SXC laser. The resonant mode power is not indicated in any of the graphs since, in each case, the evolution of the resonant mode with injection current differs by only about 1 percent from the curve in Fig. 5.1(b). The graph shown in Fig. 5.2(a) illustrates the effect of a small drift in the length of the external cavity. The external-cavity length was allowed to vary linearly with the injection current. At the maximum current value, it was assumed that the modulation of the facet reflectance resulting from the external-cavity moved toward shorter wavelengths by approximately 1/3 of a laser mode spacing. Figure 5.2(a) indicates that an external-cavity length which decreases with drive current results in an enhancement of optical power in the shorter wavelength modes and a corresponding reduction of the power in the longer wavelength modes.

Using a similar method as for the drift in the external cavity length, the predicted effect of the tuning of the intrinsic $R_m G_m$ profile toward longer wavelengths

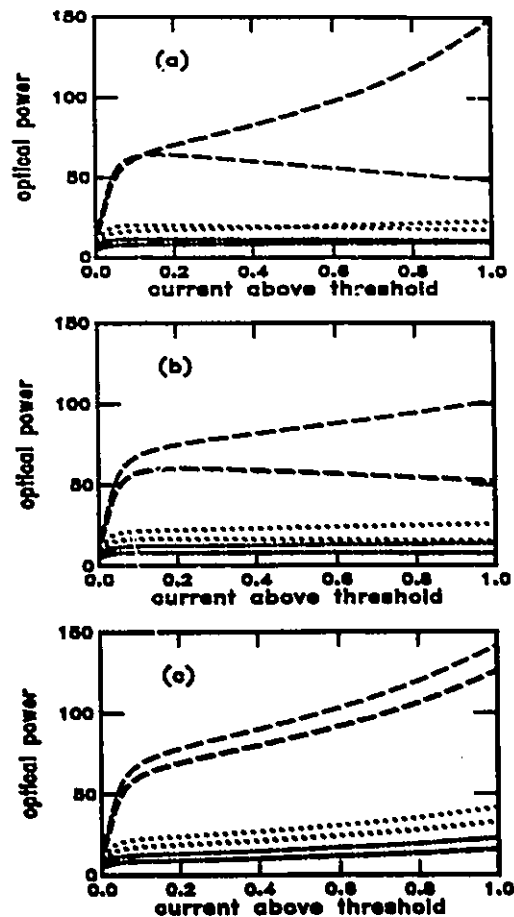


Figure 5.2

Predicted evolution of the optical power in the side modes of a short-external-cavity laser for a variety of effects. The side modes are designated by the line styles: ± 1 (---), ± 2 (···) and ± 3 (-·-). The predicted effect of a small decrease in the external cavity length is shown in (a). An increase (decrease) in the optical powers of the short (long) wavelength modes is indicated. The effect of the wavelength tuning of the gain peak with current, shown in (b), results in a predicted increase (decrease) in the optical powers of the long (short) wavelength modes. Increases in the optical powers of both the short and long wavelength side modes are indicated in (c) for a decrease in the amount of optical feedback provided by the external mirror.

with increasing current is shown in Fig. 5.2(b). For this graph, it was assumed that the peak of the $R_m G_m$ profile was centred on the resonant mode at the threshold current. The peak was then allowed to tune linearly with the current to a final position of three mode spacings (toward longer wavelengths) at the maximum current value. The result of the shift of the $R_m G_m$ profile is an increase of the optical powers in the longer wavelength modes and a corresponding reduction of the powers in the shorter wavelength modes. If the external mirror was not providing optical feedback into the active region, the magnitude of the gain peak shift used in the model would result in mode -3 becoming the strongest mode at the largest current value. However resonant enhancement of the longitudinal modes by the external cavity configuration tends to mask the effects of the wavelength tuning of the intrinsic $R_m G_m$ profile.

The effect of a decrease in the amount of optical feedback provided by the external mirror with increasing injection current is shown in Fig. 5.2(c). The peak-to-peak amplitude of the reflectance modulation resulting from the external cavity was assumed to vary linearly between 0.02 at threshold to a value of 0.01 at the highest current level. Simultaneous, supralinear increases in the optical powers of both the short and long wavelength modes are indicated.

The predicted mode evolution curves shown in Fig. 5.1 and Fig. 5.2 will serve as references for the following section to facilitate interpretation of curves derived from measured values of the optical powers in the longitudinal modes.

5.4 Experimental Technique

Figure 5.3 is a schematic diagram of the experimental configuration used to measure the effects of nonlinear gain on the optical powers in the longitudinal modes of an SXC diode laser. Separation and measurement of the intensity of the individual longitudinal modes is accomplished using a configuration similar to that described in Chapter 2 and depicted in Fig. 2.2. The only major difference in the experimental arrangements was the addition of a negative feedback loop to maintain the alignment of the short-external-cavity.

The planar mirror (PM) which provided the optical feedback necessary for resonant enhancement of the longitudinal modes was attached to a piezoelectric stack. The length of the short-external-cavity was altered by translating the planar mirror using a high voltage power supply (Lansing Lock-In Stabilizer). The power supply controlled the extension of the piezoelectric stack and provided single-mode operation for up to approximately 10 different longitudinal modes within the intrinsic $R_m G_m$ profile of the semiconductor diode laser. A bias tee was constructed which allowed the capability of superimposing a low frequency (1 kHz) AC modulation upon the high voltage DC bias applied to the piezoelectric stack.

The length of the external-cavity was susceptible to drifts caused by temperature fluctuations or mechanical instabilities. These drifts resulted in mode hops or fluctuations in the optical power of the resonant mode. Wavelength-tuning of the gain

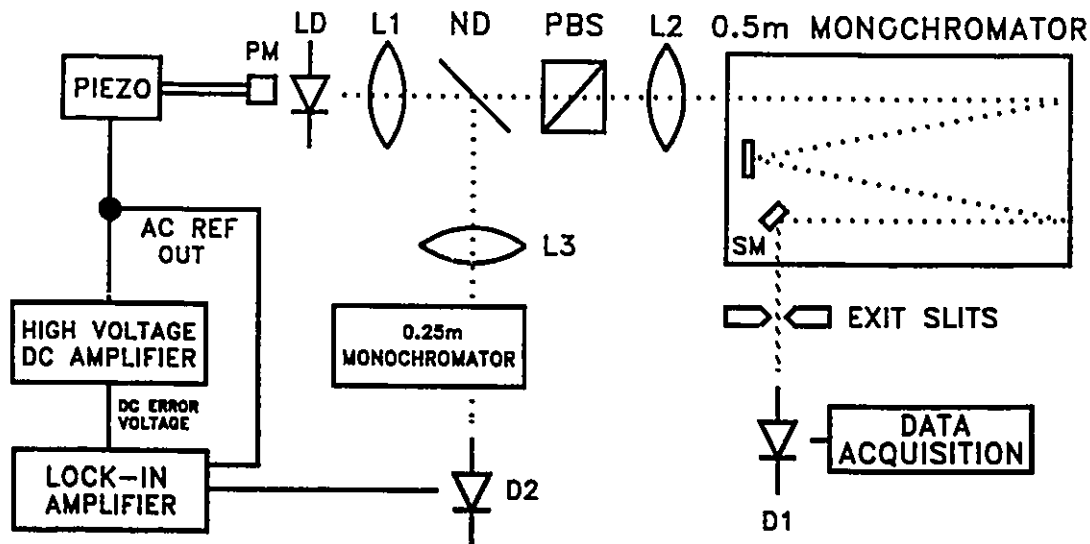


Figure 5.3

Schematic diagram of the experimental apparatus used to monitor the effects of nonlinear gain on the spectral output of SXC diode lasers. The emission spectrum was resolved by the 0.5-metre monochromator for measurement of the mode powers. The portion of the beam reflected from the neutral density filter (ND) was used in conjunction with the 0.25-metre monochromator to provide a feedback signal to the piezo for stabilization of the resonant mode power.

peak with the injection current also necessitated a correction to the length of the external-cavity in order to maintain lasing in the desired mode. The capability to modulate the external-cavity length was exploited in a feedback configuration to provide stability of the desired resonant mode. The neutral density filter (ND) shown in Fig. 5.3 reduced the deleterious effects of feedback from the optical elements and the reflection from the air-glass interface provided a small portion of the beam for locking purposes. The reflected portion of the beam was focused into a 0.25-metre monochromator (entrance slit removed)

using an AR-coated $f/1$ lens (L3). The neutral density filter was fixed to a mirror mount to optimize alignment of the beam into the monochromator. It was found that 100- μm wide exit slits on the 0.25-metre monochromator provided sufficient wavelength dispersion to yield an adequate signal to discriminate between longitudinal modes while capturing most of the optical power contained in the resonant mode. Smaller exit slits would provide better wavelength dispersion at the expense of an increased loop sensitivity to small changes in the wavelength of the resonant mode. The wavelength of the resonant mode changed with increased current injection and it was found that for smaller exit slits, the lock to the resonant mode could not be maintained over the desired current range. (An obvious improvement to the locking portion of the experiment would be to equip the 0.25-metre monochromator with a scanning mirror assembly. An additional feedback system could provide the ability to track accurately the position of the peak wavelength of the resonant mode by application of a correction signal to the scanning mirror electronics.) The signal from the detector (D2) placed at the exit slit was used as input to a lock-in amplifier which was referenced to the AC signal applied to the piezoelectric stack. The DC correction signal from the lock-in amplifier was applied to the external input port on the high voltage power supply, completing the negative feedback loop. The lock-in amplifier was used in an integration mode to reduce offsets in the DC correction signal.

With the feedback loop operating, the data acquisition procedure involved measurement of the peak optical power of the resonant mode and the three modes on

either side of the resonant mode (7 total modes), as a function of the above-threshold injection current. The emission spectra were resolved using the 0.5-metre monochromator with 50- μm wide entrance and exit slits. The procedure for acquiring the mode powers at a given injection current is subsequently described. For each of the seven modes, seven measurements of the optical power as a function of wavelength in the vicinity of the mode peak were collected. A quadratic fit to the seven points was then used to calculate the wavelength and the optical power of each of the seven mode peaks. (The seven measurements of the optical power for each mode peak were centred about the peak wavelength calculated at a previous injection current level.) The injection current was subsequently increased by a small amount (typically 1 mA) and the acquisition procedure was repeated. It should be noted that for all measurements made on the modes, conventional lock-in amplifier techniques (time constant ~ 100 ms) were used to enhance the detection sensitivity. The injection current range was typically between 30 and 80 mA, dependent on the ability of the feedback loop to maintain the desired single mode behaviour. The initial value of the injection current was typically chosen to be in the vicinity of the threshold current.

Figure 5.4 indicates the evolution of the total optical power, the peak resonant mode power and the peak side mode powers with increased above-threshold injection current for laser X, an index-guided device. It can be seen from Fig. 5.4(a) that for current levels greater than approximately 40 mA above threshold, the peak power of the resonant mode saturates. The total optical power was measured by placing a large area

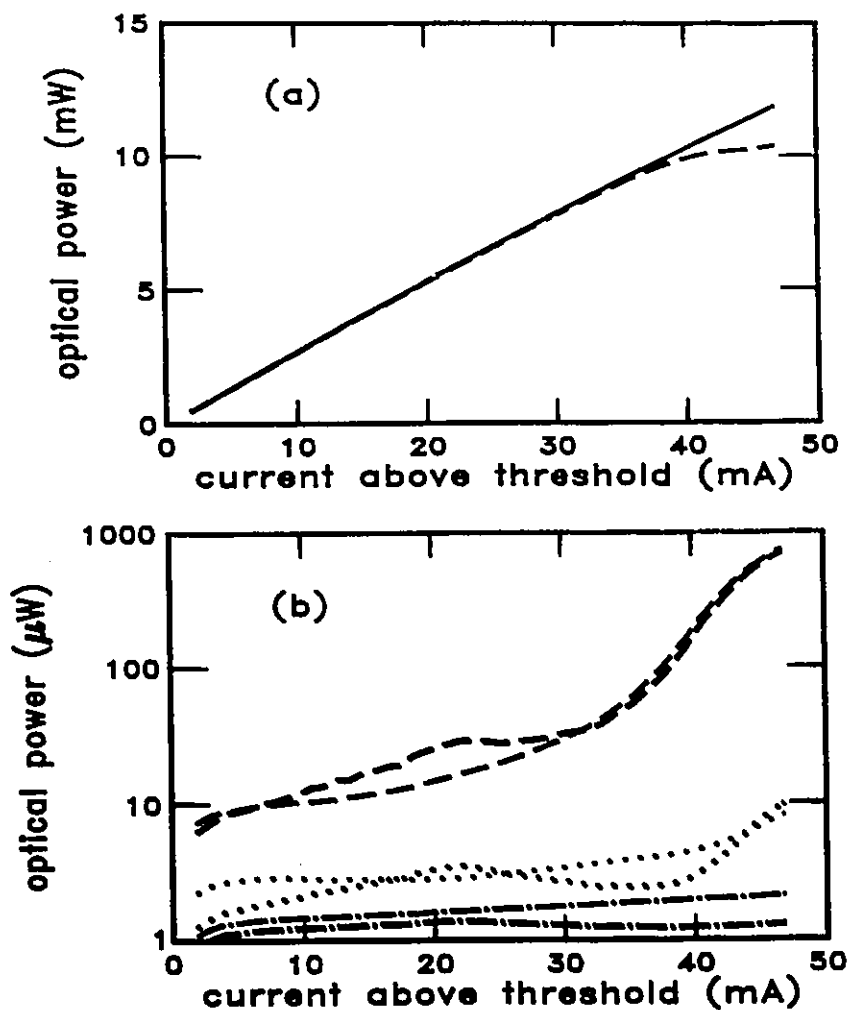


Figure 5.4

The evolution of the mode powers with increasing injection current for laser X. The total optical power (solid line) and the optical power of the resonant mode (dashed line) are shown in (a). The evolution of the optical power of the side modes is shown in (b). The side modes are designated by the line styles: ± 1 (---), ± 2 (···) and ± 3 (-·-).

(1 cm diameter) germanium detector in close proximity to the front laser facet. The total power varies almost linearly with the injection current, indicating that the optical power is being partitioned amongst the side modes as the power in the resonant mode saturates. (A decrease in the total power was often indicative of a hop to a mode greater than three mode spacings from the single mode of interest, which frequently occurred at the bounds of the free spectral range of the external cavity.) Using the same mode numbering convention as in previous chapters, Fig. 5.4(b) indicates the evolution of the peak side mode powers. The increase in the peak power of the resonant mode [mode 0 shown in Fig. 5.4(a)] coincides with a supralinear increase in the peak power of the +1 and -1 side modes. For all current values, the magnitudes of the +1 and -1 side mode powers are very similar. It is also observed that the peak intensities of the +2 and -2 side modes increases slightly with increasing injection current. (It should be noted that all of the curves displayed in this section were subjected to a 5-point sliding average to remove small ripples presumably caused by perturbations in the length of the external cavity.)

The results for another index-guided device (laser D) are shown in Figure 5.5. The variation of the peak resonant mode power with injection current shown in Fig. 5.5(a) indicates that, after reaching the current value of approximately 37 mA above-threshold, the peak power of mode 0 begins to decrease. The curve for the total optical power shown in Fig. 5.5(a) indicates that this quantity continues to increase over the entire range of current values. Figure 5.5(b) shows the evolution of the peak side mode powers with increasing injection current for the current range of 19 to 37 mA above-threshold. This

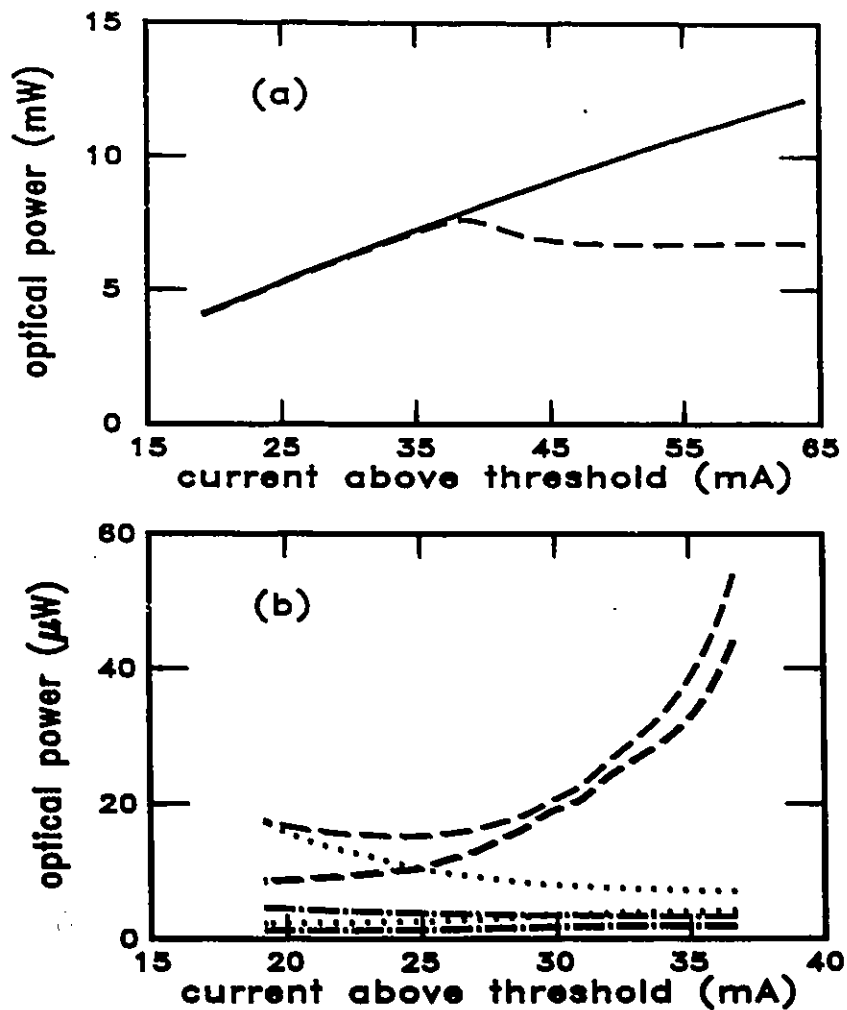


Figure 5.5

The evolution of the mode powers with increasing injection current for laser D. The total optical power (solid line) and the optical power of the resonant mode (dashed line) are shown in (a). The evolution of the optical power of the side modes for the linear region of the resonant mode power is shown in (b). The side modes are designated by the line styles: ± 1 (---), ± 2 (···) and ± 3 (-·-). The decrease in the powers of the -2 and -3 side modes is consistent with a small decrease in the external cavity length.

is the current region for which the peak power of mode 0 increases approximately linearly. The peak power of modes -1 and +1 are similar in magnitude over the current range and show a supralinear increase as the peak power of mode 0 increases. This result is similar to that obtained for laser X as shown in Fig. 5.4(b). For the higher numbered side modes (± 2 and ± 3), Fig. 5.5(b) indicates that the peak powers of the longer (shorter) wavelength side modes decrease (increase) with increasing injection current, which is consistent with a small decrease in the external cavity length [c.f. Fig. 5.2(b)].

The increase of the peak optical powers of both the +1 and -1 modes for laser D and laser X are difficult to be explain without invoking nonlinear gain phenomena. As indicated in Fig. 5.2(c), a symmetric and simultaneous increase of the powers of the ± 1 modes could result if the amount of light fed back into the cavity by the external mirror was reduced. This effect would be consistent with an increase in the angular width of the near-field light distribution with an increase in the current. This postulate was rejected for three reasons. Firstly, a reduction in optical feedback would be manifested as a simultaneous and symmetric increase in the peak optical power of each side mode [c.f. Fig. 5.2(c)]. Symmetric increases in the powers of the higher order modes (modes ± 2 and ± 3) were not observed experimentally. Secondly, measurements of the far-field patterns of InGaAsP planar-buried-heterostructure devices indicate no appreciable increase in the angular width of the output light distribution for powers up to 30 mW per facet.[60] In addition, measurements of the far-field pattern for laser X indicated no appreciable increase in the angular width of the far-field light distribution for currents up to 50 mA

above threshold.[61]

The relationship between the shape of the mode evolution curves and the amount of optical feedback provided by the external mirror is shown in Figure 5.6. Data for this figure was accumulated by measuring the mode evolution curve for a given resonant mode of laser D. The external cavity was then cycled through a number of free spectral ranges until the same resonant mode was excited. The mode evolution curve was subsequently measured and the process was repeated to generate three different mode evolution curves for the same resonant mode. Fig. 5.6(a) indicates the total optical power and peak resonant mode power (mode 0) for each of the three different lengths of the external cavity. The curves which display the total optical powers are nearly identical over the entire current range, but the evolution curves for the resonant modes indicate that the current level at which the peak power of this mode begins to decrease are different, depending on the length of the external cavity. The corresponding peak powers of the side modes for the current range of 19 to 37 mA above threshold are indicated in Fig. 5.6(b). The general features of each of the graphs are reproducible, in that there is a simultaneous and symmetric increase of the ± 1 modes. However, for the same above-threshold current level, the ± 1 modes do not attain the same peak optical powers.

From the results displayed in Fig. 5.6, it is concluded that differences in the amount of optical feedback from the planar mirror are responsible for the observed differences in the peak optical powers attained by the ± 1 side modes. Any effects on the peak mode powers caused by nonlinear gain phenomena must compete with the mode

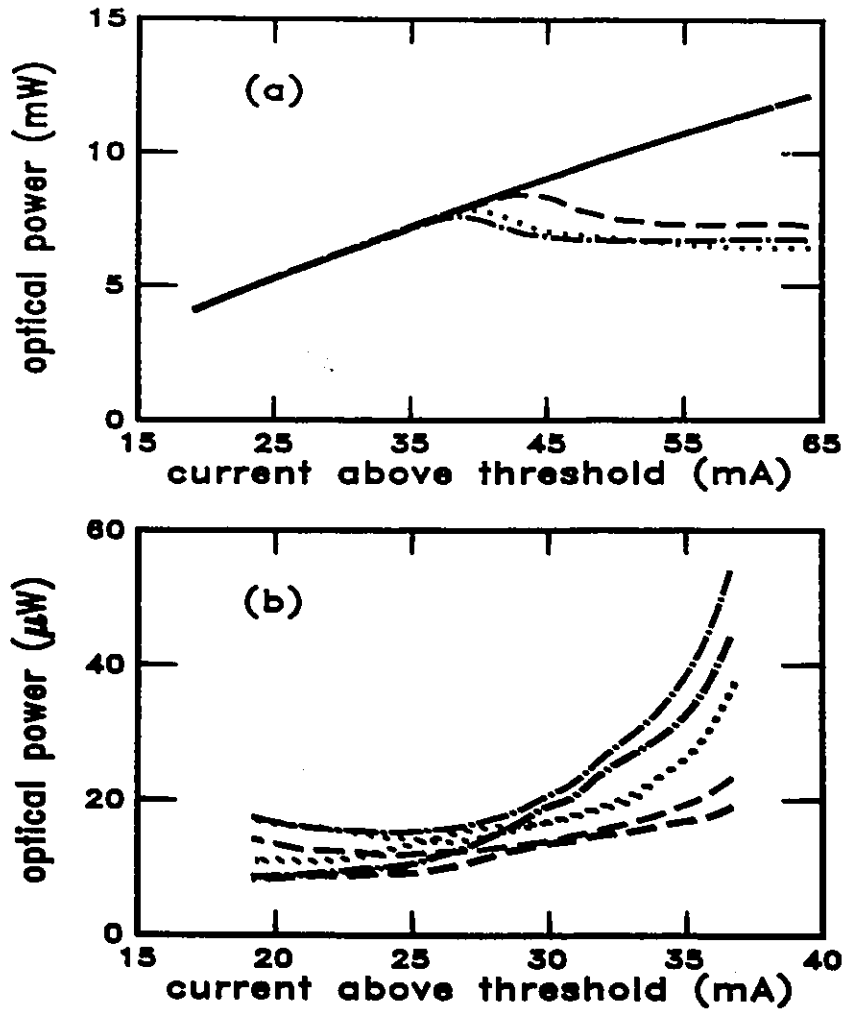


Figure 5.6

The mode evolution curves obtained by cycling through a number of free spectral ranges of the external cavity to excite the same resonant mode of laser D. The total optical power (solid line) and the optical power of the resonant mode for three different external cavity lengths are shown in (a). The evolution of the optical power of the ± 1 side modes for each of the three external cavity lengths is shown in (b). Identical line styles in (a) and (b) indicate measurements obtained at the same external cavity length.

selective effects provided by the short-external-cavity. A large amount of optical feedback would tend to mask the effects of nonlinear gain phenomena in altering the shape of the mode evolution curves. This conclusion was verified using an additional device, for which a careful alignment of the planar mirror resulted in no increase in the peak optical powers of the ± 1 side modes over a large range of current values. Deliberate misalignment of the planar mirror decreased the amount of optical feedback and resulted in the appearance of symmetric increases in the peak powers of the ± 1 side modes.

The ability to provide an indication of the optical powers required to stimulate the onset of nonlinear gain effects in an SXC laser would necessitate an accurate measurement of the feedback efficiency of the short-external-cavity. Although techniques for measurement of the optical feedback have been reported,[62] the amount of optical feedback in an SXC configuration is a difficult parameter to measure and this problem is left for further study.

The mode selective characteristics of the SXC configuration afforded the opportunity to measure mode evolution curves for a number of resonant modes lying within one free spectral range of the external cavity. The motivation for making these measurements was to examine the wavelength dependence of nonlinear gain effects. In addition, it has been suggested that the asymmetric component of the nonlinear gain is related to the slope of the gain profile in the vicinity of the strong lasing mode.[47] The effects of the gain slope were calculated to be particularly important for the side mode characteristics of distributed feedback devices.[47]

Figure 5.7 shows the results of the measurements of mode evolution curves for three different resonant modes of laser H, an index-guided device. The peak of the intrinsic $R_m G_m$ profile was determined to be the centre of the free spectral range of the external cavity at the lowest current value. The lower and higher wavelength resonant modes were chosen to be symmetrically spaced by 4 mode spacings about the resonant mode nearest the peak of the $R_m G_m$ profile. The total optical powers and the peak optical powers of the resonant modes as a function of the above-threshold current are shown in Fig 5.7(a). Saturation of the peak power was only detected for the resonant mode situated nearest the peak of the intrinsic $R_m G_m$ profile. The peak optical powers of the ± 1 side modes associated with each resonant mode are shown in Fig. 5.7(b). Increases in the peak optical powers of all the ± 1 side modes are indicated, although the side modes associated with the resonant mode nearest the peak of the $R_m G_m$ profile shows the greatest increase in optical power. The results shown in Fig. 5.7 indicate that there are no observable asymmetries in the mode evolution curves which can be directly attributed to the slope of the intrinsic $R_m G_m$ profile. The mode evolution curves for only three of the available resonant modes within the free spectral range of the external cavity are shown in Fig. 5.7. It should be noted that all nine available resonant modes were measured and there was no discernible wavelength dependence associated with either the saturation characteristics of the power in the resonant mode or the increases in the peak powers of the ± 1 side modes. For instance, the peak optical powers of the resonant modes spaced at -3, -1 and 0 mode spacings from the peak of the $R_m G_m$ profile (at the threshold current)

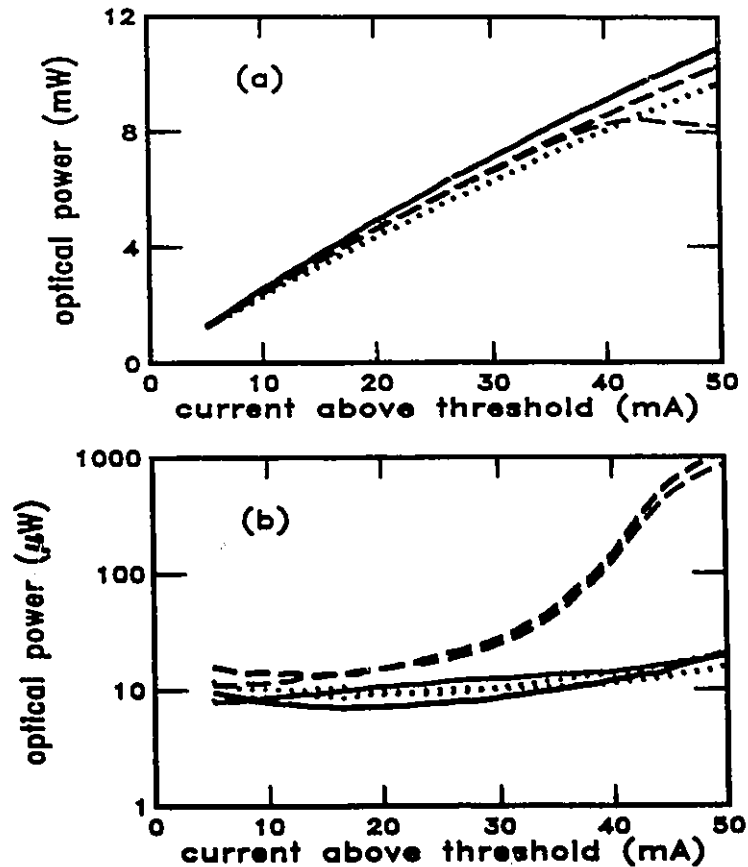


Figure 5.7

The mode evolution curves obtained for three different resonant modes within the intrinsic $R_m G_m$ profile of laser H. The total optical power and the optical power of the resonant mode nearest the peak of the $R_m G_m$ profile (at the lowest current level) are indicated in (a) by the dashed curves. The optical power of this resonant mode begins to saturate as the current increases. The solid and dotted lines in (a) indicate the total optical power and the optical power of resonant modes at four mode spacings to the long and short wavelength side, respectively, of the resonant mode designated by the dashed line. The evolution of the optical power of the ± 1 side modes corresponding to each of the three resonant modes is shown in (b). Identical line styles in (a) and (b) indicate measurements obtained for the same resonant mode.

showed saturation effects while the effect was absent in the other resonant modes.

The results depicted in Fig. 5.6 suggest that saturation of the resonant mode power depends upon the amount of optical feedback from the external mirror. The results discussed in Chapter 2 indicated that optical feedback due to the presence of scattering centres in the active region affects the spectral output of diode lasers through resonant enhancement of selected modes. Thus, an attempt was made to correlate the measured wavelength dependence of the modulations in the below-threshold $R_m G_m$ profile (the characteristic residue) of laser H with the saturation characteristics of the resonant modes for the same device in an SXC configuration. A significant correlation was not achieved, and further measurements are required to determine the role of scattering centres in masking the appearance of nonlinear gain effects in SXC lasers.

The experimental procedure to measure the effects of nonlinear gain phenomena for diode lasers in an SXC configuration was applied to six different index-guided devices. Some of the results for three of the devices have been shown in previous figures. Difficulties were experienced with one of the devices (laser Y) in that the feedback efficiency of the external mirror seemed to be consistently high. Deliberate misalignment of the cavity was attempted, but a strong resonant mode was always obtained, precluding potential increases in the side modes due to nonlinear gain effects. Attempts were also made to measure mode evolution curves for two gain-guided devices. Unfortunately, the sensitivity of the gain peak tuning to current for both devices was very high and the negative feedback loop could not lock to a resonant mode over a useful

current range.

The mode evolution curves for the five index-guided devices were carefully compared and contrasted. Patterns in several parameters were studied including the saturation characteristics of the peak optical power of the resonant mode and the magnitudes of the peak powers attained by the side modes. Patterns in these characteristics for the available resonant modes within one free spectral range of the external cavity were also sought. A number of important similarities in the mode evolution curves were observed. For all the resonant modes tested (within one free spectral range of the external cavity), for all the devices, simultaneous and symmetric increases in the peak optical powers of the +1 and -1 side modes were observed. The variations in the magnitudes of power increases of the ± 1 side modes, which is related to the amount of resonant optical feedback (c.f. Fig. 5.6 and Fig. 5.7), were such that no discernible patterns could be found. For approximately 75 percent of the resonant modes measured, some saturation effects were revealed, although the optical power of the resonant mode at the onset of saturation varied without a discernible pattern for modes tested in a given device and from device to device. For those resonant modes measured within one free spectral range of the external cavity, variations of the mode evolution curves associated with a wavelength dependence of the nonlinear gain effect were not observed. The only other general observation which could be made was that for approximately 50 percent of those resonant modes which showed saturation effects, the shorter wavelength side modes (modes +2 and +3) increased considerably after the onset

of saturation of the power in the resonant mode. The increase in these side modes could be due to a drift in the length of the external cavity [c.f. Fig. 5.2(a)].

Although specific numbers regarding the magnitude of nonlinear gain phenomena were not obtained from this experiment, clear evidence of a symmetric nonlinear gain mechanism was revealed. In the following section, a phenomenological nonlinear gain term is added to the model of an homogeneously-broadened semiconductor diode laser[20] in an attempt to explain the general shape of the mode evolution curves obtained in the experiment.

5.5 Model of Symmetric Nonlinear Gain

From the results of the experiment highlighted in the previous section, the most important general observation derived from the mode evolution curves of the index-guided devices, was that an increase in the optical power of the resonant mode resulted in simultaneous and symmetric increases in the powers of the ± 1 side modes. These observations can not be explained without invoking the prospect that nonlinear gain effects are responsible for the increases in the optical powers of the ± 1 side modes. Since the power increase in the ± 1 side modes was symmetric, the obvious candidate to explain the increase is a spectral hole burning mechanism.

In Chapter 2, a model of an homogeneously-broadened semiconductor diode laser[20] was used to predict the above-threshold spectral output of selected devices.

Nonlinear gain mechanisms were not required to model the measured results and the normalized material gain profile took the form of a Lorentzian:

$$g_m = \frac{1}{1 + \left(\frac{m}{\alpha_1}\right)^2} \quad (5-1)$$

In this equation, g_m is the material gain for mode number m and α_1 is the number of modes contained within one half-width of the Lorentzian. The value of α_1 is reported to be approximately 45,[20] although it was found in Chapter 3 that this parameter could assume a range of values between 10 and 50 with a mean value of approximately 30. In order to incorporate the spectral hole burning mechanism into the existing model, a gain suppression term linear in the mode power was added to the expression for the gain profile. The resulting expression for the gain profile becomes:

$$g_m = \frac{1}{1 + \left(\frac{m}{\alpha_1}\right)^2} - \sum_{i=-\infty}^{\infty} \left(\frac{\alpha_2 I_i}{1 + \left(\frac{m-i}{\alpha_3}\right)^2} \right) \quad (5-2)$$

where I_m is the optical power of the m^{th} mode and α_2 characterizes the depth of the Lorentzian hole of half-width α_3 . The summation in the gain suppression term allows for the gain at mode m to be affected by the holes burned by each individual mode. The Lorentzian form closely approximates the gain suppression profile calculated by Asada and Suematsu.[41] The numerical techniques required to solve the coupled system of nonlinear equations describing the mode powers are discussed in Appendix B.

The results of incorporating a gain suppression term in the homogeneously-broadened model of an SDL in a short-external-cavity configuration are shown in Figure 5.8. The SXC was modelled as a sinusoidal variation of the facet reflectance with a period of 10 mode spacings and a peak-to-peak value of 0.02.[57] The value of the spontaneous emission factor, β , was chosen to be consistent with the value used in Chapter 2 to model the above-threshold spectral output of diode lasers. Values of the parameters α_2 and α_3 which characterize the depth and width of the spectral hole were chosen to be $\alpha_2=5 \times 10^{-6}$ and $\alpha_3=1$. The evolution of the resonant mode and the total optical power with increasing injection current are shown in Fig. 5.8(a). Saturation of the optical power in the resonant mode is indicated although the total optical power remains linear throughout the current range. The total optical power was calculated by summing the optical powers of the seven modes analyzed in the model. The evolution of the side modes displayed in Fig. 5.8(b) shows a simultaneous and symmetric increase of the power in the ± 1 side modes, as well as small increases in the power of both the ± 2 and ± 3 modes. The predicted results displayed in this figure are representative of measured mode evolution curves, examples of which are shown in Fig. 5.4 through Fig. 5.7.

Figure 5.9 and Figure 5.10 indicate predicted mode evolution curves for various values of the depth and width of the spectral hole. The effect of the depth of the spectral hole, shown in Fig. 5.9, determines the characteristics of the saturation of the power in the resonant mode as well as the magnitude of the optical power attained by the ± 1 side modes. For an increased spectral hole depth, the ± 1 side modes will attain a

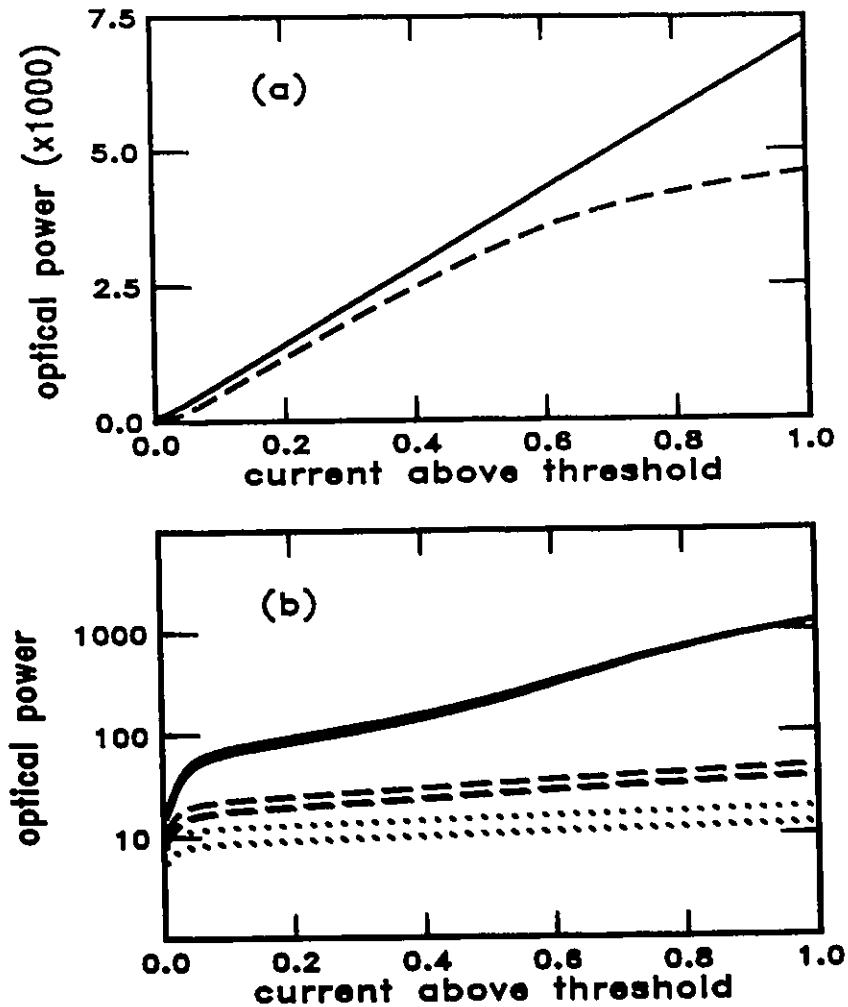


Figure 5.8

The predicted effect of a symmetric nonlinear gain mechanism on the evolution of the mode powers for a short external cavity laser. The depth (α_2) and width (α_3) of the spectral hole were characterized by $\alpha_2=5 \times 10^{-6}$ and $\alpha_3=1$. The total optical power and the optical power of the resonant mode are indicated in (a) by the solid and dashed lines respectively. The optical power of the side modes are designated by the line styles: ± 1 (solid), ± 2 (dashed) and ± 3 (dotted).

higher optical power level at the expense of the power in the resonant mode. The dependence of the shape of the mode evolution curve on the width of the spectral hole is indicated in Fig. 5.10. For a given spectral hole depth, an increase (decrease) of the width of the spectral hole, decreases (increases) the effects of the nonlinear gain mechanism on the shape of the mode evolution curves.

It is recalled from the survey of documented results in Section 5.2 that the width of the spectral hole was reported to depend upon the intraband relaxation rate.[9,37,40] The results presented in Fig. 5.10 indicate that nonlinear gain will affect the longitudinal mode spectrum regardless of the width of the spectral hole. For a spectral hole with a large width α_3 , an increase in the depth of the spectral hole α_2 will ensure saturation of the resonant mode power and the resultant increases in the power of the ± 1 side modes, although the rate of increase of the side mode power is dependent on the hole width. In other words, the mere presence of an inhomogeneous gain saturation caused by the spectral hole burning mechanism will guarantee increased multi-mode behaviour of semiconductor diode lasers at large optical power levels.

It is interesting to note that other theories of spectral hole burning[9,40,41] predict an increased single-mode operation rather than the increased multi-mode operation predicted by the model advanced in this section. However, Petermann reports that strong hole burning for light output powers above 5 mW results in an increased multi-mode behaviour of diode lasers,[32,p.76] which is consistent with the measured and predicted results discussed in this chapter.

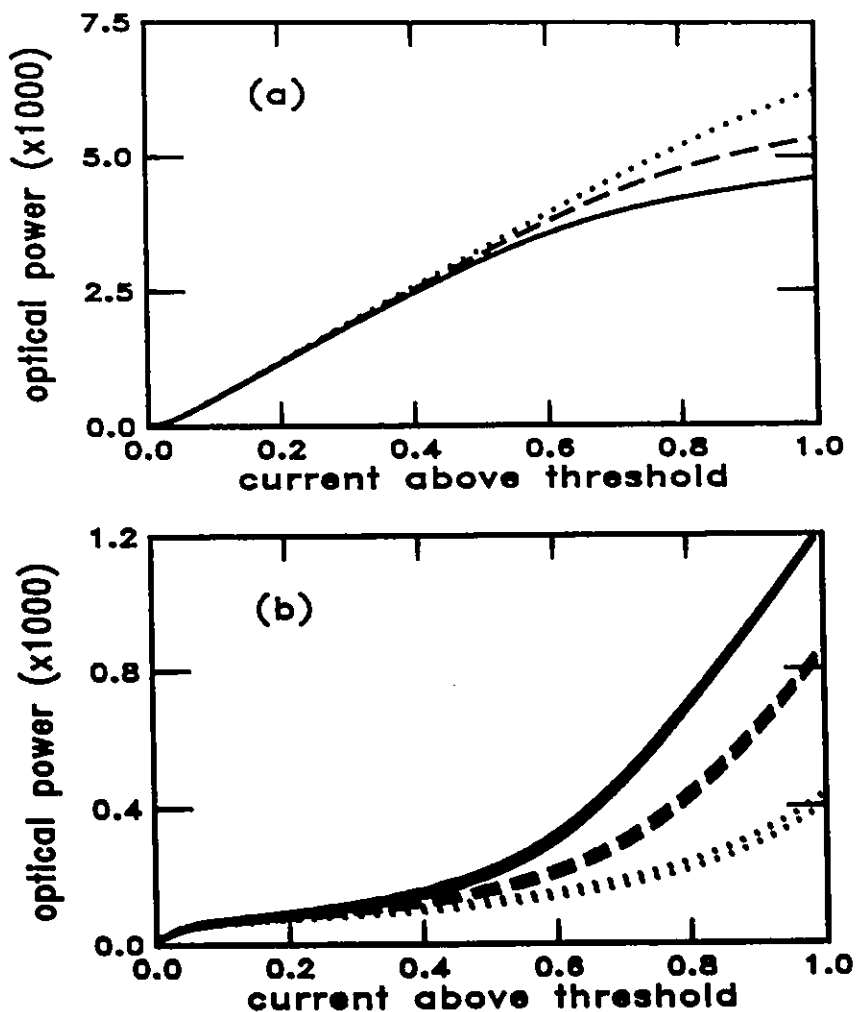


Figure 5.9

The predicted effect of a spectral hole burning mechanism on the evolution of the mode powers for various values of the hole depth α_2 . The width, α_3 , of the spectral hole was held constant at $\alpha_3=1$. The optical power of the resonant mode for hole depths of $\alpha_2=5 \times 10^{-6}$, $\alpha_2=4 \times 10^{-6}$ and $\alpha_2=3 \times 10^{-6}$ are indicated in (a) by the solid, dashed and dotted lines respectively. The optical powers of the ± 1 side modes are indicated in (b). Identical line styles in (a) and (b) indicate predictions based on the same value of the parameter α_2 .

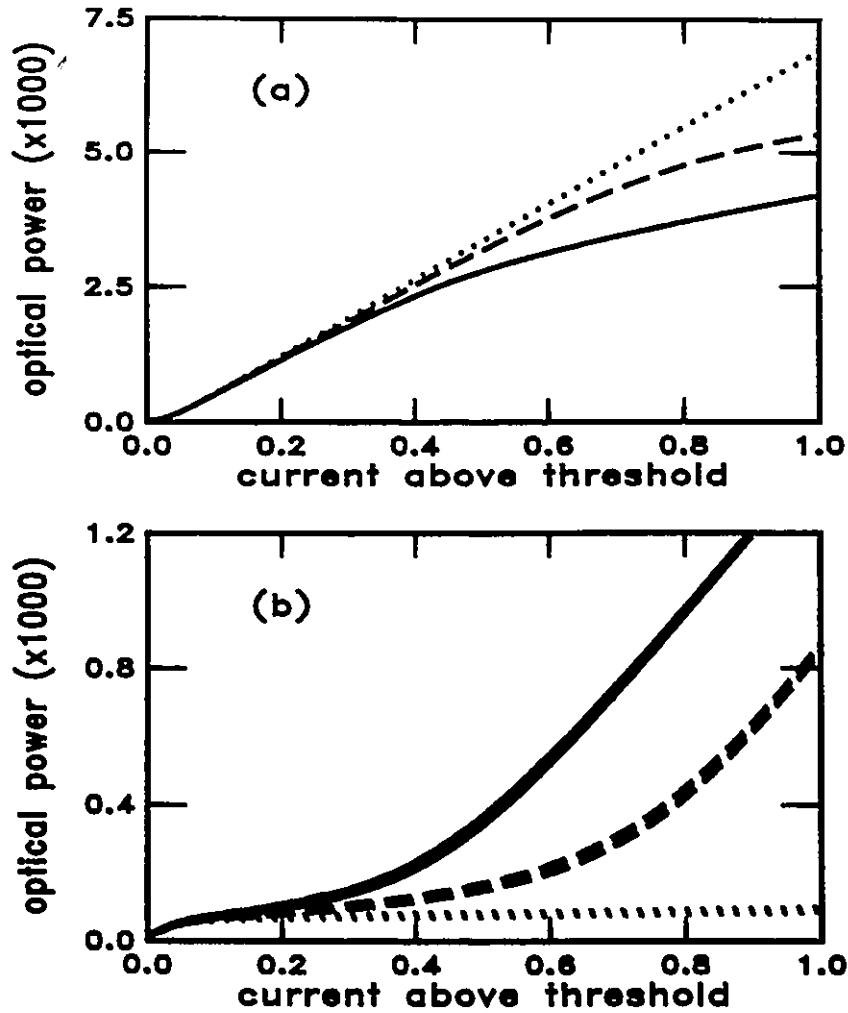


Figure 5.10

The predicted effect of a spectral hole burning mechanism on the evolution of the mode powers for various values of the hole width α_3 . The depth, α_2 , of the spectral hole was held constant at $\alpha_2=4 \times 10^{-6}$. The optical power of the resonant mode for hole widths of 0.1, 1 and 10 are indicated in (a) by the solid, dashed and dotted lines respectively. The optical powers of the ± 1 side modes are indicated in (b). Identical line styles in (a) and (b) indicate predictions based on the same value of the parameter α_3 .

The predicted effect of the competition between spectral hole burning and the amount of optical feedback from the external mirror in determining the evolution of the longitudinal mode structure of a diode laser in an SXC configuration are indicated in Figure 5.11. An increase in the amount of optical feedback from the external mirror tends to mask the effects of the nonlinear gain mechanism. Decreased saturation of the optical power in the resonant mode, as shown in Fig. 5.11(a), and a concomitant decrease in the amount of optical power distributed to the ± 1 side modes, as shown in Fig. 5.11(b), are consequences of an increase in the amount of optical feedback. The postulate that the amount of optical feedback affects the onset of the appearance of nonlinear gain effects in an SXC laser was advanced in the previous section to explain the measured results for laser D shown in Fig. 5.6 (i.e., the onset of power saturation for the same resonant mode occurred at different optical power levels for different external cavity lengths). Although the predicted results shown in Fig. 5.11 correctly explain general trends in the measured results, the amount of optical feedback provided by the external cavity mirror must be measured in order to obtain numerical estimates of the depth of the spectral hole for a given device in an SXC configuration.

The importance of the amount of optical feedback from the external mirror of an SXC laser in determining the onset of the appearance of nonlinear gain effects suggests that optical feedback resulting from scattering centres along the active region length of a device could also play an important role in determining the characteristics of the mode evolution curves. Predicted results of the nonlinear gain model for a device in

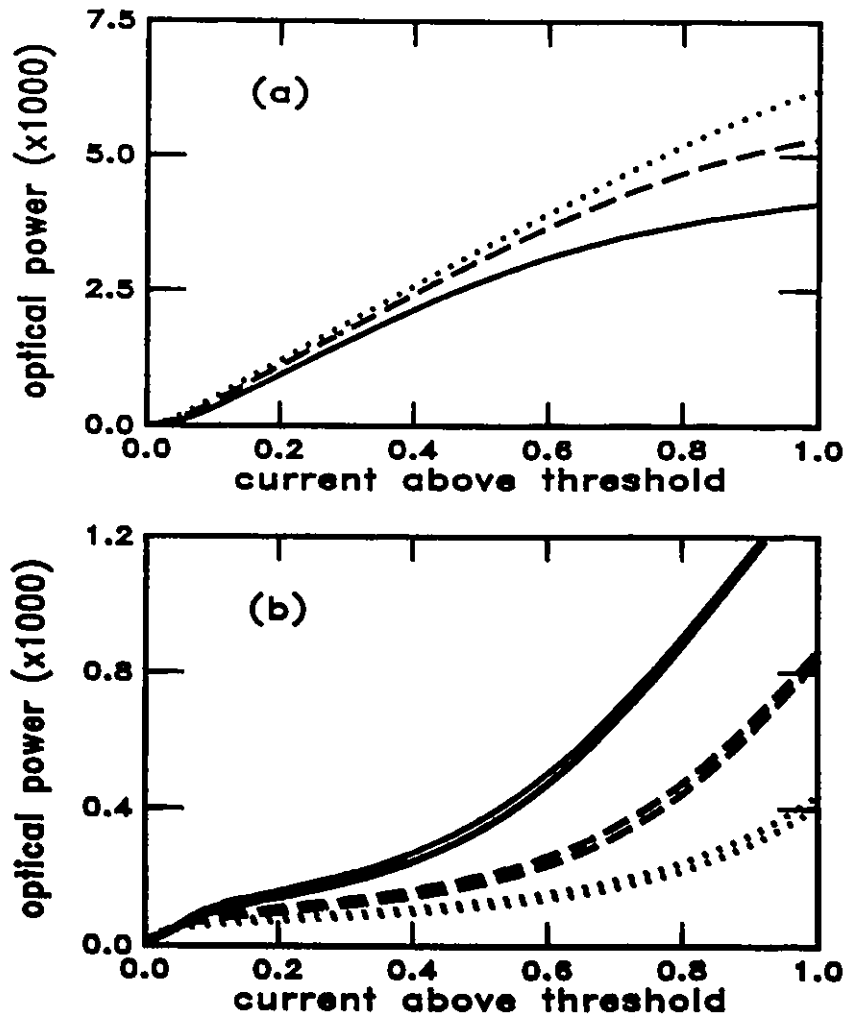


Figure 5.11

The predicted influence of the amount of optical feedback from the external mirror on the appearance of spectral hole burning effects. The depth and width of the spectral hole were held constant at $\alpha_2=3 \times 10^{-6}$ and $\alpha_3=1$ respectively. The optical power of the resonant mode for a sinusoidal modulation in the effective facet reflectance with peak-to-peak amplitudes of 0.010, 0.015 and 0.020 are indicated in (a) by the dotted, dashed and solid lines respectively. The optical powers of the ± 1 side modes are indicated in (b). Identical line styles in (a) and (b) indicate predictions based on equal amounts of optical feedback from the external mirror.

an SXC configuration with a single, isolated scatterer in the centre of the active region are shown in Figure 5.12. The results presented in Chapter 4 indicate that a sinusoidal modulation in the intrinsic $R_m G_m$ profile with a period of two mode spacings is expected for a scatterer in the centre of the active region. Phases φ , as defined in Chapter 4, of 0 and π radians are used to model scenarios in which the resonant mode is enhanced and diminished respectively, by the optical feedback from the scattering centre. Comparing the curves for a device with and without the presence of a scattering centre, Fig. 5.12 indicates that enhancement of the resonant mode by the scattering centre ($\varphi=0$) results in decreased saturation of the optical power in the resonant mode and a corresponding decrease in the power attained by the ± 1 side modes at a given current level. Note that changes in the amount of optical feedback from the external mirror (c.f. the mode evolution curves depicted in Fig. 5.11) produced similar trends.

The peak-to-peak amplitude (3.2×10^{-4}) of the sinusoidal modulation in the facet reflectance used to generate the results shown in Fig. 5.12 was comparable in magnitude to measured modulations (discussed in Chapter 2) in the below-threshold $R_m G_m$ profile for a typical index-guided device. It was expected that the optical feedback from scattering centres in the active region of a device (as characterized by the modulations in the below-threshold $R_m G_m$ profile) could explain the different saturation characteristics of the resonant modes available within one free spectral range of the external cavity of an SXC laser (c.f. Fig. 5.7). However, a significant correlation between the measured modulations in the below-threshold $R_m G_m$ profile of a device and the measured mode

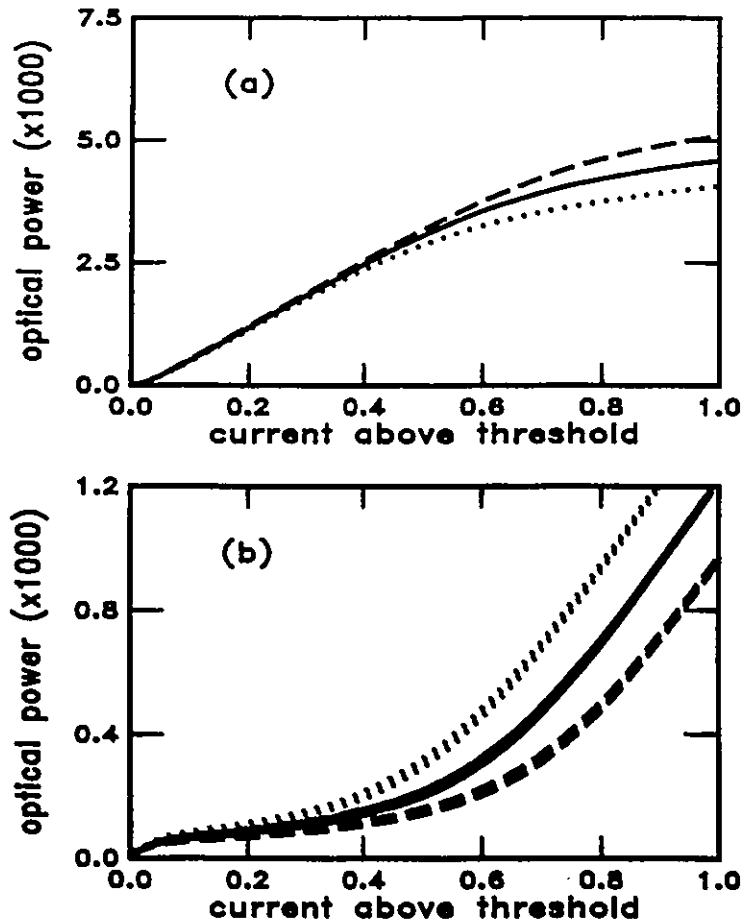


Figure 5.12

The predicted influence of a single, isolated scatterer in the centre of the active region on the appearance of spectral hole burning effects. The depth and width of the spectral hole were held constant at $\alpha_2=5 \times 10^{-6}$ and $\alpha_3=1$ respectively. The effects of the scattering centre are modelled by a sinusoidal modulation of the facet reflectance with a peak-to-peak amplitude of 3.2×10^{-4} and a period of 2 mode spacings. The optical power of the resonant modes are shown in (a) and the dashed line represents a device without a scattering centre. The solid and dotted lines in (a) indicate modulations in the facet reflectance which differ by π radians. The optical powers of the ± 1 side modes are indicated in (b). Identical line styles in (a) and (b) indicate predictions based on identical modelling parameters.

evolution curves of the same device in an SXC configuration was not found. Measurements on a larger number of devices is required to establish significant correlation statistics and to determine the importance of scattering centres in masking the appearance of nonlinear gain effects in SXC lasers.

5.6 Summary

A semiconductor diode laser in a short-external-cavity (SXC) configuration has been used to monitor the effects of nonlinear gain phenomena on the spectral output for large optical power levels. The strong single mode oscillation provided by the SXC gave the opportunity to isolate the nonlinear gain effects for the solitary mode, eliminating the complication of separating the effects of each individual mode in a multi-moded source.

The optical powers of the resonant mode (mode 0) and the 3 neighbouring modes on either wavelength side of the resonant mode were measured for 6 different index-guided devices over a large range of above-threshold current values. For 5 of the 6 devices, the evolution of the optical powers in the longitudinal modes with increasing total output power indicated a simultaneous and symmetric increase in the peak optical powers of the ± 1 side modes. Saturation of the peak optical power of the resonant mode was often associated with the power increase of the ± 1 side modes. These observations support the existence of a symmetric, nonlinear gain mechanism in the active region

material of the semiconductor.

It was found that the amount of optical feedback from the external mirror was an important parameter in determining the onset of the appearance of nonlinear gain effects in SXC lasers. Large amounts of optical feedback tended to mask the effects of the nonlinear gain phenomenon, i.e., increases in the optical powers of the ± 1 side modes as well as the saturation of the resonant mode power were delayed until higher optical power levels were obtained. (It should be noted that for the sixth device which was tested, a large optical feedback efficiency of the external cavity precluded observations of the effects of nonlinear gain on the mode evolution curves.) Further measurements to determine the amount of optical feedback from the external cavity mirror are required to provide an accurate indication of the magnitude of the nonlinear gain effects in SXC lasers.

In an attempt to model the measured evolution of the modes with increasing injection current, a Lorentzian hole in the material gain profile was incorporated into an existing model of an homogeneously-broadened injection laser.[20] The depth of the spectral hole was dependent on the optical power in the longitudinal mode and the effect of the short-external-cavity was represented by a sinusoidal variation in the facet reflectance. A fast, efficient algorithm based on the symmetry of the Jacobian matrix was developed to solve the nonlinear system of equations governing the mode powers. It was found that the saturation of the optical power in the resonant mode and the simultaneous, symmetric increases of the powers in the ± 1 side modes were predicted by the model.

It is interesting to note that, in contrast to the theoretical and measured results in this study, other models of spectral hole burning predict a decrease in the optical powers of the ± 1 side modes with increases in the injection current and hence more single-mode oscillation.[9,40,41] However, in support of the results achieved with SXC lasers, increased multi-mode behaviour for strong spectral hole burning has been reported.[32,p.76]

It was reported in Chapter 2 that the effect of internal scattering on the above-threshold spectral output of semiconductor diode lasers may dominate over nonlinear gain effects. Accurate predictions of the above-threshold mode profile were obtained for two devices for a range of output power levels from below-threshold up to approximately 5 mW. The resonant enhancement characteristics of the SXC configuration provide a source with a large amount of optical power concentrated into a single longitudinal mode. The results of this experiment indicate that nonlinear gain effects are observed for large single mode powers above approximately 5 mW. Thus, it can be concluded that nonlinear gain must be considered to model accurately the above-threshold spectral output of 1.3 μm semiconductor diode lasers. However, internal scattering appears to be the dominant effect for output power levels below about 5 mW. The effects of nonlinear gain on the other hand appear to be apparent for large single mode powers greater than about 5 mW as obtained in SXC lasers.

Chapter 6. Conclusion

6.1 Introduction

The purpose of this chapter is to suggest directions for future investigations based upon results achieved during the course of this work and to review the major results presented in the dissertation. The chapter is divided into two sections: Section 6.2 discusses the recommendations for future research and Section 6.3 provides a summary of the work.

6.2 Recommended Additional Research

The potential areas for investigation which were highlighted in the course of this work are collected in this section. Most of the recommendations for future research involve enhancements to the existing experimental technique or apparatus which could yield improved results. Proposals for new research directions in the area of nonlinear gain phenomena in semiconductor diode lasers are also advanced.

The experiment to measure the modulations in the below-threshold $R_m G_m$ profile, discussed in Chapter 2, could be enhanced by measuring a residue record over a larger number of longitudinal modes. Acquisition of the required data could be accomplished

by measuring the below-threshold spectral output for several active region temperatures, and combining the resultant residue records. Selecting the number of points based on the required spatial resolution, a Fourier transformation of the residue record could yield reliable information regarding the position of scattering centres in the active region, even for scatterers which lie close to the facets of the device. Measurements using the polarization-resolved and spatially-resolved electroluminescence technique do not provide reliable information for light scattered near the facets.[63]

The experiment which used a short-external-cavity (SXC) semiconductor laser to probe the effects of nonlinear gain phenomena, discussed in Chapter 5, could be improved by a refinement of the feedback loop which enhances the single mode stability of the source. A separate lock to the resonant mode peak should improve the single mode stability as well as increasing the current range over which the resonant mode could be tracked. This could be accomplished by equipping the 0.25-metre monochromator with a scanning mirror assembly prior to the exit slit.

The amount of optical feedback supplied by the external mirror of the SXC laser was highlighted as an important parameter for the assessment of the magnitude of nonlinear gain effects in semiconductor lasers. Designing a method to measure the amount of optical feedback is a logical evolution to the experimental technique described in Chapter 5. A method of measuring the amount of optical feedback from an external mirror has been reported.[62] This method requires mechanical chopping of the laser output within the external cavity and measurement of the optical power difference under

the conditions of feedback and no feedback. Mechanical difficulties must be surmounted in order to implement this method because the length of the external cavity is typically less than one millimetre. Accurate measurement of both the amount of optical feedback from the external mirror and the modulations imposed on the $R_m G_m$ profile due to scattering centres should allow for calculation of the magnitude of nonlinear gain effects and accurate predictions of mode evolution curves.

New research directions in the area of nonlinear gain phenomena in semiconductor diode lasers are proposed. The preference for certain semiconductor diode lasers to oscillate on a specific single mode over a large range of bias currents and active region temperatures has been termed single mode stability.[10,39] Mode hopping rather than a smooth evolution of mode intensities with the wavelength tuning of the gain profile is also a characteristic of single mode stability.[10] Single mode stability has also been observed for the SXC laser,[58] suggesting that single mode stability in Fabry-Perot semiconductor lasers may be related to mode selective mechanisms such as internal scattering rather than nonlinear gain phenomena. It would be interesting to measure the development of the above-threshold spectral output with bias current for a large number of semiconductor lasers, particularly for devices displaying a strong single mode oscillation and to correlate the mode development with the measured modulations in the below-threshold $R_m G_m$ product. It will be recalled from Chapter 2 and Chapter 4, that scattering centres induce a modulation in the effective facet reflectance which is similar to the effects induced by a short-external-cavity.

It has been reported that nonlinear gain phenomena affect the modulation characteristics of semiconductor diode lasers.[53,54] A proposal for future research involves the measurement of the electrical modulation bandwidth for all resonant modes with one free spectral range of the short-external-cavity. This study could yield new information concerning the wavelength dependence and the symmetry of the nonlinear gain mechanism.

Pump-probe experiments using a single-mode laser have been used to monitor the effects of nonlinear gain on gain saturation[63] and four-wave mixing[64] in semiconductor laser amplifiers, and on the intrinsic frequency response of semiconductor lasers.[49] SXC lasers could provide a viable alternative to the more expensive distributed-feedback lasers used for performing these measurements.

6.3 Summary

Experiments were performed to measure mechanisms responsible for the above-threshold spectral output of 1.3 μm semiconductor diode lasers. Results of these experiments indicated that scattering and nonlinear gain are important effects in determining the shape of the above-threshold longitudinal mode profile. However, the effects of scattering centres on the above-threshold spectral output appear to be the dominant effect for output powers up to approximately 5 mW. The effects of nonlinear gain on the above-threshold mode profile, as observed from SXC diode lasers become

apparent only for single-mode optical powers above 5 mW. These conclusions were based upon the measurements which are described below.

A residue that is characteristic of internal scattering was extracted from the below-threshold spectra of over 30 commercially-available devices by fitting a smooth function to the measured $R_m G_m$ profile. The residue was found to be correlated with the above-threshold spectral output and was used to predict the above-threshold spectral tuning characteristics of the devices.

The coefficients defining the smooth function which was fit to the below-threshold $R_m G_m$ profile were examined and a linear relationship between the coefficients and the peak value of the $R_m G_m$ profile was explored. The results were provided for each device and for generic gain-guided and index-guided devices as an aid to researchers desiring information regarding the shape of the $R_m G_m$ profile for a specific or generic device. The spacing of the longitudinal modes across the $R_m G_m$ profile was also examined and a linear relationship was established between the intermode spacing and the mode number.

Data obtained from two techniques on light scattering centres that are distributed along the length of the active region of 1.3 μm semiconductor diode lasers were presented and discussed. Light scattering characteristics were obtained for 16 lasers by analyzing light detected through the substrate (using spatially and polarization resolved electroluminescence) and by analyzing the facet emission for modulation features in the below-threshold reflectance-gain ($R_m G_m$) product. A Cartesian plot of the data showed the points to be dispersed about a best-fit line, but correlated. The dispersal of the points

about the best-fit line was explained by a sampling phenomena due to the discrete nature of the longitudinal modes and by the assumption of unequal or anisotropic scattering in the substrate and facet directions. The data were taken to show that the scattering is not isotropic.

Semiconductor lasers placed in a short-external-cavity configuration were used to probe the influence of nonlinear gain phenomena on the evolution of the optical power in the longitudinal modes with increasing injection current. Simultaneous, symmetric increases in the optical power of the first long and short wavelength side modes in addition to saturation of the power of the resonant mode indicated the presence of a symmetric nonlinear gain mechanism in the semiconductor material of the active region. A spectral hole with a Lorentzian lineshape was chosen to model the nonlinear gain mechanism and a fast, efficient algorithm was developed to solve the nonlinear equations governing the optical powers in the longitudinal modes. The model was able to predict the general trends of the measured results, however, accurate measurements of the amount of optical feedback from the external mirror are required to determine the magnitude of the nonlinear gain effect.

Although additional measurements are required to assess accurately the magnitude of the nonlinear gain mechanisms, it is believed that the results obtained in this work represent a significant contribution to the understanding of the physical mechanisms responsible for the above-threshold spectral output of 1.3 μm semiconductor diode lasers.

Appendix A. Variation of $R_m G_m$ Fitting Coefficients

This appendix contains tabulated values required for calculating a smooth approximation of the $R_m G_m$ profile for index-guided and gain-guided devices given a measured value of the profile peak, $(RG)_{\max}$. The values of the fitting coefficients a_i are determined from the measurement of $(RG)_{\max}$ using the formula

$$a_i = b_i + n_i(RG)_{\max} \quad , \quad i = 1 \text{ to } 5. \quad (\text{A-1})$$

In the following tables, the a_i intercept is indicated by the variable b (associated error σ_b) and the slope is indicated by the variable n (associated error σ_n). The smooth approximation of the $R_m G_m$ profile is

$$R_m G_m = R \exp \left(\frac{a_1}{a_5 m^4 + a_4 m^3 + a_3 m^2 + a_2 m + 1} \right) \quad , \quad (\text{A-2})$$

where R is the facet reflectance, m is the mode number and mode zero is defined as the mode where $(RG)_{\max}$ was measured. The laser identification label of a given device is indicated in the top left corner of the group of values associated with that device.

A detailed description of the procedure used to determine the tabulated values from measured results can be found in Chapter 3.

Table A.1: Index-Guided Devices

A	b	σ_b	n	σ_n	r	B	b	σ_b	n	σ_n	r
a ₁	-0.12	0.03	1.27	0.03	1.00	a ₁	-0.43	0.02	1.68	0.01	1.00
a ₂	6.4e-02	4.1e-03	-6.7e-02	3.5e-03	-0.99	a ₂	1.4e-01	1.0e-02	-1.6e-01	7.4e-03	-0.99
a ₃	3.1e-03	6.1e-04	-1.7e-03	5.3e-04	-0.81	a ₃	1.9e-02	5.0e-03	-1.9e-02	3.6e-03	-0.89
a ₄	4.0e-05	3.1e-05	-9.7e-06	2.7e-05	-0.16	a ₄	2.1e-03	5.4e-04	-2.5e-03	3.9e-04	-0.92
a ₅	-1.0e-06	1.1e-06	2.1e-06	9.6e-07	0.70	a ₅	7.6e-05	2.1e-05	-8.5e-05	1.5e-05	-0.90
C	b	σ_b	n	σ_n	r	D	b	σ_b	n	σ_n	r
a ₁	-0.34	0.08	1.55	0.06	1.00	a ₁	-0.18	0.02	1.35	0.02	1.00
a ₂	3.5e-02	3.9e-03	-4.1e-02	2.9e-03	-0.98	a ₂	5.5e-02	2.7e-03	-5.8e-02	2.2e-03	-1.00
a ₃	4.3e-03	1.1e-03	-4.1e-03	7.8e-04	-0.89	a ₃	2.1e-03	6.3e-04	-4.1e-04	5.1e-04	-0.31
a ₄	9.3e-04	1.6e-04	-1.0e-03	1.2e-04	-0.95	a ₄	1.1e-04	2.9e-05	-1.3e-04	2.4e-05	-0.91
a ₅	4.0e-05	6.7e-06	-4.5e-05	4.9e-06	-0.96	a ₅	3.9e-06	2.9e-06	-4.4e-06	2.3e-06	-0.60
E	b	σ_b	n	σ_n	r	F	b	σ_b	n	σ_n	r
a ₁	-0.10	0.04	1.26	0.03	1.00	a ₁	0.10	0.02	1.01	0.02	1.00
a ₂	3.0e-02	2.5e-03	-3.3e-02	2.1e-03	-0.99	a ₂	1.0e-02	1.7e-03	-1.3e-02	1.5e-03	-0.97
a ₃	2.3e-03	4.3e-04	-1.6e-03	3.6e-04	-0.88	a ₃	2.5e-04	6.8e-04	1.1e-03	6.1e-04	0.62
a ₄	3.7e-04	6.3e-05	-3.6e-04	5.2e-05	-0.95	a ₄	5.5e-05	2.2e-05	-2.7e-05	1.9e-05	-0.53
a ₅	1.5e-05	2.5e-06	-1.4e-05	2.1e-06	-0.94	a ₅	4.3e-06	1.9e-06	-6.8e-06	1.7e-06	-0.87
G	b	σ_b	n	σ_n	r	H	b	σ_b	n	σ_n	r
a ₁	0.06	0.02	1.07	0.02	1.00	a ₁	0.08	0.01	1.06	0.01	1.00
a ₂	3.7e-02	2.8e-03	-3.9e-02	2.7e-03	-0.99	a ₂	2.6e-02	3.0e-03	-2.6e-02	2.8e-03	-0.97
a ₃	1.9e-03	8.1e-04	-1.1e-03	7.7e-04	-0.56	a ₃	1.6e-05	8.0e-04	5.0e-04	7.6e-04	0.30
a ₄	4.4e-06	1.4e-05	-7.6e-06	1.3e-05	-0.26	a ₄	7.1e-05	7.1e-06	-6.1e-05	6.8e-06	-0.97
a ₅	-3.1e-06	1.2e-06	2.6e-06	1.2e-06	0.73	a ₅	5.4e-06	2.1e-06	-4.9e-06	2.0e-06	-0.77

I	b	σ_b	n	σ_n	r	J	b	σ_b	n	σ_n	r
a ₁	0.15	0.02	0.98	0.01	1.00	a ₁	-0.05	0.03	1.20	0.02	1.00
a ₂	3.1e-02	9.8e-04	-3.2e-02	9.3e-04	-1.00	a ₂	2.0e-02	4.3e-03	-2.2e-02	3.5e-03	-0.93
a ₃	8.9e-04	3.7e-04	-4.8e-04	3.5e-04	-0.55	a ₃	3.2e-03	3.2e-03	-6.8e-04	2.6e-03	-0.11
a ₄	3.9e-05	1.2e-05	-3.4e-05	1.1e-05	-0.82	a ₄	1.1e-03	3.2e-04	-1.1e-03	2.6e-04	-0.85
a ₅	7.8e-07	3.5e-07	-2.4e-07	3.3e-07	-0.32	a ₅	6.0e-05	1.4e-05	-5.8e-05	1.2e-05	-0.90
K	b	σ_b	n	σ_n	r	L	b	σ_b	n	σ_n	r
a ₁	-0.05	0.04	1.20	0.03	1.00	a ₁	-0.01	0.02	1.15	0.02	1.00
a ₂	2.6e-02	3.1e-03	-2.8e-02	2.7e-03	-0.98	a ₂	-1.7e-03	3.4e-03	-3.5e-04	2.9e-03	-0.05
a ₃	2.8e-03	6.5e-04	-1.8e-03	5.7e-04	-0.81	a ₃	4.5e-04	2.7e-04	6.8e-04	2.3e-04	0.78
a ₄	8.6e-04	6.4e-05	-8.5e-04	5.6e-05	-0.99	a ₄	2.5e-04	7.5e-05	-3.0e-04	6.5e-05	-0.89
a ₅	4.8e-05	4.0e-06	-4.5e-05	3.4e-06	-0.98	a ₅	2.1e-05	3.3e-06	-2.1e-05	2.9e-06	-0.95
P	b	σ_b	n	σ_n	r	Q	b	σ_b	n	σ_n	r
a ₁	-0.09	0.08	1.25	0.07	0.99	a ₁	-0.11	0.04	1.27	0.04	1.00
a ₂	3.5e-02	4.7e-03	-4.1e-02	3.9e-03	-0.97	a ₂	5.0e-02	3.2e-03	-5.5e-02	2.7e-03	-0.99
a ₃	1.8e-03	9.7e-04	-1.2e-03	8.1e-04	-0.54	a ₃	2.5e-03	2.9e-04	-1.2e-03	2.4e-04	-0.91
a ₄	7.4e-05	8.7e-06	-7.0e-05	7.3e-06	-0.97	a ₄	1.2e-04	1.7e-05	-1.0e-04	1.4e-05	-0.95
a ₅	2.4e-06	3.3e-06	-1.7e-06	2.7e-06	-0.25	a ₅	5.5e-06	2.2e-06	-4.9e-06	1.9e-06	-0.74
R	b	σ_b	n	σ_n	r	S	b	σ_b	n	σ_n	r
a ₁	-0.14	0.04	1.32	0.03	1.00	a ₁	-0.51	0.06	1.76	0.05	1.00
a ₂	3.3e-02	3.2e-03	-4.2e-02	2.5e-03	-0.99	a ₂	4.1e-02	3.3e-03	-5.1e-02	2.4e-03	-0.99
a ₃	8.4e-03	6.8e-04	-7.9e-03	5.3e-04	-0.99	a ₃	-1.2e-02	1.9e-03	1.6e-02	1.4e-03	0.97
a ₄	1.1e-03	1.7e-04	-1.1e-03	1.3e-04	-0.96	a ₄	-1.1e-05	4.1e-05	-1.3e-05	3.0e-05	-0.15
a ₅	6.7e-05	1.6e-05	-7.4e-05	1.3e-05	-0.91	a ₅	6.8e-05	1.1e-05	-8.0e-05	8.1e-06	-0.96

T	b	σ_b	n	σ_n	r	U	b	σ_b	n	σ_n	r
a ₁	-0.08	0.02	1.24	0.01	1.00	a ₁	-0.09	0.03	1.25	0.02	1.00
a ₂	3.3e-02	2.2e-03	-3.5e-02	1.9e-03	-0.99	a ₂	6.8e-04	2.8e-03	-4.7e-03	2.2e-03	-0.65
a ₃	2.8e-03	4.3e-04	-2.2e-03	3.7e-04	-0.93	a ₃	-5.2e-04	8.4e-04	2.1e-03	6.7e-04	0.78
a ₄	1.1e-04	6.8e-06	-9.9e-05	5.8e-06	-0.99	a ₄	9.3e-05	1.4e-05	-9.0e-05	1.1e-05	-0.95
a ₅	5.2e-08	2.7e-06	1.5e-06	2.3e-06	0.27	a ₅	3.5e-06	3.4e-06	-4.2e-06	2.7e-06	-0.53
1	b	σ_b	n	σ_n	r	2	b	σ_b	n	σ_n	r
a ₁	-0.01	0.03	1.15	0.03	1.00	a ₁	-0.11	0.03	1.25	0.02	1.00
a ₂	7.4e-03	9.9e-03	-3.7e-03	9.0e-03	-0.18	a ₂	8.7e-02	5.0e-03	-8.6e-02	4.6e-03	-0.99
a ₃	-1.9e-03	8.6e-04	3.5e-03	7.8e-04	0.90	a ₃	6.4e-03	5.5e-04	-4.9e-03	5.0e-04	-0.98
a ₄	6.1e-04	6.9e-05	-5.7e-04	6.3e-05	-0.97	a ₄	-2.8e-05	2.3e-05	6.8e-05	2.1e-05	0.83
a ₅	4.1e-05	3.1e-06	-3.9e-05	2.8e-06	-0.99	a ₅	-7.2e-06	3.0e-06	6.9e-06	2.7e-06	0.76
3	b	σ_b	n	σ_n	r						
a ₁	0.05	0.02	1.09	0.02	1.00						
a ₂	3.4e-03	9.6e-04	-5.3e-03	8.9e-04	-0.94						
a ₃	1.2e-03	3.0e-04	-5.1e-04	2.8e-04	-0.65						
a ₄	1.7e-04	1.1e-05	-1.5e-04	1.0e-05	-0.99						
a ₅	2.4e-06	8.4e-07	-1.9e-06	7.7e-07	-0.76						

Table A.2: Gain-Guided Devices

a	b	σ_b	n	σ_n	r	b	b	σ_b	n	σ_n	r
a ₁	-0.03	0.08	1.17	0.08	0.99	a ₁	-0.04	0.02	1.19	0.01	1.00
a ₂	-5.2e-02	5.0e-02	5.5e-02	4.7e-02	0.48	a ₂	-3.9e-03	3.4e-03	2.5e-03	2.8e-03	0.34
a ₃	4.7e-04	9.7e-04	3.8e-04	9.1e-04	0.19	a ₃	1.7e-03	5.7e-04	-1.0e-03	4.7e-04	-0.66
a ₄	1.6e-04	5.6e-05	-1.6e-04	5.3e-05	-0.82	a ₄	2.8e-05	3.3e-05	-1.3e-05	2.7e-05	-0.19
a ₅	-5.0e-06	3.4e-06	6.2e-06	3.2e-06	0.68	a ₅	2.3e-06	2.5e-06	-1.1e-06	2.0e-06	-0.21
c	b	σ_b	n	σ_n	r	d	b	σ_b	n	σ_n	r
a ₁	-0.13	0.02	1.30	0.02	1.00	a ₁	-0.06	0.02	1.21	0.02	1.00
a ₂	3.6e-02	5.1e-03	-4.2e-02	4.0e-03	-0.97	a ₂	1.8e-02	1.0e-03	-2.2e-02	8.2e-04	-1.00
a ₃	4.6e-03	3.1e-04	-3.1e-03	2.5e-04	-0.98	a ₃	3.2e-03	3.0e-04	-1.8e-03	2.5e-04	-0.95
a ₄	7.8e-04	3.7e-05	-8.5e-04	3.0e-05	-1.00	a ₄	1.9e-04	2.3e-05	-2.0e-04	1.9e-05	-0.97
a ₅	5.2e-05	5.0e-06	-5.2e-05	3.9e-06	-0.98	a ₅	1.8e-05	2.2e-06	-1.6e-05	1.8e-06	-0.97
e	b	σ_b	n	σ_n	r	f	b	σ_b	n	σ_n	r
a ₁	-0.09	0.01	1.25	0.01	1.00	a ₁	-0.12	0.03	1.29	0.02	1.00
a ₂	1.0e-02	7.5e-04	-1.3e-02	6.1e-04	-0.99	a ₂	1.2e-02	1.6e-03	-1.5e-02	1.3e-03	-0.98
a ₃	3.3e-03	1.7e-04	-2.1e-03	1.4e-04	-0.99	a ₃	1.6e-03	4.6e-04	-2.4e-04	3.7e-04	-0.25
a ₄	1.5e-04	1.7e-05	-1.6e-04	1.3e-05	-0.98	a ₄	1.6e-04	2.3e-05	-1.7e-04	1.8e-05	-0.97
a ₅	1.8e-05	1.8e-06	-1.6e-05	1.5e-06	-0.98	a ₅	2.6e-05	3.5e-06	-2.4e-05	2.8e-06	-0.96
g	b	σ_b	n	σ_n	r	h	b	σ_b	n	σ_n	r
a ₁	-0.11	0.02	1.27	0.02	1.00	a ₁	-0.04	0.01	1.19	0.01	1.00
a ₂	-1.2e-03	9.4e-04	2.9e-03	7.6e-04	0.84	a ₂	1.1e-02	1.7e-03	-1.6e-02	1.4e-03	-0.98
a ₃	2.9e-03	4.7e-04	-1.2e-03	3.8e-04	-0.78	a ₃	1.7e-03	4.2e-04	-3.4e-04	3.6e-04	-0.38
a ₄	9.5e-05	1.8e-05	-1.0e-04	1.4e-05	-0.95	a ₄	1.5e-04	1.9e-05	-1.5e-04	1.6e-05	-0.97
a ₅	1.9e-05	3.2e-06	-1.7e-05	2.6e-06	-0.94	a ₅	1.6e-05	2.4e-06	-1.4e-05	2.0e-06	-0.95

l	b	σ_b	n	σ_n	r	j	b	σ_b	n	σ_n	r
a₁	-0.02	0.02	1.16	0.02	1.00	a₁	0.03	0.02	1.11	0.01	1.00
a₂	1.3e-02	9.5e-04	-1.3e-02	8.0e-04	-0.99	a₂	6.5e-03	9.0e-04	-6.0e-03	7.9e-04	-0.96
a₃	1.6e-03	4.6e-04	-5.4e-04	3.9e-04	-0.50	a₃	6.2e-04	4.2e-04	2.3e-04	3.7e-04	0.26
a₄	1.3e-04	1.5e-05	-1.2e-04	1.3e-05	-0.97	a₄	1.3e-04	9.4e-06	-1.2e-04	8.3e-06	-0.99
a₅	8.8e-06	1.3e-06	-8.1e-06	1.1e-06	-0.95	a₅	7.5e-06	1.1e-06	-6.7e-06	9.3e-07	-0.95
k	b	σ_b	n	σ_n	r						
a₁	-0.03	0.01	1.18	0.01	1.00						
a₂	1.1e-02	4.5e-03	-1.3e-02	3.9e-03	-0.81						
a₃	1.7e-03	3.2e-04	-7.4e-04	2.8e-04	-0.75						
a₄	7.4e-05	2.5e-05	-7.1e-05	2.1e-05	-0.82						
a₅	9.7e-06	2.8e-06	-8.3e-06	2.4e-06	-0.83						

Appendix B. Numerical Technique for Determining Longitudinal Mode Powers

The analytic expression for the steady-state optical power I_m of the m^{th} mode of an homogeneously-broadened injection laser with facet reflectivity R is:

$$I_m = \frac{c_m(G_m - 1)}{1 - RG_m} , \quad (\text{B-1})$$

where c_m is related to the amount of spontaneous light coupled into the mode. The single-pass gain, G_m , is an exponential function whose argument contains a term which is dependent on the sum of the mode powers. Hence, the optical power in one mode is a function of the optical powers in all the other modes:

$$I_m \equiv I_m(I_1, I_2, I_3, \dots, I_n) , \quad (\text{B-2})$$

where n is the number of modes considered. The problem of evaluating the mode powers can be formulated as the solution to a set of n coupled, nonlinear equations of the form:

$$f_m(I_1, I_2, I_3, \dots, I_n) = I_m - \frac{c_m(G_m - 1)}{1 - RG_m} = 0 , \quad m=1, 2, \dots, n. \quad (\text{B-3})$$

The partial derivatives of the functions f_m with respect to the mode powers evaluated at

$I = (I_1, I_2, I_3, \dots, I_n)$ are:

$$\left. \frac{\partial f_m}{\partial I_n} \right|_I = \delta_{m,n} - \left. \frac{\partial}{\partial I_n} \left(\frac{c_m(G_m - 1)}{1 - RG_m} \right) \right|_I = \delta_{m,n} - a_m \quad (\text{B-4})$$

where $\delta_{m,n}$ is the Kronecker delta and a_m is a constant, specific to the m^{th} mode.

One technique to obtain the solution to the nonlinear system of equations is based upon a Newton-Raphson iteration scheme and involves solving a matrix equation which incorporates the Jacobian:[66,p.269]

$$\begin{pmatrix} 1-a_1 & -a_1 & -a_1 & \dots & -a_1 \\ -a_2 & 1-a_2 & -a_2 & \dots & -a_2 \\ -a_3 & -a_3 & 1-a_3 & \dots & -a_3 \\ \dots & \dots & \dots & \dots & \dots \\ -a_n & -a_n & a_n & \dots & 1-a_n \end{pmatrix} \quad (\text{B-5})$$

At high pump levels, the Jacobian matrix for the present set of equations (B-3) is often very close to being a singular matrix and solution of the matrix equation is hampered by round-off errors. However, a simplified iteration algorithm can be derived which does not require matrix inversion.[67]

Following the Newton-Raphson method, the function f_m is expanded in a

Taylor series about the point $I = (I_1, I_2, I_3, \dots, I_n)$:

$$0 = f_m(I_1 + \Delta I_1, \dots, I_n + \Delta I_n) \approx f_m(I_1, \dots, I_n) + \sum_{j=1}^n \left. \frac{\partial f_m}{\partial I_j} \right|_I \Delta I_j \quad (\text{B-6})$$

Using the value of the derivative shown in (B-4):

$$f_m + \Delta I_m - a_m \sum_{j=1}^n \Delta I_j = 0 \quad , \quad (\text{B-7})$$

and summing both sides of the above equation over the index m :

$$\sum_{m=1}^n f_m + \sum_{m=1}^n \Delta I_m - \sum_{m=1}^n a_m \sum_{j=1}^n \Delta I_j = 0 \quad . \quad (\text{B-8})$$

Since j is a dummy index, the two sums over ΔI_m and ΔI_j can be collected and the solution for the sum over ΔI_m can be substituted into (B-7) to yield the final expression for ΔI_m :

$$\Delta I_m \approx -f_m + \frac{a_m \sum_{j=1}^n f_j}{-1 + \sum_{j=1}^n a_j} \quad . \quad (\text{B-9})$$

The final form of the iteration algorithm for the mode power I_m becomes:

$$I_{m,new} = I_{m,old} + \Delta I_m = I_{m,old} - f_m + \frac{a_m \sum_{j=1}^n f_j}{-1 + \sum_{j=1}^n a_j} \quad (\text{B-10})$$

The value of the mode power I_m can then be iterated until a suitable convergence criterion has been met.

The iteration algorithm described above provided solutions to the longitudinal mode powers in cases where the method using the Jacobian matrix (B-5) failed due to the singular condition. In addition, the simplified algorithm is more efficient since inverting the Jacobian matrix requires on the order of N^3 floating-point operations, where N is the number of modes considered.[66,p.37]

References

1. B. E. A. Saleh and M. C. Teich, *Fundamentals of Photonics*, (John Wiley and Sons, New York, 1991).
2. D. T. Cassidy, "Trace gas detection using 1.3- μm InGaAsP diode laser transmitter modules," *Appl. Opt.* **27**, 610-614 (1988).
3. D. Renner and J. E. Carroll, "Simple system for broad-band single-mode tuning of D. H. GaAlAs lasers," *Electron. Lett.* **15**, 73-74 (1979).
4. H. Naito, H. Nagai, M. Yuri, K. Tateoka, M. Kume, K. Hamada, and H. Shimizu, "A new composite-cavity laser with two different waveguide cores for stable longitudinal mode operation," *J. Appl. Phys.* **66**, 5726-5730 (1989).
5. K. Petermann, "Calculated spontaneous emission factor of double-heterostructure injection lasers with gain-induced waveguiding," *IEEE J. Quantum Electron.* **QE-15**, 566-570 (1979).
6. G. P. Agrawal, "Heuristic approach to spontaneous emission factor of gain-guided lasers," *J. Opt. Soc. Am. B* **1**, 406-408 (1984).
7. D. T. Cassidy, "Spontaneous-emission factor of semiconductor diode lasers," *J. Opt. Soc. Am. B* **8**, 747-752 (1991).
8. A. Yariv and S. Margalit, "On spontaneous emission into guided modes with curved wavefronts," *IEEE J. Quantum Electron.* **QE-18**, 1831-1832 (1982).
9. M. Yamada and Y. Suematsu, "Theory of single mode injection lasers taking account of electronic intra-band relaxation," *Proceedings of the 10th Conference on Solid State Devices, Tokyo, 1978*, *Jpn. J. Appl. Phys., Suppl.* **18-1**, 347-354 (1979).
10. R. F. Kazarinov, C. H. Henry, and R. A. Logan, "Longitudinal mode self-stabilization in semiconductor lasers," *J. Appl. Phys.* **53**, 4631-4644 (1982).

11. M. Willatzen, A. Uskov, J. Mørk H. Olesen, B. Tromborg, and A.-P Jauho, "Nonlinear gain suppression in semiconductor lasers due to carrier heating," *IEEE Photon. Tech. Lett.* **3**, 606-609 (1991).
12. C. B. Su, "Nonlinear gain caused by cavity standing wave dielectric grating as an explanation of the relationship between resonance frequency and damping rate of semiconductor diode lasers," *Appl. Phys. Lett.* **53**, 950-952 (1988).
13. F. H. Peters and D. T. Cassidy, "Spectral output of 1.3 μm semiconductor diode lasers," *IEE Proc. J* **138**, 195-198 (1991).
14. F. H. Peters and D. T. Cassidy, "Model of the spectral output of gain-guided and index-guided semiconductor diode lasers," *J. Opt. Soc. Am. B* **8**, 99-105 (1991).
15. J. E. Hayward and D. T. Cassidy, "Correlation of spectral output and below-threshold gain profile modulation in 1.3 μm semiconductor diode lasers," *Appl. Phys. Lett.* **59**, 1150-1152 (1991).
16. J. E. Hayward and D. T. Cassidy, "Experimental confirmation of internal scattering as a dominant mechanism determining the longitudinal mode spectra of 1.3 μm semiconductor diode lasers," *J. Opt. Soc. Am. B* **9**, 1151-1157 (1992).
17. J. E. Hayward and D. T. Cassidy, "Correlation between experiments to measure scattering centres in 1.3 μm semiconductor diode lasers," accepted for publication in *IEEE J. Quantum Electron.* (1992).
18. J. E. Hayward and D. T. Cassidy, "The effects of nonlinear gain in short-external-cavity semiconductor diode lasers," submitted to *IEEE J. Quantum Electron.* (1993).
19. L. F. DeChiaro, "Damage-induced spectral perturbations in multilongitudinal-mode semiconductor lasers," *J. Lightwave Technol.* **LT-8**, 1659-1669 (1990).
20. D. T. Cassidy, "Analytic description of a homogeneously broadened injection laser," *IEEE J. Quantum Electron.* **QE-20**, 913-918 (1984).
21. D. T. Cassidy, "Technique for measurement of the gain spectra of semiconductor diode lasers," *J. Appl. Phys.* **56**, 3096-3099 (1984).

22. H. Ishikawa, H. Imai, T. Tanahashi, K.-I. Hori, and K. Takahei, "V-grooved substrate buried heterostructure InGaAsP/InP laser emitting at 1.3 μm wavelength," *IEEE J. Quantum Electron.* QE-20, 1704-1711 (1982).
23. I. Mito, M. Kitamura, K. Kobayashi, S. Murata, M. Seki, Y. Odagiri, H. Nishimoto, M. Yamaguchi, and K. Kobayashi, "InGaAsP double-channel-planar-buried-heterostructure laser diode (DC-PBH LD) with effective current confinement," *J. Lightwave Technol.* LT-1, 195-201 (1983).
24. J. C. Dymont, "Hermite-Gaussian mode patterns in GaAs junction lasers," *Appl. Phys. Lett.* 10, 84-86 (1967).
25. G. P. Agrawal and N. K. Dutta, *Long-Wavelength Semiconductor Lasers* (Van Nostrand Reinhold, New York, 1986).
26. P. R. Bevington, *Data Reduction and Error Analysis for the Physical Sciences* (McGraw-Hill Book Company Inc., New York, 1969).
27. D. T. Cassidy and F. H. Peters, "Spontaneous emission, scattering and the spectral properties of semiconductor diode lasers," *IEEE J. Quantum Electron.* QE-28, 785-791 (1992).
28. R. A. Damon and W. R. Harvey, *Experimental Design, ANOVA, and Regression* (Harper and Row, Cambridge, 1987).
29. K. Y. Lau and A. Yariv, "A theory of longitudinal modes in semiconductor lasers," *Appl. Phys. Lett.*, 40, 763-765 (1982).
30. D. Marcuse, "Computer model of an injection laser amplifier," QE-19, 63-73 (1983).
31. J. T. Verdeyen, *Laser Electronics* (Prentice-Hall, Inc., New Jersey, 1981).
32. K. Petermann, *Laser Diode Modulation and Noise* (Kluwer Academic Publishers, Massachusetts, 1991).
33. H. Burkhard, "Effective phase and group indices for $\text{In}_{1-x}\text{Ga}_x\text{P}_{1-y}\text{As}_y/\text{InP}$ waveguide structures," *J. Appl. Phys.*, 55, 503-508 (1984).
34. G. H. B. Thompson, *Physics of Semiconductor Laser Devices* (John Wiley and Sons, New York, 1980).

35. S. H. Woodside, *Linewidth of Short External Cavity Semiconductor Lasers*, M. Eng. Thesis, (McMaster University, 1992).
36. F. H. Peters and D. T. Cassidy, "Scattering, absorption and anomalous spectral tuning of 1.3 μm semiconductor diode lasers," *J. Appl. Phys.* **71**, 4140-4144 (1992).
37. Y. Nishimura and Y. Nishimura, "Spectral hole-burning and nonlinear-gain decrease in a band-to-level transition semiconductor laser," *IEEE J. Quantum Electron.* **QE-9**, 1011-1019 (1973).
38. A. P. Bogatov, P. G. Eliseev and B. N. Sverdlov, "Anomalous interaction of spectral modes in a semiconductor laser," *IEEE J. Quantum Electron.* **QE-11**, 510-515 (1975).
39. M. Nakamura, K. Aiki, N. Chinone, R. Ito, and J. Umeda, "Longitudinal-mode behaviours of mode-stabilized $\text{Al}_x\text{Ga}_{1-x}\text{As}$ injection lasers," *J. Appl. Phys.* **49**, 4644-4648 (1978).
40. M. Yamada and Y. Suematsu, "An approximate analysis of gain suppression in injection lasers for band-to-band and band-to-impurity-level transitions," *Jpn. J. Appl. Phys.*, **18**, 1531-1541 (1979).
41. M. Asada and Y. Suematsu, "Density-matrix theory of semiconductor lasers with relaxation broadening model - gain and gain-suppression in semiconductor lasers," *IEEE J. Quantum Electron.* **QE-21**, 434-442 (1985).
42. M. P. Kessler and E. P. Ippen, "Subpicosecond gain dynamics in GaAlAs laser diodes," *Appl. Phys. Lett.* **51**, 1765-1767 (1987).
43. K. L. Hall, J. Mark, E. P. Ippen and G. Eisenstein, "Femtosecond gain dynamics in InGaAsP optical amplifiers," *Appl. Phys. Lett.* **56**, 1740-1742 (1990).
44. J. Mark and J. Mørk, "Femtosecond gain dynamics in InGaAsP optical amplifiers: Experiment and theory," *Appl. Phys. Lett.* **61**, 2282-2283 (1992).
45. R. Frankenberger and R. Schimpe, "Origin of nonlinear gain saturation in index-guided InGaAsP laser diodes," *Appl. Phys. Lett.* **60**, 2720-2722 (1992).

46. J. Eom and C. B. Su, "Determination of the gain linearity time constant in 1.3 μm semiconductor lasers," *Appl. Phys. Lett.* **58**, 234-236 (1991).
47. G. P. Agrawal, "Gain nonlinearities in semiconductor lasers: Theory and application to distributed feedback lasers," *IEEE J. Quantum Electron.* **QE-23**, 860-868 (1987).
48. M. Sargent III, S. Koch, and W. W. Chow, "Side-mode gain in semiconductor lasers," *J. Opt. Soc. Am B* **9**, 1288-1298 (1992).
49. J. Eom and C. B. Su, "Observation of positive and negative nonlinear gain in an optical injection experiment: Proof of the cavity standing-wave-induced nonlinear gain theory in 1.3 μm semiconductor diode lasers," *Appl. Phys. Lett.* **54**, 1734-1736 (1989).
50. H. E. Lassen, H. Oleson and B. Tromborg, "Gain compression and asymmetric gain due to the Bragg grating induced by the standing waves in Fabry-Perot lasers," *IEEE Photon. Tech. Lett.* **1**, 261-263 (1991).
51. G. P. Agrawal, "Spectral hole-burning and gain saturation in semiconductor lasers: Strong-signal theory," *J. Appl. Phys.* **63**, 1232-1235 (1988).
52. D. J. Channin, "Effect of gain saturation on injection laser switching," *J. Appl. Phys.* **50**, 3858-3860 (1978).
53. R. S. Tucker, "High-speed modulation of semiconductor lasers," *IEEE J. Lightwave Technol.* **3**, 1180-1192 (1985).
54. R. Olshansky, P. Hill, V. Lanzisera, and W. Powazinik, "Frequency response of 1.3 μm InGaAsP high speed semiconductor lasers," *IEEE J. Quantum Electron.* **23**, 1400-1418 (1987).
55. P. A. Morton, R. F. Ormondroyd, J. E. Bowers and M. S. Demokan, "Large-signal harmonic and intermodulation distortions in wide-bandwidth GaInAsP semiconductor lasers," *IEEE J. Quantum Electron.* **25**, 1559-1567 (1989).
56. K. A. Shore and M. W. McCall, "Nonlinear and quantum optics in semiconductor lasers," *Prog. Quant. Electr.* **14**, 63-129 (1990).

57. L. J. Bonnell and D. T. Cassidy, "Alignment tolerances of short-external-cavity InGaAsP diode lasers for use as tunable single-mode sources," *Appl. Opt.* **28**, 4622-4628 (1989).
58. D. T. Cassidy, D. M. Bruce and B. F. Ventrudo, "Short-external-cavity module for enhanced single-mode tuning of InGaAsP and AlGaAs semiconductor diode lasers," *Rev. Sci. Instrum.* **62**, 2385-2388 (1991).
59. D. T. Cassidy and L. J. Bonnell, "Trace gas detection with short-external-cavity InGaAsP diode laser transmitter modules operating at 1.56 μm ," *Appl. Opt.* **27**, 2688-2693 (1988).
60. I. Mito, M. Kitamura, Ke. Kobayashi, and Ko. Kobayashi, "Double-channel planar buried-heterostructure laser diode with effective current confinement," *Electron. Lett.* **18**, 953-954 (1982).
61. J. Abu-Dayyeh, private communication.
62. D. T. Cassidy, "Influence on the steady-state oscillation spectrum of a diode laser for feedback of light interacting coherently and incoherently with the field established in the laser cavity," *Appl. Opt.* **23**, 2070-2077 (1984).
63. F. H. Peters, *Spatially Resolved and Polarization Resolved Electroluminescence of 1.3 μm InGaAsP Semiconductor Diode Lasers*, Ph. D. Thesis, (McMaster University, 1991).
64. T. Mukai, K. Inoue, and T. Saitoh, "Homogeneous gain saturation in 1.5 μm InGaAsP traveling-wave semiconductor laser amplifiers," *Appl. Phys. Lett.* **51**, 381-383 (1987).
65. L. F. Tiemeijer, "Effects of nonlinear gain on four-wave mixing and asymmetric gain saturation in a semiconductor laser amplifier," *Appl. Phys. Lett.* **59**, 499-501 (1991).
66. W. H. Press, B. P. Flannery, S. A. Teukolsky, and W. T. Vetterling, *Numerical Recipes* (Cambridge University Press, Cambridge, 1986).
67. D. T. Cassidy, private communication.